School of Civil and Mechanical Engineering

Faculty of Science and Engineering

Numerical Modelling for Design of Ram-compacted Bearing Base Piling Foundations

Zhaodong DU

0000-0002-9148-9838

This thesis is presented for the Degree of

Master of Philosophy

of

Curtin University

November 2020

DECLARATION

This work contains no material which has been accepted for the award of any other degree or diploma at any university or other tertiary institution and, to the best of my knowledge and belief, this thesis contains no materials previously published or written by another person, except where due reference made in the text.

I give consent to this copy of my thesis, when deposited in the University Library, being available for loan and photocopying.

Signature:

Date: 01 November 2020

To my partner and family

ABSTRACT

Ram-compacted Bearing Base (RBB) piles are one of the typical enlarged base piling solutions that are relatively new and can provide higher bearing capacity at lower costs compared to traditional piles. However, the current design of RBB piles relies on semi-empirical equations that are typically over-conservative and inconsistent, often necessitating costly pilot pile loading tests before construction. The root cause of the available semi-empirical equations lies in the fact that they do not correlate the pile bearing capacity with the typical soil properties and also ignore the compaction effects associated with the installation process, urging the need for more accurate, consistent and economical design solutions.

This research aims to develop a new design method for RBB piles based on finite element (FE) numerical modelling, using the commercial software package ABAQUS, and validated with historic field cases. Five significant inputs of RBB piling foundations were considered in the FE models, including the pile shaft length, rubble base diameter, soil elasticity (Young's Modulus), soil cohesion and soil friction angle, and the load-settlement (*Q*-*S*) curve of the RBB pile was obtained. The compaction effect of the installation process was also considered in the FE models. However, for simplicity, this preliminary RBB modelling ignored the presence of groundwater, and thus zero pore pressure was set throughout the models. In a subsequent phase of future work, the presence of groundwater and its impact on the modelling results should be investigated. In addition, this research was undertaken for a single RBB design; the study for RBB pile group design is recommended based on the research outcome of the single RBB pile from this thesis.

The developed FE modelling procedure was then used to perform an extensive parametric study simulating a set of 1008 combinations of different input parameters involving a wide range of hypothetical cases of various of RBB piling configurations, including the soil properties, pile geometry and strata feature covering all soil types except pure clay. Each case yielded (*Q*-*S*) curve, and the ultimate bearing capacity (Q_u) was obtained from that curve at two different settlement values equal to 40 mm and 60 mm. The database obtained from the parametric study was then used in an

Artificial Intelligence (AI) approach via Evolutionary Polynomial Regression (EPR) analysis and returned two relatively simple equations for predicting (Q_u) at settlement values of 40 mm and 60 mm. The EPR equations were applied to two historic cases for further validation; these have confirmed that the prediction results using the EPR equations were economic and accurate, and the over-conservatism was eliminated. The developed EPR equations can serve as a new standalone method for the design of RBB piles. However, the developed equations should be ultimately verified with more field loading tests whenever possible, once the calibration reveals a consistent prediction gap, a unified constant can be applied to increase the prediction result close to the measured value in the load test; then the ultimate RBB design equations can then be confirmed for use by the piling practitioners.

PUBLICATIONS AND ATTRIBUTING CO-AUTHORSHIPS DECLARATION

The following publications are produced from the research work conducted in this Master thesis:

1- Du, Z. & Shahin, M. A. (2020). "Design of Ram-compacted Bearing Base Piling Foundations using Numerical Modelling." *Computers and Geotechnics*, submitted.

Contributing Authors:

Du, Zhaodong

Master Candidate, Department of Civil Engineering, Curtin University, WA 6845, Australia.

Shahin, Mohamed

Associate Professor, Department of Civil Engineering, Curtin University, WA 6845, Australia.

	Background /literature	Numerical modelling	Data Presentation interpretation and analysis	Discussion	paper writing/ preparation/ proofread/ final approval
Co-Author #1	20%	30%	20%	20%	20%
I acknowledge that these represent my contribution to the above research output.					
Signed:					

2- Du, Z., Walske, M., Shahin, M. A. & Ghadimi, B. (2019). "Numerical modelling of ram-compacted bearing base piles." *Proceedings of the 13th Australia New Zealand Conference on Geomechanics*. Acosta-Martínez & Lehane (Eds.), Australian Geomechanics Society, Sydney, Australia, 333–338, ISBN 978-0-9946261-0-3.

Contributing Authors:

Du, Zhaodong

Master Candidate, Department of Civil Engineering, Curtin University, WA 6845, Australia.

Walske, Megan

Lecturer, Department of Civil Engineering, Curtin University, WA 6845, Australia.

Shahin, Mohamed

Associate Professor, Department of Civil Engineering, Curtin University, WA 6845, Australia.

Ghadimi, Behzad

Research Associate, Sustainable Engineering Group, Curtin University, WA 6845, Australia.

	Background /literature	Numerical modelling	Data Presentation interpretation and analysis	Discussion	paper writing/ preparation/ proofread/ final approval
Co-Author #1	10%	5%	10%	10%	60%
I acknowledge that these represent my contribution to the above research output.					
Signed:					
Co-Author #2	10%	10%	10%	10%	10%
I acknowledge that these represent my contribution to the above research output.					
Signed:					
Co-Author #3	10%	10%	5%	5%	5%
I acknowledge that these represent my contribution to the above research output.					
Signed:					

3- Du, Z., Shahin, M. A. & Neeson, J. (2016). "Ram-compacted Base Bearing (RBB) piling technology for infrastructure developments." *The 2016 New Zealand Society for Earthquake Engineering (NZSEE) Annual Technical Conference*, New Zealand Society for Earthquake Engineering (NZSEE), Proceedings on USB.

Contributing Authors:

Du, Zhaodong

Master Candidate, Department of Civil Engineering, Curtin University, WA 6845, Australia.

Shahin, Mohamed

Associate Professor, Department of Civil Engineering, Curtin University, WA 6845, Australia.

Neeson, Jethro

Geotechnical Engineer, RDCL, New Zealand

	Background /literature	Numerical modelling	Data Presentation interpretation and analysis	Discussion	paper writing/ preparation/ proofread/ final approval
Co-Author #1	15%	-	15%	20%	20%
I acknowledge that these represent my contribution to the above research output					
Signed:					
Co-Author #2	5%	-	5%	5%	-
I acknowledge that these represent my contribution to the above research output					
Signed:	THIS AUTHOR WAS UNABLE TO CONTACT.				

ACKNOWLEDGEMENT

First and foremost, I would like to sincerely thank my supervisor, Associate Professor Mohamed Shahin, Department of Civil engineering, Curtin University, for all of his advice, help, support and everything he had done for me during my research and thesis writing, and for being so approachable. Dr Shahin initiated the research project, helped me choose the research methods, and optimise the thesis structure. Dr Shahin assisted me with the Artificial Intelligence (AI) approach for regression of the development of the new equations. I greatly appreciated all his contribution in assisting my research.

I would like to attribute my research and thesis to the Thesis Committee members: Dr Prabir Sarker, Dr Mohamed Shahin, and Dr Hamid Nikraz, for their direction and warm-hearted support during my study. I also wish to thank Dr Behzad Ghadimi for his numerous supports in my early-stage modelling assisting me with the static simulation in Abaqus code. Acknowledgement goes to Dr Hina Ismail and Dr Megan Walske for their involvement in numerical modelling and supervision in the early stage, respectively.

I wish to thank the Department of Civil Engineering and the Graduate Research School of Curtin University for the provision of great research support, scholarship, and facilities. Heartfelt acknowledgements are expressed to all academic and non-academic members, in particular, thanks to Dr Ranjan Sarukkalige, Cheryl Cheng, Frankie Sia, for their assistance and support, especially Cheryl did a very impressive job in sourcing an advanced computer for me in a short time. Thanks to my fellows Mohamed Shams, Elham Mohammadi, Mahtab Nezhadasl, and Hayder Abdullah for their help and laugh together to relax for a spell in the busy research work.

I would like to greatly acknowledge the contribution of the Australian Government Research Training Program Scholarship in supporting this research. Also, it has been so lucky for me to have been working for MTU Australia over four years. This has not only provided me the income for my living costs, most importantly, offered me a valuable stage to work in a great team contributing my capabilities in administration,

office supports and event organising, thanks to MTU team and the Managing Director Mr. Moerl.

Finally, I am indebted to my family, especially my partner Charlene (Xiaoling), my sister Juan and brother–in-law Yong, and my nephew Si for their support, encouragement, and company, mentally and physically, in my busy study time. Without their sacrifices, I may never have come this far in my research. Sincerely thanks to my friends, particularly Guangping, Xuwei, Fengdi and Xiaohan, the Song's, Amy, and Wu's for their support, and keeping me sane, and occasionally and friendly distracting me from the addictive data work and thesis writing. All the supports, and encouragement above have guided me through the difficult time to achieving the success of the research!

TABLE OF CONTENTS

LIST OF FIGURES

LIST OF TABLES

NOTATIONS

ΔQ_u	$\Delta Q_u = Q_M - Q_P$, difference of pile capacities between the measured value Q_M from load test and predicted value Q_P
ΔQ_u	$\Delta Q_u = Q_{u-60mm} - Q_{u-40mm}$, increase of bearing capacity at 40, 60 mm
Δt	Total time for deceleration
α	Coefficient
a_j	Constant
β	Coefficient (2.0 for Franki piles and 1.0 for in-situ concrete driven piles)
γ	Unit weight of soil
θ	Soil improvement coefficient
μ	Coefficient of friction
ν	Poisson's ratio
ρ	Soil density
$\sigma_1^{'}$, $\sigma_2^{'}$	Effective vertical stress at the bulb base and stem base, respectively
ϕ	Friction angle
ψ	Dilation angle of soil
ψ_c	Casting method coefficient (0.8 for precast piles and 0.75 for in-situ piles)
Ω	Angular frequency of loading

a	Constant
a_0	An optional bias
$a_1,\ a_2,\ a_3$	Cohesion factors of soil
a_j	Constant
A_b	The bearing area of the pile end
A_e	The equivalent bearing area of the bearing base
A_p	Shaft cross-sectional area
A_s	Side surface area of the pile shaft
$A_{s.i}$	Nominal pile shaft surface area in stratum number *i*
B	Width of the falling weight $= r_0\sqrt{\pi}$
C_b	Mean shear strength of the soil at and just below the base level
c	Cohesion of soil
C_1, C_2	Constants
d	Pile shaft diameter
D	Rubble base diameter
D_b	Base diameter
D_1	Diameter of bulb
E	Young's Modulus of soil
e_h	Constant equal to 0.75 for drop hammers

E_h	Constant equal to 0.85 for other hammers
ES	Matrix of exponents
f	User-defined function
f_a	Characteristic value for bearing capacity of soil in the bearing layer, referring to Standard GB 50007 - Code for Design of Building Foundations
f_c	The design value of the axial compressive strength of RBB shaft concrete following GB50010 - Code of Concrete Structure Design
f_s	Unit side friction
F	Function created by the regression process
G	Shear modulus of soil
H	Free fall distance of ram
I_L	Liquidity Index
k	Soil type factor
K	Factor of safety (K = 2)
K_0	At-rest coefficient of lateral earth pressure
l_1, l_2	Bucket length of belled piles
L	Pile shaft length
m	Number of terms of the expression as target (the expression length)
M	Mass of ram
n	Empirical coefficient factor that varies between (0.3 and 1.0)

n	Amount of bulbs/bases of one pile
$N_{0.03}$	Count of blows required to compact 0.03 m^3 of concrete into soil
N	SPT blow counts near the pile base
N_c, N_q, N_γ	Terzaghi's bearing capacity factors depending on soil friction angle
N_V	Design vertical load applied in the standard loading situation
P_s	Tip resistance before pile installation
$P_s^{'}$	Tip resistance after pile installation
q_b	Unit base bearing capacity of soil at the base
q_c	Cone resistance of CPT to DIN 4094
$q_{s.k.i}$	Characteristic pile skin friction of soils in stratum *i*
Q_b	Ultimate base resistance
$Q_{b.all}$	Allowable pile base bearing capacity at a factor of safety (FOS = 2.5)
Q_c	Bearing load of conventional piles
Q_M , Q_P	Design/predicted value of pile bearing capacity and site measured value of pile bearing capacity
Q_r	RBB pile bearing capacity
Q_s	Ultimate shaft side resistance
Q_u	Pile ultimate capacity

$Q_{M@S}$	Bearing capacity measured at settlement (S)
$Q_{P@S}$	Bearing capacity predicted at settlement (S)
P_t	Three drive penetration
r_0	The radius of the falling mass
R	Bearing capacity ratio (Q_r/Q_c) of RBB pile against conventional piles
$R_{b.k}$, $R_{s.k}$	Characteristic pile base resistance and shaft side resistance
s	Depth beneath the impacted surface (m)
S	Settlement of pile
V	Base bulk volume
V_s	Shear wave velocity of compacted soil
W	Ram weight
X, $\boldsymbol{X_i}$	Matrix of variables as inputs; Vector(s) of (k) variables as inputs
$\boldsymbol{y}$	Vector of regression output
$\bar{Y}$	Vector of output values
z	Distance from the rubble base bottom to the layer interface below the base
Z	Depth of footing (depth of embedment)

ABBREVIATIONS

AI	Artificial Intelligence
BH	Bore Hole
CPT	Cone Penetration Test
DCIS	Driven Cast In-situ
DPH	Dynamic Penetrometer (Heavy)
EPR	Evolutionary Polynomial Regression
FE	Finite Element
FEM	Finite Element Method
GD	Geotechnical Data
LL	Liquid Limit
MAE	Mean Absolute Error
PI	Plasticity Index
PIF	Pressure Injected Footing
Q-S	Load-Settlement
RBB	Ram-compacted Bearing Base
RMSE	Root Mean Squared Error
SPT	Standard Penetration Test

CHAPTER 1 INTRODUCTION

In this chapter the basic information of the ram-compacted bearing base piling technology is introduced first, followed by a discussion of the research background, objectives and scopes. The research significance is then highlighted before the entire structure of the thesis is finally outlined.

1.1 Research background

The Ram-compacted Bearing Base (RBB) piling technology was invented in 1998 by Mr Jizhong Wang at Beijing Puissant Geotechnical Engineering Company, China. The essence of the method is using the rubble to create a compacted enlarged bearing base under a concrete pile shaft to significantly increase the bearing capacity. Since its invention, the RBB piling technique has been utilised in China for over 20 years. This technology was primarily managed by the first edition of the Chinese National Professional Standards JGJ135-2001 and JGJ94-94, and currently by its latest edition JGJ135-2007 and JGJ 94-2008 (Chinese Ministry of Construction 2007, 2008). To date, nearly 279 major cities in China have authorised agencies and joint companies to locally exploit the RBB piling technology, resulting in its use as a foundation solution in a wide range of applications such as buildings, roads, railways, power factories, concrete mills, storage and mining plants (Chen et al. 2013; Liu, Xiao, and Fu 2008; Shen 2004; Tan and Wang 2010). It was reported that about 4 million tonnes of construction rubble were being used per year in the RBB piling foundation constructions in China (Wang 2007). The RBB piling technology has taken a key role in the rebuilding of the Province of Sichuan after the 2008 M8.0 earthquake. It is endorsed by the Chinese Ministry of Science and Technology and the Chinese Ministry of Construction as one of the three main piling technologies in the Sichuan Rebuilding (Chinese Ministry of Science & Technology 2008). In addition to China, RBB piling technology was also used in Burma (Myanmar) for a main plant building in the Myanmar Tagaung Taung Nickel resource project in 2009. A total of 388 RBB piles were installed, each having a diameter of 400 mm and a length of 6.0 m (Wang

2009). RBB piles were also negotiated in the United Arab Emirates in 2012, but no further progress was published.

The current design procedures for RBB piles rely on semi-empirical equations that typically lead to over-conservative designs, often necessitating costly pilot pile loading tests before construction. To improve the design method, this research undertakes a detailed numerical study to determine the soil parameters that mostly affect the performance of the RBB piles and evaluate the impact of each of these parameters. To this end, a numerical finite element (FE) model using the commercial software package ABAQUS was first developed to simulate the behaviour of RBB piles under axial loading conditions. The developed FE model was validated using field data, ultimately providing a robust methodology for further parametric analyses. Over 1,000 sets of hypothetical cases were used in the parametric study and were input into the validated ABAQUS model, and the output results were interpreted. The correlations between the RBB pile bearing capacity and the typical soil properties, RBB pile features and strata profiles were obtained using one of the Artificial Intelligence (AI) techniques, namely Evolutionary Polynomial Regression (EPR). According to the work undertaken above, it was found that the current RBB design method can be improved by two new EPR correlation equations, based on which the RBB piling specification can be updated for design practice by geotechnical engineers.

Owing to the over-conservative design of the current design approaches, this thesis investigates the ability of numerical modelling (using FE analysis) to accurately simulate the performance of RBB piles under axial loading. In the FE approach adopted herein, the RBB structure was modelled using a predefined or 'wished-in-place' pile structure with a spherical rubble base, with the surrounding soil represented by the Mohr-Coulomb elastic-perfectly plastic constitutive law (or Mohr-Coulomb model for simplicity). In the literature, the unknown properties and dimensions of the densified zone are dealt with by either: (1) assuming an increase of the soil properties (e.g. 20% to 50% increase of density and Young's Modulus) of the densified zone in excess of the in-situ material in the strengthened/bearing layer (Yu 2007); or (2) ignoring the effect of compaction on the densified soil zone, and instead of increasing

the rubble zone dimension to account for the strength increase of the soil. For example, the Chinese Standard uses the effective bearing area to implicitly include some compaction effect, which increases the bearing area value (Jin 2011; Luo 2010; Zhang 2012). More details refer to Section 2.1.4.

The study undertaken for this research follows an approach that is different from the two simplifications presented above. The study intends to indirectly include the compaction effect by manipulating the coefficients of the regression analysis performed on the results obtained from the simulation of the finite element method. Specifically, the study, therefore, has three stages: (1) constructing sophisticated 3D axisymmetric finite element models to simulate the RBB pile-soil interaction; the models were validated by comparison with historical study cases; (2) performing a comprehensive parametric study using the validated FE models, and exploring the characteristics of the soil-pile interaction of RBB piling foundations using the results of the parametric study; and (3) the results of the previous stage were processed using EPR analysis to derive design equations using artificial intelligence.

1.2 Research significance

The primary purpose of the study presented herein is to improve the safety aspects in the design of RBB piles whilst reducing the over-conservatism associated with the current design methods. This is possible by defining and evaluating the actual parameters that affect the bearing capacity of RBB piles, and this is the first time such an attempt is made in this area. More specifically:

- The research highlights some of the shortcomings that exist in the current methods commonly used to predict both axial capacity and settlement response of RBB piles.
- The research aims to provide more accurate, consistent and economical design methodology by defining the specific parameters that mostly affect the design performance of RBB piles. This will improve the reliability of RBB design by avoidance of over-conservatism and ensuring safety.

- The research is economically important, since optimising the design can reduce considerable material and labour costs.
- The first attempt in RBB piling design to use a set of significant influencing parameters to replace non-typical parameters.
- The first attempt to quantify the lower layer distance and its impact on the variations of the RBB pile capacity.
- It comprehensibly explores the impacts of the pile profile and soil properties on the RBB piling bearing capacity.

Overall, this research provides initial numerical evidence for introducing this technology to global society, hence, providing notable benefits to the global economy and environment.

1.3 Objective and scope

As iterated above, the primary objective of this research is to improve and optimise the current design methods of RBB piles. To this end, the following scope was undertaken:

- Analyse the process associated with RBB piles and the associated mechanism as a precursor to creating suitable FE numerical models, using proper constitutive material models to simulate the behaviour of a single RBB pile under axial loading, and validate the numerical models against field case studies.
- Carry out a comprehensive parametric study using the validated numerical models, and provide charts to investigate the behaviour of RBB piles under various conditions of soil properties, pile features and ground profile.
- Process the simulation outputs of the parametric study using artificial intelligence and develop design equations via EPR analysis to determine the correlation between the single RBB pile bearing capacity and the associated parameters. Provide the developed design equations as the basis for updating

the design guidelines and current design practice for the geotechnical engineers and practitioners.

1.4 Thesis structure

This thesis is divided into five chapters, as follows:

Chapter 1 provides an introduction to RBB piling foundation technology and research background. The chapter also outlines the thesis objectives, significance, and structure.

Chapter 2 presents a literature review on the RBB piling foundation technology and an overview of the RBB piling foundation mechanism. The chapter also discusses the current problems associated with RBB design and proposes methods that can improve the design approaches. Chapter 2 then reviews the enlarged base piles, discusses their common characteristics, compares the RBB piles with the Franki piles, and provides bases for further discussion of the RBB piling methods.

Chapter 3 presents the major research methodology used in this research, i.e. finite element (FE) modelling. This chapter mostly discusses the development of sophisticated axisymmetric 3D FE numerical models that correctly simulate the performance and behaviour of RBB piling foundations, including validation of the developed FE models with historic cases. This chapter then undertakes the parametric analysis involving a wide range of RBB piling foundation configurations; it includes the detailed investigation (quantity analysis based on the sophisticated model developed) on the parametric impact of those parameters on the variations of the RBB pile bearing capacity using visualisation methods. five significant parameters and some insignificant parameters relevant to the RBB piling are determined as inputs into numerical modelling for development of the new RBB design equations.

Chapter 4 develops the new design method with equations based on the results of the extensive parametric study performed using the FE numerical models combined with artificial intelligence (AI) approach. Chapter 4 first presents the AI approach used and

explains how it processed the output of the FE numerical models to develop a new design formula for RBB piles. The outputs are interpreted and presented in a set of simple equations that can be readily used by professionals for design purposes. This chapter validates the new RBB pile design equations developed against the historic cases.

Chapter 5 summarises the research carried out in the thesis and provides the research contributions and limitations. This chapter concludes the research with recommendations for potential future work.

CHAPTER 2 LITERATURE REVIEW

The literature review presented in this chapter introduces the concept of RBB piling foundations technique, including pile installation, mechanism, strengths and weaknesses. The chapter then discusses the available design methods and existing problems of the RBB piles, including assumptions and limitations. The chapter also provides suggestions to improve the existing design approaches. The chapter then reviews the development and practical application of enlarged base piles, including piling techniques that produce enlarged bases and compares them with RBB piles. The data reviewed and collected will be theoretically analysed to determine the current technical levels and profile of these technologies, and the problems existing. The aim is to provide some insights into the contribution of enlarged bases and better understand the RBB piles. Eventually, this understanding will help to develop a new design method for RBB piles in the following chapters.

2.1 RBB Piling Technology

Ram-compacted bearing base (RBB) piles have been used as a foundation solution in China since 1998, but the technology is virtually unknown in the western world. Reviewing the literature published in the past 20 years showed that available publications mostly focus on case studies, ground investigations and primary experimental techniques (Jin 2011; Li et al. 2002; Shen 2004; Yang and Wang 2011). Only a few publications contributed to RBB piling research. Qiu et al. (2002) discussed the mechanism of load transfer and proposed the soil-base interaction model using FEM to simulate the load-settlement response. Su and Ge (2005) reported the application of RBB piles in saturated sandy clay, and experimental results by Yu (2007) showed that the influence zone extends to twice the base diameter in soils under the base, and once the base diameter in the soil surrounding the base above the bottom level. Apparently, no rigorous research was undertaken to tune the design process, and several authors highlighted the over-conservatism associated with the current design methods (Jin 2011; Qiu et al. 2002; Wang 2014; Yang 2011).

Generally speaking, RBB pile usually comprises a cylindrical concrete shaft overlaying a solid spherical bearing base, as shown in Figure 2-1. An array of RBB piles works as a load-transmitting truss that conveys the outer loads to the bearing base spheres which sequentially spread the loads to the underlying soil stratum. RBB pile is comparable to traditional concrete piles, and the upper segment of the RBB pile is similar to that of conventional concrete piles in terms of materials (concrete and reinforcement bar cage), but its shaft diameter is smaller and the length is shorter. The overall length of the RBB pile usually varies from 5 m to 10 m with a usual diameter of 400 mm, but the diameter may vary from 320 mm up to 650 mm. The ultimate capacity per pile ranges from several tens of tonnes to approximately one thousand tonnes (Chinese Ministry of Construction 2007; Shen 2004; Zhu and Wang 2005). The pile spacing varies from 1.6 m (for sand) to 2 m (for clayey soil). Based on the site tests and laboratory experiments, Li et al. (2002) discovered that the optimal spacing of RBB piles is four times the diameter of the pile shaft.

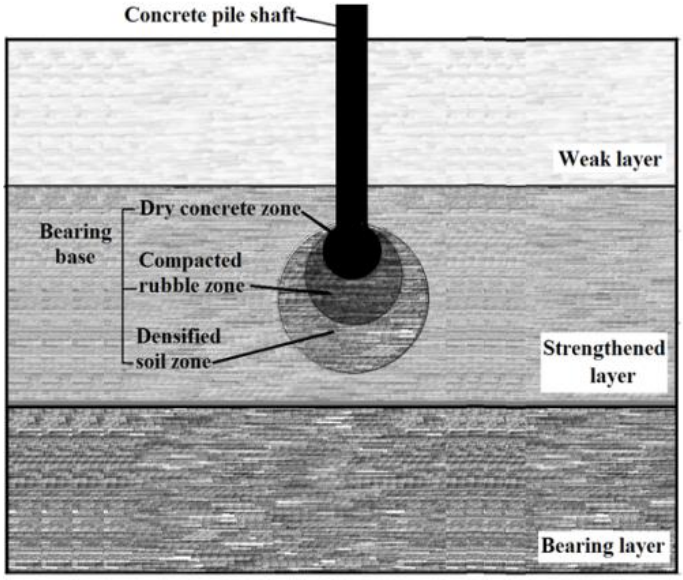

Figure 2-1 Typical structure of single RBB pile system with a predefined profile (pile-in-place) (Du et al. 2019).

The spherical bearing base created by the RBB piling method has three zones (see Figure 2-1), including: (1) a concrete zone (dry or half-dry, approximately 0.5 m^3 in volume); (2) a ram-compacted filling material zone (approximately 0.5-1.8 m^3); and (3) a densified surrounding soil zone (Tang 2012; Zhu 2008). Dry or half-dry concrete is the concrete mix with no or low water content. During the RBB base creation, the

dry concrete is used when the hole bottom is wet; otherwise, the half-dry concrete is used when the bottom is dry. The dry concrete zone connects the upper concrete pile shaft with the bearing base, and the ram-compacted filling material zone is made of demolition rubble (installation of RBB pile is introduced in Section 2.1.1). As can be seen in Figure 2-1, across the entire RBB pile profile, three categories of natural sub-surface soil layers are formed, as follows: a weak layer (1st layer from top), a strengthened layer (2nd layer from top) and a load-bearing layer (3rd layer). The RBB pile extends through the weak layer (e.g., topsoil, saturated silt, peat and landfills) into the strengthened layer where the bearing base sphere is created. The strengthened layer is denser than the upper weak layer and can comprise any soils except the saturated clay (to be discussed in Section 2.1.3) and those in the weak layer above it. The load-bearing layer has engineering characteristics similar or superior to those of the strengthened layer and could be of the same lithological formation (Tang 2012; Yang and Wang 2011). Basic details regarding the RBB piles can be found in Du et al. (2019, 2016).

The rubble consists of any materials of clean landfill waste and rough fragments of brick, concrete stone or a mixture thereof sourced from building demolitions, quarries, tailings, etc. These materials are recognised and approved in the policies on *Demolition and Construction Waste Minimisation and Recycling* in many countries, such as USA, New Zealand and Australia (Department of Environment Australia 2011; Ministry for the Environment New Zealand 2002).

2.1.1 Installation of RBB piles

The installation process of the RBB piles is presented herein to better understand the mechanism discussed later in Section 2.1.3. RBB piles are installed using a special patented piling machine in nine main stages (Figure 2-2), as follows (Wang 2007; Zhang 2014):

1) Mark out all the RBB pile positions according to the site survey plan; dig a 0.5 m deep hole at each pile location immediately before the new installation;

place the piling machine at the marked position and align the casing vertically into the hole.

2) Drop the 3.5 tonnes ram freely through the casing and let it protrudes out of the casing bottom about 0.3-0.5 m.
3) Successively drive the casing 0.3-0.5 m into the ground by pulling downwards the steel wire powered by a winch.
4) Repeat Steps 2 and 3 above until the desired foundation level is reached; retain the piling casing in position; Figure 2-3a shows the detail of Stage 4 with the first batch of rubble fill at bottom.
5) Construct the rubble base by hammering sequential small batches of the rubble material until the inserted rubble reaches a certain amount (e.g., 1.5 m^3) and the advancement of the hammer becomes slow; the energy level used to compact the rubble at depth can be approximately 250 kN.m up to 617 kN.m (see Table 2-1).
6) Conduct measurement of the three-drive-penetrations (P_t, generally ranging from 10 to 30 cm) after the complete hammering of the last rubble batch and drop the 3.5 tonnes hammer three times with a motion of free-falling body and 6.0 m drop distance; record the reach penetration:
    - Every penetration should not be larger than the previous one;
    - The sum of the three penetrations should comply with the design requirement (i.e. P_t should be less than a designed value) and the RBB pile installation is then regarded as being compacted to "refusal"; and
    - If the above criteria are not met, continue to fill materials and compact until the three penetrations meet the design requirement. However, if the volume of the filling materials is too excessive, the adjacent pile may be adversely driven away or even twisted. In these circumstances, the piling engineer should liaise with both the designer and owner to adjust the piling parameters.
7) Drop the (half) dry concrete into the hole and compact.
8) Withdraw the hammer from the casing and install the reinforcing cage to the designed level. The upper concrete shaft is then constructed by pouring a high

slump concrete into the casing and the casing should be pulled out gradually towards the end of this process.

9) Complete a single RBB pile installation (Figure 2-3b presents details of a complete RBB pile with enlargement).

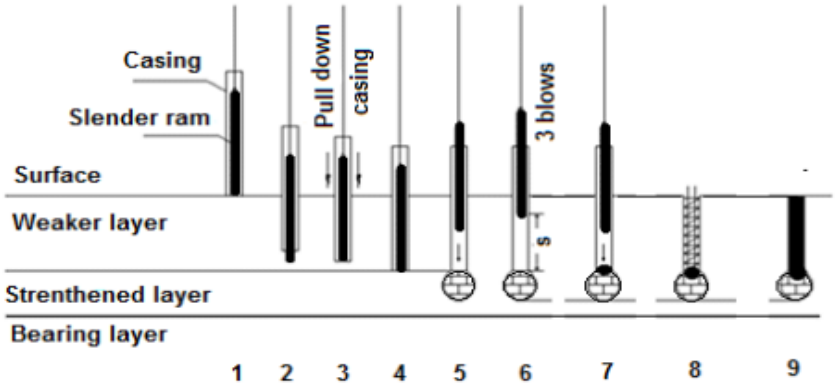

Figure 2-2 RBB pile installation process (Du et al. 2016).

Table 2-1 Standard driving energy level for RBB pile three-drive-penetration tests.

Tube diameter (mm)	Ram weight (kN)	Drop height (m)	Number of blows	Standard driving work (kN.m)
425	34.3 (3.5 ton)	6.0	3	617

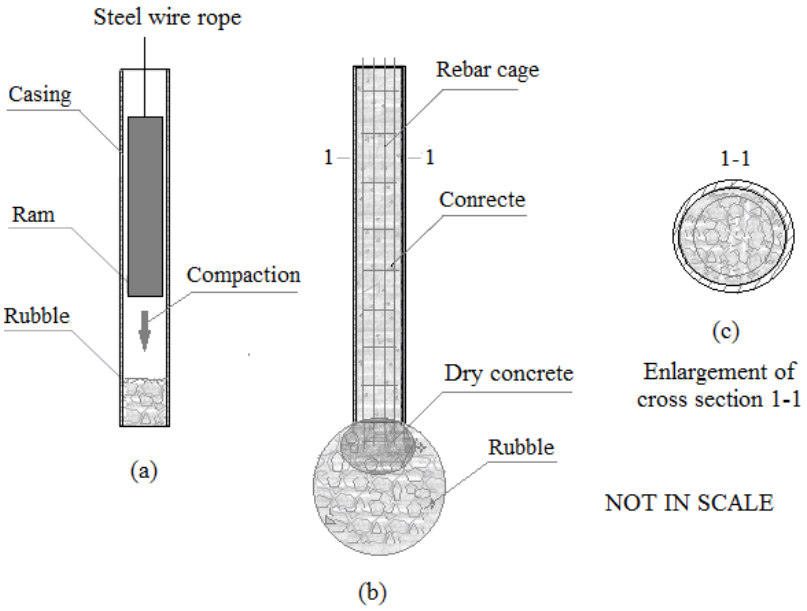

Figure 2-3 Details of RBB pile for: (a) start of the first rubble batch compaction; (b) complete RBB pile after installation; and (c) enlargement of the cross-section 1-1.

Patented RBB piling machines use a hydraulic walking mechanism. Figure 2-4 shows two machines on RBB piling sites in Heze city (China) and Figure 2-5 displays the material filling window in the casing. The main components of the RBB machines are as follows:

- 15 m vertical frame mast made of a hollow tube.
- 50 kN fast release winch, used to lift and release a hammer, and 30 kN additional winch, used for back pulling and lifting the casing.
- 3.5 tonnes ram with a length of 3.5 m and a diameter of 355 mm.
- Casing used to guide the direction of the hammer and protect the walls of the hammered hole, made of 327 mm to 600 mm steel pipe; the length is determined by the pile length.

Figure 2-4 RBB piling machine on site.

Figure 2-5 Material infill window in casing.

2.1.2 Testing of RBB piles

Pile load testing has been used in the geotechnical engineering practice to verify pile capacity obtained from theoretical and empirical design formulae and to provide information regarding the expected deformations under working loads (Elkateb, Law, and Tweedie 2003). Herein, a brief description of the pile load testing program is presented to help understand the similarities and differences between the RBB piles and traditional piles. This will help to determine the bearing capacity, Q_u, in Section 3.1.3.

Two main RBB pile load testing methods are currently used, namely “static load test” and “low strain test” (Ministry of Housing and Building of China 2014). Similar to most traditional piles, the RBB static load test is commonly conducted by jacking against a beam fastened to several RBB reaction piles (generally four or more); each reaction pile is reinforced with a cage strengthening both the shaft and the base. The test pile is always installed in the centre of the reaction pile group. Loading of the pile starts as soon as the shaft concrete achieves the specified strength−usually about ten days for piles in sandy soils, and 26 days in silty and clayey soils after installation. The test results are presented in the form of a load-settlement (*Q*-*S*) curve measured at the pile head (Ministry of Housing and Building of China 2014; William 1991).

Although the static load test method is the same as that conducted for conventional piles, interpretation of the results is different, because the bearing mechanism of RBB piles is different. Traditional piles exhibit two types of load-settlement response: (1) a curve with a definitive yield point that can be recognized from the sudden drop of the rate at which the load increases with the settlement; and (2) a curve with no definitive yield point. The ultimate bearing capacity for traditional piles exhibiting type (1) response is taken at the yield, whereas for type (2) it is taken as the value that corresponds to a certain settlement magnitude. Review over 10,000 (*Q*-*S*) curves of RBB piles (Li 2007; Qiu et al. 2002) showed that the (*Q*-*S*) curve falls into type (2) where the rate of loading gradually decreases with the settlement, with no distinctive yield point. This interpretation for certain settlement criteria will be detailed in Section 3.1.3.

The low strain testing is mostly used to test the structural integrity of piles; it is also utilised for verifying the structural integrity of the segments of the RBB piles (shaft, base and joint). The test starts by striking the pile head with a hammer. The response of the pile top to the low strain shockwave generated is used to confirm the pile length and approximate position and extent of any major deficiencies or abnormality (Curtin et al. 2006). The low strain testing method is adopted by the RBB Standard to examine the completeness of the RBB concrete piles. Care must be exercised during the interpretation of the signals due to the reverse-phase section at the joint interface of the RBB concrete shaft and the rubble base (at 7 m in Figure 2-6), because the bearing

structure of the RBB piles is different from that of conventional piles. The defects that can be revealed by the low strain testing of the RBB piles are commonly associated with a poor connection between the concrete shaft and the bearing base, resulting from the inappropriate piling operations, e.g. lifting the casing too fast or at a wrong time (Yue and Yang 2002).

Figure 2-6 Typical low strain test curve showing a complete RBB pile (Zhang 2014).

2.1.3 Mechanism of RBB piling foundation technique

2.1.3.1 Influence depth of surface ram-compaction

During the formation of the bearing base, the ram compaction induces dynamic stress in the surrounding soils. Distribution and variation of the dynamic stress determine directly the extent and shape of the compacted soil. The extent and shape of the compacted soils further correlate to the formed RBB base shape and dimension, and the magnitude of the RBB bearing capacity. Several research studies have been carried out on the depth of the compaction effect and the induced stress in the soils. Although the compaction in these researches was applied above ground (not in a deep hole as in the case of RBB piles); furthermore, most of these studies involved compaction of natural soils, not two different materials (rubble and natural soils), the results shed some light into the process of the RBB compaction.

Most of the equations found in the literature were based on the technique and theory firstly devised and developed in the 1960s by Menard. Wayne and Jones (1983) studied the stress induced by dynamic compaction (mass impact) and proposed a formula presented in Mayne and Jones (1983). Berry et al. (2000) reviewed the

prediction of ground improvement made by dynamic compaction and pointed out that a few formulas may be used to provide a preliminary estimate for the degree of improvement. However, none of the formulas produced appears to accurately predict the outcomes of dynamic compaction. Berry et al. (2000) suggested that a revision and/or combination of these formulas into one model may be needed to produce reliable predictions.

According to Menard and Broise (1975) (cited by Bo et al. (2009) and Nazhat (2013)) the degree of granular soil improvement by rammed dynamic compaction increases with the applied energy, and the influence depth correlates with the ram-weight and drop-height. Most existing equations are based on the formula first proposed by Menard and Broise (1976) as $D = \sqrt{W \times H}$, where: W = compactor mass (tonne) and H = Ram drop distance (metre). Lukas (1992) (cited by Bo et al. (2009) and Nazhat (2013)) proposed an equation that provides an estimation of the influence depth D (m), as follows:

$$D = n \times \sqrt{W \times H} \qquad \text{Equation 2-1}$$

where: W = weight of ram (tonne); H = ram free drop height (metre) and n = an empirical coefficient factor varies between 0.3 and 1.0.

Equation 2-1 can be initially used to estimate the influence depth associated with compaction of RBB piles, as follows: W = 3.5 tonnes, H = 6 m and n = 0.5 (Nazhat 2013). This produces a depth $D = 0.5 \times (3.5 \times 6)^{½} = 2.3$ m meaning a 2.3 m thickness of the soil below the compacted rubble base will be densified. However, an accurate estimation of the empirical coefficient, n, requires further studies because the compaction in RBB piling is transferred by the compacted rubble to the underneath soil, i.e. it is indirect compaction. In addition, the formula used is based on the surface compaction, and the equation also does not indicate how the influence changes over the affected depth. Berry et al. (2000) reported a case where the compaction influenced the foundation soil down to a maximum depth of 2.2 m. However, the maximum strain has occurred at a depth of only 1 m (Figure 2-7). The maximum strain

depth is as important as the maximum influence depth in terms of the performance of RBB piles.

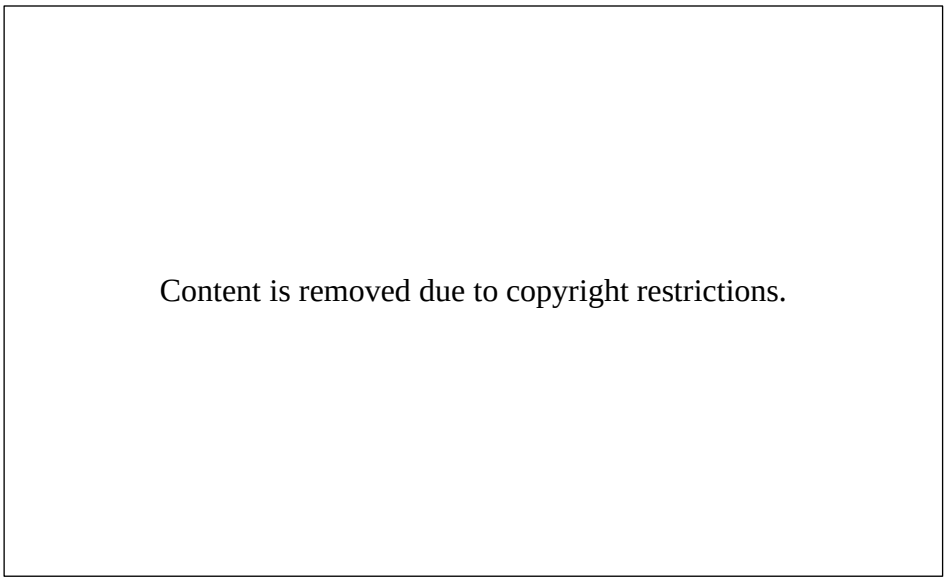

Figure 2-7 Variation of compaction-induced strain with depth (Berry et al. 2000).

2.1.3.2 Lateral extent of compaction due to RBB installation

Li et al. (2002) undertook a field test in the City of Tianjin, China, to verify the lateral improvement effected by installing a single RBB pile. Five soil samples were retrieved from the edge of the compacted rubble base covering a horizontal distance of up to 3 m from the base edge. The diameter of the compacted rubble zone was 1.05 m (Figure 2-8a). Laboratory test results from the five samples showed that the soil porosity decreased from 44.7% (native) to 41.1% at the base edge after compaction (Figure 2-8b). This means that the soil dry density increased from 1.92 g/cm^3 to 2.05 g/cm^3 (Figure 2-8c). The results of this test are encouraging; however, further testing is still required to determine how the influence distance changes with the variation of the rubble base diameter. Besides, this test did not explain how the subsoil layer below the bearing base impacts the overall settlement of the RBB pile. Figure 2-8 (b and c) shows that the significant improvement occurred at approximately 90 cm from the edge of the base.

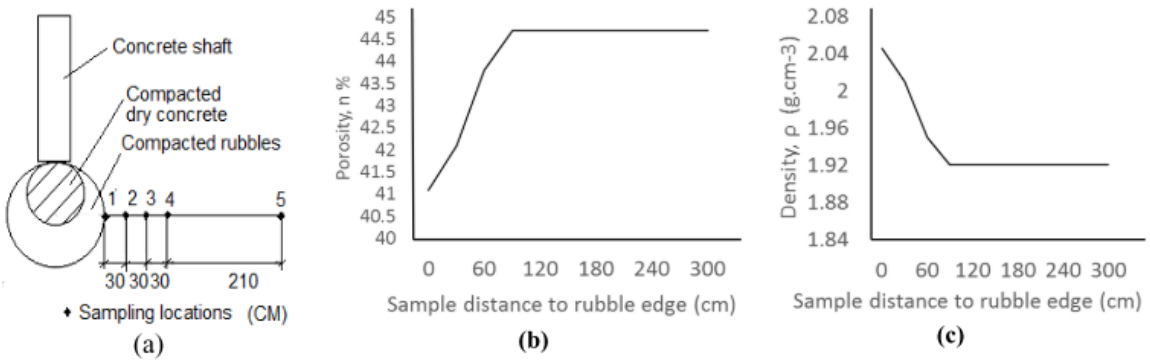

Figure 2-8 Field tests conducted in Tianjin China to evaluate RBB piling effects: (a) sample locations; (b) porosity changes; and (c) density changes (Du et al. 2016).

Heijnen (1974) (cited by Tomlinson and Woodward (2007)) measured the cone penetration resistance of loose to medium-dense silty fine sand before and after installation of a Frankipile, and the improved penetration resistance at several distances away from the enlarged base of the pile is presented in Table 2-2. Table 2-2 indicates that the significant improvement of the soil occurred within 1 m from the edge of the base, agreeing with the finding by Li et al. (2002) discussed above.

Table 2-2 Improved penetration resistance outside the enlarged base.

Distance from pile axis	*Increase in static cone resistance*
(m)	*(%)*
1	50–100
2	About 33
3.5	Negligible

2.1.3.3 Improvement of liquefaction resistance by RBB piles

The effect of RBB piling on improving the liquefaction resistance of soils was assessed through an in-situ test undertaken in the District of Tongxian, Beijing (Yang and Wang 2012). In this test, the length of the RBB pile shaft was 4.4 m. Two boreholes (BH1 and BH2) were located midway between two RBB piles installed 2 m apart. Standard Penetration Tests (SPTs) were performed every 1 m from 4.4 m to 8.4 m depth to assess the effect of RBB piling. Table 2-3 shows that the SPT readings increased from 6% at 6.3 m (BH 1) to 160% at 4.4 m (BH 2) after RBB compaction, except the one at 7.3 m (BH 2) in which the SPT reading did not change. Assessing

the liquefaction potential using the improved values of SPT readings proved that RBB compaction changed the classification of the soil from being liquefiable to non-liquefiable. It is worth noting that because the compacted rubble had a height of around 2 m, the ram- compaction influence depth under the rubble base was found to be approximately 2 m, which is close to that previously predicted using Equation 2-1 (cited by Bo et al. (2009)).

Table 2-3 Comparison of soil SPT readings before and after RBB compaction (Yang and Wang 2012).

Bore hole	Test depth (m)	SPT critical blows	SPT blows before compaction	SPT blows after compaction	Liquefaction potential before	Liquefaction potential after	SPT improvement %
1	4.4	11.31	7	12	yes	no	71
	5.3	12.21	10	14	yes	no	40
	6.3	13.21	16	17	no	no	6
	7.3	14.21	13	16	yes	no	23
	8.2	15.11	9	19	yes	no	111
2	4.4	11.31	5	13	yes	no	160
	5.3	12.21	7	14	yes	no	100
	6.3	13.06	8	16	yes	no	100
	7.3	14.06	17	17	no	no	0
	8.2	15.26	13	18	yes	no	38

Another in-situ test using a heavy dynamic penetrometer (DPH) was undertaken to verify RBB compaction effect in a railway foundation project in Langfang District of Beijing. The soil profile comprised 8.4 m interbedded silty clay and clay, overlying a 3.6 m thick fine sand layer (Zhang 2012). The pile diameter was 0.43 m and pile spacing was 2 m. The test was conducted from the surface down to a depth of about 10 m. The test results showed that the DPH blows increased from 19 for the intact (native) soil to 33 at around 10 m depth after RBB piling. The state of the sand between the bearing bases changed from being medium dense to dense and very dense. It was concluded by Zhang (2012a) that the RBB pile bases were effectively connected with the now densified−non-liquefiable soil. It was also noted that after the second base was installed, the consistency in the soil properties was improved significantly compared to the single base installation.

Wu and Tang (2000) performed 20 Cone penetration Tests (CPTs) below the bearing base before and after the RBB pile installation. The results were used to develop the following correlations:

In sandy soils, the CPT resistance after RBB installation is:

$$p_s' = 2.979 \times p_s^{0.642}$$ Equation 2-2

In silty soils, the CPT resistance after RBB installation is:

$$p_s' = 2.972 \times p_s^{0.561}$$ Equation 2-3

where: p_s = tip resistance before RBB pile installation and p_s' = tip resistance after installation.

Table 2-4 shows that the tip resistance of the weak soil tripled because of the installation effect of the RBB piles. However, as the tip resistance of the native soil increases, the degree of improvement vanishes when the tip resistance of the native soil exceeded 19 MPa for sand and 12 MPa for silt. This finding is consistent with the results of the parametric study presented later in Sections 3.2.3 and 3.3.2. To avoid the lateral influence on the neighbouring piles, the Chinese standard suggested that the minimum RBB pile spacing varies from 1.6 m (for sandy soils) to 2 m (for clay). Li et al. (2002) found that the optimum interval of RBB piles is four times the RBB pile shaft diameter.

Table 2-4 CPT test results – Tip resistance.

No.	Sand Soil		Silt Soil		No.	Sand Soil		Silt Soil	
	P_s (MPa)	P_s' (MPa)	P_s (MPa)	P_s' (MPa)		P_s (MPa)	P_s' (MPa)	P_s (MPa)	P_s' (MPa)
1	1.1	2.5	0.5	2.0	13	5.5	9.4	3.2	5.7
2	1.2	2.8	0.8	2.7	14	6.0	10.0	3.5	5.9
3	1.5	3.8	1.0	3.0	15	6.5	10.4	3.8	6.3
4	1.8	4.4	1.2	3.2	16	7.0	10.7	4.0	6.4
5	2.5	5.9	1.4	3.5	17	7.5	10.9	4.5	6.9
6	3.0	6.6	1.8	4.1	18	8.2	11.2	4.8	7.3
7	3.5	7.5	2.0	4.5	19	8.4	11.4	5.0	7.4
8	3.7	7.8	2.1	4.6	20	9.0	11.6	5.5	7.8
9	4.0	8.2	2.2	4.7	21	9.7	11.9		
10	4.3	8.4	2.5	5.0	22	10.0	12.0		
11	4.6	8.7	2.8	5.2	23	10.5	12.1		
12	5.0	9.0	3.0	5.4	24	12.4	12.0		

2.1.3.4 Stress induced by ram dynamic compaction

Mayne and Jones (1983) proposed equations for the maximum dynamic force, F_{max}, and peak dynamic stress, σ_{zmax}, beneath the centre of a falling ram, as follows:

$$F_{\max} = (32W \times H \times G \times \frac{r_o}{1-\nu\pi^2})^{0.5} = \frac{2W \times \sqrt{2g \times H}}{g} \times \Delta t; \cdot \sigma_{z-\max} = V_s \frac{\sqrt{W \times H \times B}}{(B+s)^2}$$

Equation 2-4

where: W = ram weight (kg); H = ram free fall height (m); G = soil shear modulus (MPa); r_o = radius of the falling mass (m); ν = Poisson's ratio; Δt = total time for deceleration (sec); V_s = shear wave velocity of the compacted soil (m/s); B = width of the falling weight $= r_0\sqrt{\pi}$ (m); and s = depth beneath the impacted surface (m). This equation was applied to the surface compaction and no attempt was made when the compaction occurs at depth.

Yang (2004) presented an equation for calculating the dynamic pressure generated by the hammer compaction (ignoring soil viscosity), as follows:

$$\sigma = \sin(\omega t) \times \frac{\sqrt{4g \times H \times W \times E}}{\pi \times (1-v^2)^2 \times r_0 \times \sqrt{r_2}}; \qquad \omega = [2 \times r_0 \times E / (W - W \times v^2]^{0.5}$$

Equation 2-5

where: W, r_o & H = mass (kg), radius (m) and free fall distance of ram (m); E = Young's Modulus (Pa); v = Poisson's ratio of soil under ram compaction; and ω = angular frequency of loading.

Equations 2-4 and 2-5 suggest that the stress-induced by the dynamic compaction is proportional to the shear wave velocity, V_s, Young's Modulus, E, and Poisson's ratio, v. This indicates that the bearing capacity of the RBB piles is proportional to these factors; this is used to identify the parameters affecting a soil response to RBB piling in Section 3.1. The improvement in the soil properties is progressive as the

compaction continues since the values of V_s , E and v keep increasing; this recursive process accelerates the increase in the induced dynamic stress with every new cycle of rubble addition and compaction. The Civil-Engineering-World (2011) published a sketch of the distribution of the stress contours during the surface dynamic compaction (Figure 2-9), and this is in agreement with what was reported by Shah and Shroff (2003).

Figure 2-9 Isobars of vertical stress under a uniformly loaded circular area (Shah and Shroff 2003).

2.1.3.5 RBB pile profile and base shape

The base shape of RBB piles were examined by excavating on a few sites after construction to expose the piles. For example, the project of Inner Mongolia Puissant (2015) and the one reported by Yang (2011) revealed that the dug-out rubble base of the RBB piles had a near ball shape (Figure 2-10).

Figure 2-10 Near sphere shape of rubble part of RBB bearing base (Inner Mongolia Puissant Ltd 2015).

Laboratory tests conducted by Li and Qiu (2009) showed that the base shape was close to an ellipsoid in both clay and sand. Combining the above with the findings by other researchers, it can be concluded that the RBB base has a spherical or a near-spherical shape in most circumstances, and this is what will be assumed in the theoretical analysis of the current research.

Zhang (2014) presented an interesting numerical modelling case study demonstrating the relationship between the RBB pile diameter, bearing area, rubble base volume and bearing capacity, and the data are listed and analysed in Table 2-5. It can be observed that when the pile base diameter increases from 0.6 m to 1.2 m, the bearing area increases 4.4 times from 0.28 m^2 to 1.54 m^2; the bearing load increased from 3080 kN to 4460 kN by about 45%. This improvement corresponded to a rubble volume which increased from 0.11 m^3 to 1.44 m^3 (11.7 times).

Table 2-5 Pile diameters, bearing area, rubble base volume and bearing capacity for case study by Zhang (2014).

Pile Number	H1	H2	H3	H4	H5
Base diameter (m)	0.6	0.8	1.0	1.2	1.4
Base bearing area (m^2)	0.28	0.50	0.79	1.13	1.54
Bearing area increase by (%) (per increase)		0.78	0.56	0.44	0.36
Bearing area increase by (%) (H5/H1)					4.44
Base volume (m^3)	0.11	0.27	0.52	0.90	1.44
Base volume increase by (%) (per increase)		0.33	0.25	0.20	0.17
Base volume increases by (%) (H5/H1)					11.70
Capacity at 60 mm (kN)	3080	3600	4020	4320	4460
Capacity increases by (%) (per increase)		16.9%	11.7%	7.5%	3.2%
Capacity increases by (%) (H5/H1)					0.45
Rubble volume calculated (m^3)	0.11	0.27	0.52	0.90	1.44
Rubble volume used (m^3)	0.15	0.35	0.68	1.18	1.87
Rubble compressional ratio	0.75	0.77	0.77	0.77	0.77

Even though the rubble cost may be low and could be ignored, the labour and machine costs may on contrary be too significant to ignore. Relying on enlarging the base size to increase the bearing capacity per a single RBB pile is not economic and efficient. Note also that an excessively large base requires larger pile spacing, which may further increase the cost of the cap beam (Zhang 2014). Efficiency entails seeking a

solution where an optimum base diameter can be adopted to achieve the desired bearing capacity at the minimum cost. This is why RBB standards require the base volume should optimally range from 0.5 m^3 to 1.5 m^3.

2.1.3.6 RBB pile group

Based on the experimental results presented earlier, a single RBB pile can produce an entire subsurface mass of compacted rubble and densified soil of about 3–5 m in thickness and 2–3 m in diameter. The group of RBB piles can thus create a platform under a cap or foundation (Yang and Wang 2011). The three-drive-penetrations, P_t, value of each RBB pile is not larger than one design value to ensure all the piles in one group have the capacities higher than an allowable capacity. The building seated on this group of RBB piles has small and even settlements. The RBB pile group is efficient in transferring the load; it readily neutralises the partial fluctuation of the stress in the group, which may result from some partial small defects in the design or construction. The differential settlements can therefore be avoided or mitigated (Jin 2011; Shen 2004; Yang and Wang 2011).

When a bearing base is created using RBB piling in a liquefiable soil, it pushes on the soil mass (i.e. consolidates/densifies it), bridges and separates possible lower liquefiable layers and mitigates or eliminates the liquefaction potential, not only in the base-worked layer but also in the lower liquefiable layer. Besides the in-situ tests discussed above, other case studies were reported, such as (Jingsong Yang 2011; Yang, Wang, and Shen 2007) where the potential of soil liquefaction was eliminated in an approximately 4 m zone from the top of the compacted dry concrete to the bottom of the affected surrounding soil.

2.1.3.7 Discussion and conclusion

Based on the dynamic compaction theory of Menard and analysis of dynamic compaction and field testing, the RBB compaction mechanism can be described as follows (Wu and Tang 2000):

- RBB piling improves the soil surrounding the base by delivering compression and shear shock waves around and below the enclosed hole, which improves the soil mass in a localised manner compared with surface compaction (Wu and Tang 2000).
- In saturated sandy and silty soils, the RBB hammer compacts the soil, repelling the water and air entrapped in the soil, and the shear fracture forms. The soil consolidation accelerates under free drainage after installation; therefore, strength and Young's Modulus of the sand and silt increase considerably after compaction.
- In saturated highly plastic clayey soil, the strength decreases instead of increasing after compaction. Following further compaction, the softening effect worsens and this is why a saturated clay layer is deemed unsuitable for RBB piling (Chinese Ministry of Construction 2007; Wu and Tang 2000).
- As RBB base diameter increases, the extent and density of the compacted soils increase, leading to improved bearing capacity but in a deficient manner compared with the increasing volume of the used rubble, letting alone the additional labour and machine cost. Moreover, when the base volume is too large, the ground heave becomes an issue, therefore, the optimal base diameter should be sought in RBB design (Zhang 2014).

It follows from the discussion above that RBB piling in suitable soils can be useful in reducing settlement, increasing bearing capacity and mitigating liquefaction risk as Menard Group (2020) found in Franki pile construction.

2.1.4 Design methods of traditional and RBB piles and associated concerns

As noted in the previous sections, research into RBB pile technology is behind the practice, which justifies the existing uncertainties and inconsistencies in the design, installation and testing (Zhu 2008). This section first overviews the general design methods of the traditional piles, and then critically introduces the current RBB design methods and briefly proposes the approach to be followed to improve the design, with more elaboration later in the following sections and Chapter 3.

General considerations associated with pile foundation design (Suman 2015):

- The design of the pile should ensure that the applied load from the upper structures can be tolerated without safety issues that may result from soil shear failure or excessive differential or total settlement. The pile designed should work within the allowable vertical and lateral loads or combinations of the two during the life of the structure.
- The construction of the proposed pile shall not risk the surrounding structures with vibration, noise and deep excavations that may cause critical lateral land spreading.
- The material selected to fabricate the pile must be physically rigid to take the loads applied and transfer the load to surrounding media (soils).

Pile foundations are extensively utilised in industries of civil and construction. However, due to the irregular behaviour of soil and the dependency of pile bearing resistance on various factors, no one definite equation has been found to predict the pile resistance and to embrace all the factors systematically (Suman 2015). The problem common to all piling is to determine the appropriate design parameters so that shaft and base capacities can be assessed as realistically as possible. The densification effects of driving the casing and subsequent formation of the enlarged base must be taken into account if realistic results are to be achieved (Paikowsky 2014). For RBB piles only the base bearing capacity is considered as the friction is omitted. Methods proposed by Kishida (1967) and Meyerhof (1959) offer solutions to cater for these effects (cited by Paikowsky (2014). Two major measures are provided in the literature to include the compaction effects: (1) dynamic modelling automatically includes the densification effects in simulating the process of filling material insertion and compaction by hammering; (2) if the static load model is used, then the increased coefficient or parameters can implicitly include the densification effects as suggested by Wang et al (2006), which is to be detailed in Section 3.1.4.

Several other methods have been developed to alleviate the uncertainty in the prediction, which involve using assumptions, simplifications, or empirical coefficients associated with the soil-pile interface, soil stratigraphy properties, and

calculation of soil resistance along the side surface of the pile shaft. As a result, they do not offer straightforward measurable values suitable for foundation design (Eslami, Tajvidi, and Karimpour-Fard 2014; Shariatmadari, Eslami, and Karimpour-Fard 2008; Suman 2015).

A single pile capacity can be defined by one or combination of the following common methods: static equations (static analysis), dynamic equations (dynamic analysis), static load testing and dynamic load testing (Shooshpasha, Hasanzadeh, and Taghavi 2013). Dynamic load testing requires more experience in operation and the estimation of capacities is only available after pile completion (Coyle and Sulaiman 1970; Shooshpasha et al. 2013), and is not discussed further herein. Mostly, all of these techniques provide the estimation of pile capacities with capricious accuracy (Zein and Ayoub 2016). Numerical modelling is also another method that can be used to investigate the pile capacity and will be discussed in Chapter 3.

2.1.4.1 Pile Capacity from static equations

Static equations generally utilize static soil properties to calculate the pile capacity. Curtin et al (2006) define this method as the Soil Test method and Elsamee (2013) delineated it as a theoretical prediction equation method. The static equation method primarily relates soil shear strength to two components: the end-bearing resistance at pile end and the skin friction along the pile side surface. These two components add together to predict the pile ultimate capacity for any variety of pile length and diameter of various pile types. Thus, the total bearing capacity in the static equation method is calculated by the following equation (Fellenius 2006; Tomlinson and Woodward 2007):

$$Q_u = Q_s + Q_b = A_s \times f_s + A_b \times q_b \qquad \text{Equation 2-6}$$

where Q_u = pile ultimate bearing capacity; Q_s = ultimate shaft side resistance, Q_b = ultimate base resistance; A_s = the side surface area of the pile shaft, A_b = the base area

of the pile, f_s = unit side friction, q_b = the unit base bearing capacity of the soil at the base.

The values of f_s and q_b are usually calculated from empirical coefficients, in-situ tests or laboratory tests. Laboratory tests on soils can be unreliable as taking intact undisturbed soil samples is costly and difficult. The properties of soils are better derived from in-situ tests, such as standard penetration test (SPT) and static cone penetration test (CPT or Dutch penetration) (Curtin et al. 2006) because the pile end-bearing resistance can be directly related to the force necessary to push the cone tip into the soil, and the side friction correlates with the cone friction measured. All the prediction results assessed by these measures include both empirical and experience factors with uncertainties and should be calibrated by pile static load tests (Curtin et al. 2006). Depending on the availability of the values of f_s and q_b, several of the static equation methods are reviewed:

(1) Terzaghi method: Practical formulas of predicting the pile bearing resistance for either shallow or deep foundations customarily depend on the use of Terzaghi's equations with a few empirical coefficients.

Unit tip resistance:

$$q_b = c \times N_c + \gamma \times L \times N_q + \tfrac{1}{2} \times \gamma \times Z \times N_\gamma \qquad \text{Equation 2-7}$$

Unit shaft resistance:

$$f_s = a \times c + K_0 \times \bar{\sigma} \times \tan\phi \qquad \text{Equation 2-8}$$

where, N_c, N_q, N_γ = Terzaghi's bearing capacity factors depend on soil friction angle ϕ; c = Cohesion of soil (apparent cohesion intercept); Z = depth of footing (depth of embedment); γ = unit weight of soil; K_0 = passive pressure coefficient; a = constant.

Equation 2-7 uses the Terzaghi original approach with the bearing capacity coefficients $N_c, N_q,$ and N_γ. For a deep foundation, Terzaghi has indicated that the above equation can approximate the bearing capacity by the Equation 2-7 plus the skin friction along the side surface of the foundation/piles and the shearing stress-induced vertically from the mass of soil surrounding the foundation, represented by Equation 2-8 (Meyerhof 1951).

The coefficients were initially proposed for a surface strip foundation assuming a failure occurred associated with overall upwelling of soil from the base of foundation onto the ground surface. Corrections to the calculations using these equations are related to a burial depth of the foundations and the form of the load applied. However, predictions made from these formulas produce substantially larger results compared with static test results (Grevtsev and Fedorovskii 2013). There is presently no such precise design correlation reported specifically for enlarged bearing base piles. It has been reported that the N_γ value varies extremely, such as 60 – 300 in gravel, 30 – 150 in sand; so the N_γ value is very empirical and experience-based (Fellenius 2006), which means that it is impractical for use in RBB design.

(2) Laboratory testing method: The ultimate capacity of the base of a pile can be obtained by the formula (Cooke and Whitaker 1961):

$$Q_b = A_b \times (N_c \times C_b + \gamma \times H) \qquad \text{Equation 2-9}$$

Where $N_c =$ the bearing capacity factor; $A_b =$ the bearing area of the base; $C_b =$ the mean shear strength of the soil at and just below the level of the base; γ = the mean density of the soil, and H = the height of the free surface of the soil to the base bottom (Cooke and Whitaker 1961). Herein, the value of the base bearing capacity factor N_c is found to be very complex to determine, meaning that it is impractical for use in RBB design.

(3) In-situ testing method: Estimation of the bearing capacity of piles is complicated in several aspects, including the technical difficulties in soil sampling and testing, the

substantial variation of soil properties induced by pile driving, and the intrinsic variability of numerous natural formations. As a result, the routine design of pile foundations is essentially empirical by its nature. It necessitates the import of correlations established between data revealed by the in-situ soil tests and the data derived from field static loading tests. Here in-situ soil tests mainly include the standard penetration test (SPT) and Cone Penetration tests (William 1991). The derived soil properties from in-situ tests not only assist to establish correlation equations between the bearing capacity and the soil properties but also can be utilised as inputs into RBB numerical modelling which is to be discussed later.

For many years, the application of SPT and CPT techniques has been increasingly used for designs in geotechnical engineering because CPT and SPT are the closest simulation to the pile driving and load-bearing mechanism (Shooshpasha et al. 2013). This is necessary for large projects to acquire a more accurate value of bearing capacity (Coyle and Sulaiman 1970).

The SPT performance varies with many factors like the experience of operators, drilling machine and procedures, hammer profile and efficiency and compaction of the hammer, resulting in great uncertainty associated with SPT data. Instead, the CPT is a fast and simple method providing continuous and direct readings of soil friction, resistance and several other soil property data. The CPT method has become superior to SPT and other techniques as its readings can be reduced analytically or empirically for pile design (Suman 2015) in two ways: (1) using a direct correlation between the CPT results and the end bearing capacity and side resistance of pile shaft (Suman 2015); (2) building a relationship between the SPT or CPT readings with typical strength parameters of soil, e.g., E, S_u, and φ, which are input into static equations to predict the capacity. This section only discusses the first approach as below.

The approach proposed by Bu (2012) is applied to driven piles allowing calculation of a resistance-settlement curve; the relationship is:

End resistance

$$q_b = \beta \times (\frac{S}{b})^{1/c}$$ Equation 2-10

Skin resistance

$$f_s = \alpha \times q_c$$ Equation 2-11

Where: S = pile settlement [mm]; q_c = cone resistance of the CPT to DIN 4094 [MN/m²]; α, β, b, c = coefficients, of which β is 2.0 for Franki piles, and 1.0 for In-situ concrete driven piles. Obviously, there are too many coefficients associated with this estimation, emphasizing the questionable reliability of these formulas if used for RBB prediction design (Bu 2012).

Based on the research by Meyerhof (1956), the ultimate capacity of expanded base piles with a length up to 10 times the base diameters ($\frac{L}{D_b} < 10$) can be calculated using the empirical correlation (cited by Neely (1990)):

$$q_b = 0.28 \times 95.8 \times N \times \frac{D}{D_b}$$ Equation 2-12

where N = SPT blow count value near the pile base; L = pile length / driven depth; D_b = base diameter. The average of the ratio of calculated capacity to measured capacity reached 0.93, providing a better prediction than most of the other methods (Neely 1990). For long piles, i.e. ($\frac{L}{D_b} \geq 10$), the averages of measured ultimate pile tip resistance are calculated with the following equation, which provided results with considerable scatter (Neely 1990).

$$q_b = 2.8 \times 95.8 \times N$$ Equation 2-13

Gwizdala (1984) analysed the performances of large-diameter drilled piles in sandy soils and recommended formula for predicting pile bearing capacity from CPT data.

Gwizdala (1984) collected 20 datasets from static loading tests on drilled shafts having diameters of 1.00-2.14 m and with a length of 6.0-16.5 m to validate the accuracy of his equations. The datasets consisted of eight data measured from tests of enlarged base piles. The end bearing capacity and coefficient of friction related to soil type and CPT reading of q_c values. The influences of the diameter of the shaft and enlarged base were also integrated into the design formulas (Niazi and Mayne 2013). Because the data samples in this method were very limited, the reliability of these equations if applied in RBB piling is questionable.

Blackwell (2014) provided substantial design equations, tables and charts for Franki pile designs based on empirical data ranges, including complex parameters derived from SPT and CPT in cohesive and non-cohesive soils (cited in Johnson (2014)). These equations are too cumbersome for RBB piling design and will not be discussed further in this thesis.

In the scenarios of the applications of the static equations above, it can be found that more factors and coefficients were used than those applied in current RBB design methods, and most calculations were associated with several empirical factors from tables and charts, other than directly relying on the typical parameters of soil properties.

(4) Chinese standards method: This method is the curently used formula for the RBB piling foundations, and regulated by the Chinese Standards JGJ135-2007 (Chinese Ministry of Construction 2007) and JGJ 94-2008 (Chinese Ministry of Construction 2008). The characteristic value of the bearing capacity, R_a , per pile can be derived from the trial pile static testing, as follows:

$$R_a = Q_u / K \qquad \text{Equation 2-14}$$

where: K = factor of safety (K = 2) and Q_u = ultimate bearing capacity from the static load test *(kN).*

Generally speaking, the load sharing between friction along the pile shaft and end bearing varies according to the pile types. For example, it ranges from 20% to 70% (friction to end bearing) in continuous flight auger piles (Elsamee 2013). However, this ratio is generally less than 10% for RBB piles shorter than 15 m. Shaft friction is implicitly included in the equivalent bearing area of the bearing base, A_e, which is back-calculated from the data collected from historic cases across China (Chinese Ministry of Construction 2007).

Also, most RBB piles are installed with casing from digging the hole to completion. Therefore, the lateral pressure of the soil surrounding the shaft is relatively small. The coefficient of friction is smaller than other types of piles due to the smooth interface between the contiguous soil and formed concrete shaft. This is why the piles with cased shafts are assumed as end-bearing piles in the design (William 1991). Similarly, the RBB piles are considered as end-bearing piles in the Chinese standards. In the initial design of the RBB piles, for simplicity R_a is derived from the following semi-empirical equation without considering the friction addition:

$$R_a = f_a \times A_e \qquad \text{Equation 2-15}$$

where: f_a = characteristic value of bearing capacity of soil in the bearing layer (kPa), referring to the Standard GB 50007, Code for Design of Building Foundations (Chinese Ministry of Construction 2012) and A_e = equivalent bearing area of the bearing base (m^2). The value of f_a can be determined from laboratory or in-situ testing (Chinese Ministry of Construction 2008), assuming conventional piles. However, using a conventional bearing capacity value does not account for the effects of soil densification achieved by the ram compaction. Moreover, A_e is an empirical parameter provided in Table 4.2.3 of the Chinese Standards JGJ135-2007 (refers to Table 2-6) (Chinese Ministry of Construction 2007).

Table 2-6 Effective base bearing area, A_e (m^2) (Chinese Ministry of Construction 2007).

Soil Properties of Strengthened Layer		Three-drive-penetrations, P_t (cm)				
		<10	10	20	30	>30
Clay or clayey soils	$0.75 < I_L \leqslant 1.0$	—	2.0~2.3	1.6~1.9	1.4~1.7	<1.8
	$0.25 < I_L \leqslant 0.75$	—	2.3~2.6	1.9~2.2	1.7~2.0	<2.1
	$0.0 < I_L \leqslant 0.25$	2.7~3.2	2.6~2.9	2.2~2.6	2.0~2.3	<2.2
Silt	e > 0.8	2.4~2.7	2.2~2.5	1.9~2.2	1.6~1.9	<1.7
	0.7 < e ⩽ 0.8	2.7~3.0	2.5~2.8	2.2~2.5	1.9~2.2	<2.0
	e ⩽ 0.7	3.0~3.4	2.8~3.1	2.5~2.8	2.2~2.5	<2.3
Fine sand	Medium dense	2.7~3.1	2.4~2.8	2.1~2.5	1.8~2.2	<1.9
	Slightly dense	3.1~3.5	2.8~3.2	2.5~2.9	2.2~2.6	<2.2
Medium to coarse sand	Medium dense	2.9~3.4	2.7~3.1	2.4~2.8	1.9~2.4	—
	Slightly dense	3.4~3.8	3.1~3.5	2.8~3.2	2.4~2.8	—
Gravels	Medium dense	3.2~3.8	2.9~3.4	2.6~3.0	—	—
	Slightly dense	3.8~4.5	3.4~3.8	3.0~3.4	—	—

Note: I_L is the liquidity index; e is the void ratio of soil.

To start the design, a three-drive-penetration is firstly selected (10 cm, 20 cm or 30 cm) from Table 2-6, based on the designer; the high value of 30 cm may be selected in soft soils (silt), whilst the lower value can be selected in stiff sandy soils selected (i.e., 10 or 20 cm). A corresponding A_e value can then be determined following the properties of the strengthened layer. The characteristic value of the bearing capacity of the soil f_a can be deduced from laboratory or field testing, e.g., Plate Bearing Test, Standard Penetration Test (SPT) and Cone Penetration Test (CPT). Here, the value of f_a does not consider the effect of soil densification by the ram compaction. The empirical data in Table 2-6 were back-calculated from RBB piling case histories across China.

Once the two values f_a and A_e are determined, the characteristic value of the RBB pile bearing capacity R_a is calculated by Equation 2-15, and verification of the strength of the RBB pile shaft is made, as follows (Chinese Ministry of Construction 2007)：

$$N_V \leq \psi_c \times f_c \times A_p \qquad \text{Equation 2-16}$$

where: N_V = design vertical load applied in a standard loading situation (kPa); ψ_c = casting method coefficient (0.8 for the precast pile and 0.75 for in-situ casting pile); f_c = design value of the axial compressive strength of the RBB shaft concrete (kPa) in accordance with GB50010, Code of Concrete Structure Design; and A_p = shaft cross-sectional area (m^2).

From the analysis above, three problems can be identified in connection with determining the three values f_a, A_e and R_a, as follows:

1. The majority of the data used to determine f_a were collected from in-situ plate loading tests performed at shallow depths, and these do not represent the relatively deep soil affected by the RBB method. In other words, the f_a value does not consider the deep densification of the soil.
2. The empirical data for determining A_e values in Table 2-6 were back-calculated from RBB piling cases, only relying on the soil liquidity index (I_L) for clays; void ratio (e) for silts; and compactness (dense, medium dense, and slightly dense) for sand, gravel and fills. A single soil parameter is not expected to be a good representative for providing accurate A_e values. Moreover, the wide range of values in these options of the equivalent bearing areas A_e with varying three-drive-penetrations P_t emphasises the questionable reliability of those formulas (Coyle and Sulaiman 1970).
3. The choice of three-drive-penetrations to determine refusal is arbitrary, as the direct correlation between the bearing capacity and three-drive-penetrations has not been reported. The over-conservative design during the 20 years since the RBB pile application confirms the unreliability of the three-drive-penetration method as a means to determine installation refusal.

Is there a correlation between the last three blows, P_t, and the bearing capacity, Q_u? After analyzing 482 datasets prepared on Franki piles, it was found that the average progress of the last three blows correlates with the bearing capacity of the enlarged

base piles only in the gravel at a coefficient of correlation $r = -0.789$. However, in sand and clay, no obvious correlation was found (Pusztai 2005).

The abovementioned parameters of soil liquidity index, I_L, void ratio, e, and soil compactness are not direct mechanical parameters of soil. The current design method mostly relies on using those data and the abovementioned equations in association with several assumptions and idealisations (Cheng 2006; Chinese Ministry of Construction 2007; Yang and Wang 2011). These increase uncertainties and inconsistency in the design method often lead to over-conservative design, due to both ignoring the densification effect of the compaction and erroneous estimation of the effective bearing area (Jin 2011). This is why the current design standard JGJ135-2007 dictates performing trial piling before the commencement of RBB piling projects to examine the reliability and accuracy of the initial design. This prerequisite is both costly and time-consuming.

From Figure 2-11a, it can be seen that the soil bearing capacity and the pile bottom end bearing area of traditional piles can be readily determined. The soil bearing capacity can be obtained from in-situ tests, such as CPT or SPT. The end bearing area can be calculated directly from the nominal design diameter of the pile. Thus, the end bearing capacity of a traditional pile is easy to obtain.

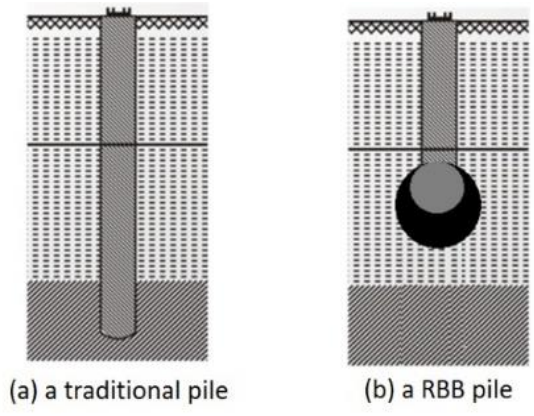

Figure 2-11 Comparison sketches of: (a) conventional pile; and (b) RBB pile.

However, for RBB pile (Figure 2-11b) the soil bearing capacity and pile end bearing area are difficult to determine. The three problems described above are responsible

for the over-conservatism that is currently associated with the design of RBB piles. An alternative design method excluding these problems is thus required for the RBB piles.

Over-conservatism has been overwhelmingly known to the RBB piling industry since the invention of the technique (Wang 2014; Yang 2004; Zhang 2014). Previous research showed that most static load tests stopped loading at 20-30 mm, before reaching 60 mm while the load applied reached the designed ultimate value, indicating that most designs are over-conservative by some 50% to 200% in terms of bearing capacity. This uncertainty in the design outcomes justifies the need for costly pilot piling tests before commencement of the any RBB project. To solve this problem, the values of A_e in the design reference datasets was increased once in 2007 based on the initial A_e data published in 2001, as compared in Table 2-7 (Chinese Ministry of Construction 2007, 2018). However, the predictions proved still too conservative.

Table 2-7 Equivalent bearing area A_e (m^2) (Chinese Ministry of Construction 2007).

Soil Properties of Strengthened Layer		Three Drive/strike Penetration Pt (cm)							
		<10	10		20		30		>30
		2007	2001	2007	2001	2007	2001	2007	2007
Clay or clayey soils	0.75 < IL ≤ 1.0	-	2.3-2.6	2.0-2.3	2.1-2.5	1.6-1.9	1.8-2.3	1.4-1.7	<1.8
	0.25 < IL ≤ 0.75	-	2.2-2.5	2.3-2.6	1.8-2.0	1.9-2.2	1.6-2.2	1.7-2.0	<2.1
	0.0 < IL ≤ 0.25	2.7-3.2	2.2-2.5	2.6-2.9	1.7-2.2	2.2-2.6	1.5-2.0	2.0-2.3	<2.2
Silt	e > 0.8	2.4-2.7	1.8-2.1	2.2-2.5	1.6-2.0	1.9-2.2	1.5-1.9	1.6-1.9	<1.7
	0.7 < e ≤ 0.8	2.7-3.0	1.7-2.0	2.5-2.8	1.6-1.9	2.2-2.5	1.5-1.8	1.9-2.2	<2.0
	e ≤ 0.7	3.0-3.4	1.6-1.9	2.8-3.1	1.5-1.8	2.5-2.8	1.2-1.7	2.2-2.5	<2.3
Fine sand	Medium dense	2.7-3.1	1.6-1.9	2.4-2.8	1.4-1.7	2.1-2.5	1.3-1.6	1.8-2.2	<1.9
	Slightly dense	3.1-3.5	1.8-2.0	2.8-3.2	1.6-1.9	2.5-2.9	1.4-1.7	2.2-2.6	<2.2
Medium to coarse sand	Medium dense	2.9-3.4		2.7-3.1		2.4-2.8		1.9-2.4	-
	Slightly dense	3.4-3.8		3.1-3.5		2.8-3.2		2.4-2.8	-
Gravely soils	Medium dense	3.2-3.8		2.9-3.4		2.6-3.0		-	-
	Slightly dense	3.8-4.5	1.5-1.7	3.4-3.8	1.3-1.6	3.0-3.4	1.2-1.5	-	-
Fills		2.4-2.9		2.1-2.5		1.8-2.2		1.5-1.9	<1.6

Note: IL is the Liquidity Index; e is the Void Ratio of soil.

The conservatism was quantified and used as one of the terms to evaluate the prediction quality in RBB piling practice. When a predicted value, Q_P in the design is lower than the site measured result, Q_M, the difference of ($Q_M - Q_P$) is defined as conservation of the bearing capacity (Wang 2014). Then, the Underestimation ratio (conservative ratio) of a design can be presented as follows:

$$\text{Underestimation ratio} = (Q_M - Q_P)\,/Q_P \times 100\% \qquad \text{Equation 2-17}$$

When the conservation ratio reaches 50%, the prediction is deemed too conservative, causing wastes of piling resources. Also, the designed value Q_P should not exceed the measured value Q_M according to RBB standards, because the difference $(Q_M - Q_P) < 0$ indicates a failed design.

It is necessary to inspect how conservative the current design method and its results are. Table 2-8 shows the degree of conservatism of 224 Q_u values predicted by the RBB standard design method, based on existing publications. Table 2-8 reveals that the design capacity of 93% of the piles was much lower than the tested values by more than 50% and up to 200%. On the other hand, nearly 3% of the piles were found to have negative conservation, indicating faulty piles. In fact, it is that wide range of uncertainty which forces the current design standard to entail full-scale testing prior to the commencement of any RBB piling. Satisfying this requirement is both expensive and time-consuming. Motivated by the lack of confidence in the current design method, some investigators (Cheng 2006; Zhang and Chen 2008) developed alternative design equations to improve the predicted bearing capacity of RBB piles. However, these methods were not reported to produce reliable results.

Table 2-8 Conservatism of RBB piles designed according to the current standard (Wang 2007, 2008; Yang 2004).

Conservation range	No of Piles	Percentage of piles	Remark
-30% to 0 %	6	2.6%	Negative conservation: faulty design
0% to +50%	10	4.4%	Economic design
+50% to +100%	137	61%	Too conservative design
+100% to +200%	71	32%	Extremely conservative design

Also, the degree of conservatism in the table above varies, indicating an unknown amount of uncertainty in estimating the RBB pile capacity using the current method (Elkateb et al. 2003). The results in Table 2-8 designate that higher than expected bearing capacities were achieved across 93% of the piles studied (Engelbrecht and Kgole 2016). According to Corson (1989), a calculation is fairly accurate when

predicting the capacity within 30% of measured values. Then the predictions 93% of piles above were neither accurate nor economic.

In the current design formulas, the soil parameters are implicitly included in the bearing capacity factor, N_q. For example, the soil friction angle, ϕ has a function with N_q and declines over depth. Hence, N_q value also decreases with depth. However, the increase of pile bearing capacity is not at the same rate as the increase of depth (William 1991). The use of N_q and N_c would bring in more assumptions and uncertainties than simply developing an equation that is directly based on the typical soil parameters, and this research prioritises such an option.

Several approaches are merely represented with empirical formulas that correlates identified pile behaviour with some basic soil geotechnical parameters, such as shearing strength, Young's Modulus and relative density, using observed coefficients to work out the end bearing capacities and shaft friction (Tomlinson and Woodward 2007). According to Wrana (2015), the following factors influence the pile bearing capacity: friction angle of soil, dilation angle, Poisson's ratio, shear modulus and effective stress at the pile tip. Therefore, in calculating RBB bearing capacity, if A_e is only determined by referring to I_L value for clayey soil, e value for silts, and soil compactness level for sand and gravel, the results will be most likely inconsistent and inaccurate.

2.1.4.2 Pile Capacity from dynamic equations

The current common term "dynamic formula" may refer to "dynamic analysis", "dynamic test", as well as "wave equation analysis". The current dynamic formula refers to dynamic measurements using a Pile Driving Analyzer® (PDA) and signals interpretation software (Likins, Fellenius, and Holtz 2012). Dynamic formulas have been used as an indication of site refusal over measuring and determining the pile bearing capacity. Dynamic analysis is based on wave transmission mechanics for studying the ram-pile-soil interaction. The uncertainties occurring in the ram compaction, along with modifications of soil properties during both pile driving and

pile loading, generate subsequent uncertainties in the determination of bearing capacity (Coyle and Sulaiman 1970; Shooshpasha et al. 2013). The dynamic formulas assess the total resistance to the entire pile by measuring the energy entailed in driving the pile. Some researchers have disputed that the dynamic analysis is inaccurate, e.g. Cummings (1940); Davisson (1979) (cited by Alkroosh (2011)). Numerical assessment of the dynamic methods conducted by Hannigan et al. (1996) has presented a poor correlation with static load test results. The main limitation of the dynamic methods is that they encompass uncertainties related to varying energy losses in an actual driving procedure during pile installation and measurement. These losses are difficult to quantify accurately (Coduto (1994) cited by Alkroosh (2011)). The second drawback of the dynamic methods is that they can only be measured while the pile is driven or after completion (Shariatmadari et al. 2008).

The wave analysis equation is another method of dynamic analysis to assess pile bearing capacity. Smith (1960) recommended a numerical approach applying the wave analysis theory to explore pile capacity (cited by Suman (2015)). These methods correlated pile capacity estimation with hammer information, compaction energy and pile sets, combined with the historic variants of piling velocity and force during driving measured on the PDA (Long, Hendrix, and Jaromin 2009).

Although many dynamic formulas have been developed, only several are widely used (Fragaszy, 1989). A few of those techniques have been developed for the design of Franki piles. Elkateb, Law, and Tweedie (2003) used the empirical relationship developed by Nordlund (1982) to assess the allowable end bearing capacity of piles, $Q_{b\ all}$ through the equation:

$$Q_{b.all} = W \times H \times N_{0.03} \times V^{2/3} / k \qquad \text{Equation 2-18}$$

Where: $Q_{b.all}$ = allowable pile base bearing capacity at a factor of safety (FOS) 2.5; W = compactor weight (lb); H = drop height of the used hammer (ft.); $N_{0.03}$ = count of blows required to compact 0.03 m^3 of concrete into the surrounding soils; V = base bulk volume (ft^3); and k = soil type factor referred to Table 2-9.

Table 2-9 Recommended values of *K* for varying soil types (Elkateb et al. 2003).

Soil Type	K Value	
	Uncased Shaft	Cased Shaft
Gravel	9	12
Medium to coarse sand	11	14
Fine to medium sand	14	18
Coarse sand	18	23
Medium sand	22	28
Fine sand	27	35
Very fine sand	32	40
Silty medium to coarse sand	14	18
Silty fine to medium sand	17	22
Silty fine sand	24	30
Till with granular matrix	20	27
Till with clayey matrix	30	40

Through back analysis of the pile ultimate end bearing resistances used to determine the actual field values of the soil factor (*K*), the values of *K* were 14, 11, and 23 for tested piles Nos. 1, 2, and 3, respectively, and were not in close agreement with the values presented in Table 2-9. It should be noted that Equation 2-18 is not reliable in predicting the bearing capacity for RBB piles if adopted.

Fragaszy, Argo and Higgins (1989) carried out a comparison of 11 dynamic formula predictions with normal pile load test outcomes, analysed the coefficient of variation for each formula, and announced that the Gates formula is the most accurate.

$$Q_u = 27 \times (1 - \log S) \times \sqrt{e_h \times E_h} \qquad \text{Equation 2-19}$$

Where: e_h = 0.75 for drop hammers (ft-kips); E_h = 0.85 for other hammers (ft-kips); Q_u = pile ultimate capacity (kips); *S* = settlement of pile.

The resistance to pile driving theoretically is equal to the pile capacity, but partial kinematic energy is lost in deformation of soil, vibration and elastic strains of the pile. Furthermore, the soil properties always vary during pile driving even after installation(Coyle and Sulaiman 1970)**;** these changes have to introduce several empirical coefficients and constants for constituting formulas (Coyle and Sulaiman 1970)**.** These two coefficients and one settlement measurement have no direct correlation to any soil property parameters and are only site-specific. Limitations and

constraints above emphasize the questionable reliability of these dynamic formulas (Coyle and Sulaiman 1970).

The literature review from the early 1940s has shown a straightforward agreement about the uncertainty, unscientific basis, unreliability and concerns in the practical use of dynamic formulas. Later researches have further endorsed these, such as Lawton et al., (1986), Olson and Flaate (1967) (cited by Likins et al. (2012)). A grand analysis of all dynamic methods is beyond the scope of this study. The three-drive-penetration method is one of the dynamic formulas and has been analysed in Section 2.1.4.1 illustrating its unsuitability in practice for the RBB piling refusal. Thus, all these dynamic formulas are not considered for improving RBB piling designs.

2.1.4.3 Pile Capacity from static loading tests

Static loading test also refers to "load testing", "loading tests" or simply "tests". It is the most reliable method in determining pile capacity; so the capacity determined was the standard benchmark in assessing the accuracy of any other prediction methods of the pile capacity (Likins et al. 2012). However, these tests are time-consuming and costly, so are seldom used for small projects. These methods are only carried out after pile installation (Coyle and Sulaiman 1970; Shooshpasha et al. 2013). The capacity obtained from an equation is theoretically equal to resistance the pile suffers in penetration or measured blow-count value. Correspondingly, the capacity derived from a static load test can be delineated as the load that pushed the pile downwards with a certain settlement. The concern is how to correlate these two dissimilar distinctive definitions (Likins et al. 2012), that is, how to derive an ultimate bearing capacity value from a load-settlement (Q-S) curve in a static loading test.

Normally, the (Q-S) curves drawn from the pile loading test have three different shapes as shown in Figure 2-12. Many analysis methods have been raised in the literature for the estimation of the failure loads from pile load test data by following three main criteria to solve the three curve shapes of A, B, and C (Zein and Ayoub 2016). The ultimate capacity of the test pile is defined by the peak reading of curve A or the asymptote reading of curve B in this figure, which has rapidly increasing

settlement. If the load-settlement correlation matches curve C, which is mostly the case for enlarged base piles and large diameter piles, then it is challenging to define the ultimate pile capacity (Suman 2015; Zein and Ayoub 2016). As discussed in Section 2.1.2, the (*Q*-*S*) curves derived from static loading tests on RBB piles mostly have a similar appearance to curve C. The bearing capacity determination from curve C is to be discussed in Section 3.1.3 for the RBB piles.

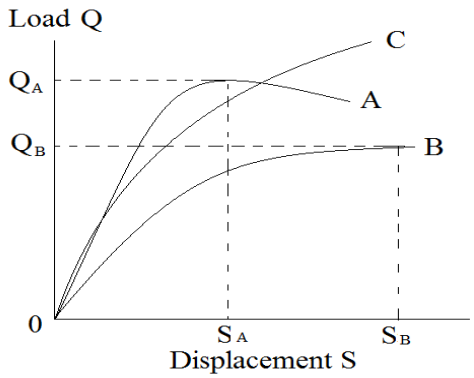

Figure 2-12 Typical load-displacement curves of pile load tests (Zein and Ayoub 2016).

2.1.5 Strengths and weaknesses of RBB piling foundations

Ram-compacted bearing base (RBB) piling technology have a number of characteristics that qualify it as one of the most successful foundation techniques (Shen 2004; Wang 2008; Yang and Wang 2011; Yang et al. 2007). Specifically, RBB piling foundations have the following strengths:

- Wide application: RBB piling is suitable for most engineering and geological conditions, especially for most weak grounds, except in saturated clay, which is not suitable as either being a strengthened or bearing layer.
- Fewer material costs: RBB pile shaft is thinner and shorter than traditional pile shaft, generally saving 50% of concrete and reinforcement (Luo 2010).
- High bearing capacity: RBB piles provide a bearing capacity of 3-5 times that of traditional piles. Mostly RBB piling foundations are suitable for residential and industrial buildings, and the single pile ultimate capacity is generally 10,000 kN.

- Quality control: RBB piling foundations serve as 3D spatial bearing platform under buildings when installed in an appropriate pattern. The fill materials used to construct RBB piles displaces, compacts and consolidates the surrounding weak/liquefiable layer. According to Ishihara (Ishihara 1985), ground damage due to liquefaction will be avoided when RBB piles are used.
- Environmental and ecological benefits: each RBB pile uses around 1.0 m^3 to 1.5 m^3 of demolition or industrial wastes. RBB engineering sites are tidy without mud, dewatering and excavation.
- Economic benefits: material cost per RBB pile is approximately less than 50% the cost of a traditional concrete pile, while still providing the same or much higher bearing capacity. Generally, RBB piling foundations can save 10% to 30% and reduce the project leading time by 30% (Yang 2004).
- Reliability and consistency: no building quality incidents have been ever reported in the past on RBB piles.

Despite its advantages, RBB piling technology has some limitations, as follows (Yang and Wang 2011):

- The piling speed has room for improvement; it generally takes 1.0 to 2.5 hours to complete one RBB pile, depending on the specific site conditions and design requirements.
- RBB piling machine requires further development to become fully automated.
- Ground heaving around piling needs attention in design and during piling work to prevent the impact on nearby installed piles.
- More advanced site technologies such as SPT and CPT need to be applied for testing accurate soil properties and evaluating ground improvement effects.
- On some sites, the vibration and noise produced from RBB piling may be an issue for adjacent buildings and residents in crowded urban areas. Currently the increasing use of silent jacking machines to replace the compaction machines solves these problems.
- Furthermore, RBB piling technology has been mainly developed from practice, using a number of empirical equations for design, and lacks systematic scientific theory (Yu 2008; Zhang 2014).

In summary, RBB technology has many advantages compared to traditional piling. It is suitable for most ground profiles and groundwater conditions. Particularly, RBB piling eliminates the potential of liquefaction risk and provides even and small foundation settlements. The technique supports national policies aiming to minimize demolition wastes. RBB piling technology can save 10% to 30% of costs and provide much higher bearing capacity than traditional piles. The operation of RBB piling is quiet compared with most other piling technologies and is thus suitable for urban areas. Its worldwide promotion would provide significant benefits to the global economy and the environment.

Additionally, RBB concrete shaft diameter ranges from 320 mm to 650 mm, but the typical diameter is 400 mm. For traditional piles, the pile shaft diameter directly controls the magnitude of its surface area and bearing areas, which calculates the pile capacity straightforward. However, the selection of the shaft diameter of RBB piles neither relates to the total bearing capacity nor the rubble base diameter, because most of the pile capacity is derived from the sizeable enlarged base, for which exact estimation of the area, thickness, even the bearing capacity is not straightforward. The next section provides discussion and comparison on enlarged base piles, including RBB piles.

2.2 Enlarged Base Piles

Pile foundations are very efficient in transferring loads from structures to deep stiff soil strata. The enlarged-base piles such as Franki piles and RBB piles remain the most economical and effective types that provide remarkable resistance at a relatively shallower piling depth than other pile types. The principle largely relies on the densification of in-situ soils, which improves the soil properties dynamically during driving the casing and construction of bulged bearing bases (Tchepak 1986). This section introduces a number of piling techniques that produce enlarged bases and compares them with RBB piles. The section then reviews the development and practical application of enlarged base piles. The data reviewed and collected will be theoretically analysed to determine the current technical levels and profile of these technologies, and the problems existing. The aim is to provide some insights into the

contribution of enlarged base piles and better understand the RBB piles. Eventually, this understanding will help develop the new RBB pile design method in the following sections.

Several approaches are used to improve the bearing capacity of piles by magnifying the pile base. Examples include belled piles, Franki piles, pedestal piles, RBB piles, squeezed branch piles, base-grouting piles, under-reamed piles, bottom pressure injected footing (PIF) piles and multiple bases/bells piles. The most common type of enlarged piles is "Franki piles" (Mainroads Western Australia 2011). The common characteristics of the enlarged base piles related to the axial pile bearing capacity are the deliberately enlarged bearing base underlying the upper cylindrical concrete shaft. This is achieved by various piling methods and procedures (Johnson 2014). For an enlarged base formed by compaction, the soil surrounding the pile toe is driven radially outward as the base portion expands (Qi et al. 2015). For a belled pile, the enlarged base is constructed mechanically to increase the toe horizontal sectional bearing area. Regarding Franki piles or RBB piles, the enlarged base is created by adding and driving out small batches of filling materials, i.e. zero slump concrete for the former, rubble for the latter (Chinese Ministry of Construction 2007; Hannigan et al. 2006). Tension piles with an enlarged base and sufficient reinforcement can provide significant uplift resistance (Mainroads Western Australia 2011). The following sections briefly introduce each type of enlarged base piles to highlight their similarities and differences and to help understand RBB piling foundations.

2.2.1 Franki piles

Franki piles have several names, including “enlarged-base driven cast-in-situ pile (DCIS)”, “Franki pile” (Jaksa, Griffith, and Grounds 2002; Neely 1990), “compacted concrete pile”, “pressure injected footing (PIF)” (Rogers 2009) or just “enlarged-base pile” (Chang and Markides 2016; Cooke and Whitaker 1961; Jaksa et al. 2002). Franki piles are cast in-situ concrete piles with enlarged bases obtained by a powerful driving method. Some Franki piles have a rebar cage (Paikowsky 2014; Tomlinson and Woodward 2007) and other have only a concrete shaft (Pusztai 2005). Frank piles were first used in the 1900s as an effective foundation type for cohesionless soil

primarily due to the densification of the soil around the pile base (bulb). Since then, several studies have been carried out to determine the engineering behaviour of these piles. Examples of such studies include De Beer et al. (1977), Nordlund (1982), McAnally and Douglas (1984) and Neely (1990) (cited by Elkateb et al. (2003)).

The well-known Franki piles are still used worldwide, because of their reliability. The enlarged base in dry concrete enables limiting and controlling the length of the piles and achievement of high bearing capacities, even in weak soils (Bottiau 2006). Franki piles are high-capacity piles that can be constructed using different methods, generally with the assistance of a casing at a diameter of approximately 400-700 mm. They can be installed either vertically or inclined at an angle of up to 14^{o} to cope with the horizontal dynamic loads. The characteristic capacity ranges from 1-6 MN, depending on the pile profile and ground conditions (Johnson 2014).

Generally speaking, enlarged base piles have excellent capacity and load-settlement performance compared with conventional piles, and this is attributed to the preloading/compaction of the soils at the enlarged-base (Srbulov 2010; Tchepak 1986). The characteristic axial pile resistance of Franki pile, $R_{c.k}$ is determined using empirical values for the skin friction and base bearing capacity, as follows (Johnson 2014).

$$R_{c.k} = R_{b.k} + R_{s.k} = R_{b.k} + \sum_{i} q_{s.k.i} \times A_{s.i} \qquad \text{Equation 2-20}$$

where: $R_{b.k}$ = characteristic pile base resistance; $R_{s.k}$ = characteristic pile shaft side resistance; $A_{s.i}$ = nominal pile shaft surface area in stratum number i; and $q_{s.k.i}$ = characteristic pile skin friction of soils in stratum i. The required empirical data are referred to in Figure 2-13.

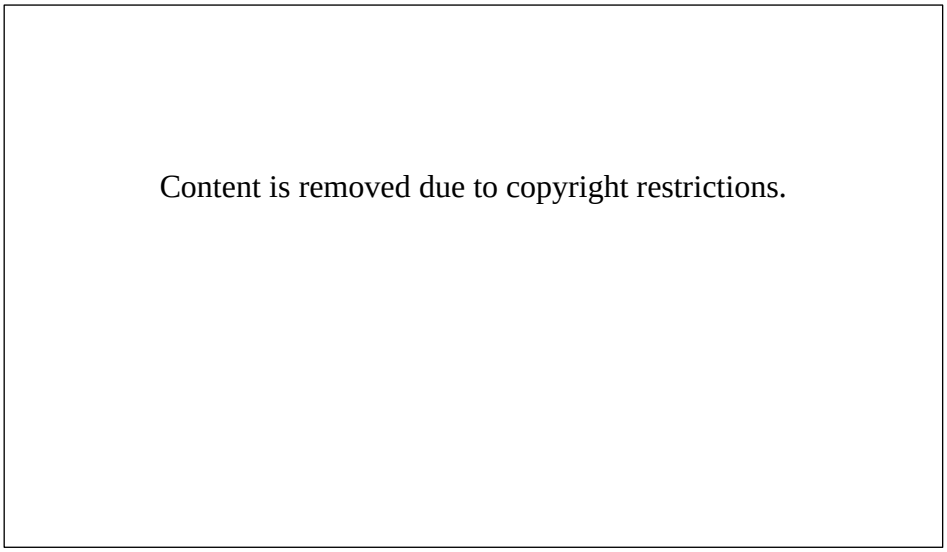

Figure 2-13 Empirical data of lower bound base resistance and required volume of Franki pile base in sandy soils (Johnson 2014).

Franki piles are installed by hammering a plug of low slump concrete mix or gravel at the bottom of a steel casing letting the casing to penetrate the surrounding soils. The internal hammer weighs is 2-8 tonnes (Figure 2-14) (Johnson 2014), when penetrating an aquifer the plug formed can prevent soil and groundwater from entering the casing. When the casing tube reaches the designed depth, the casing is lifted a little and kept in position.

Figure 2-14 Schematic diagram showing details of construction of Franki piles (Johnson 2014).

The internal ram continues to compact the filling materials into the soils to radially form an enlarged bearing base. The reinforcement cage can be installed into position either before or after the formation of the enlarged bases, but before pouring concrete (Fleming et al. 2009). The ram and casing are withdrawn concurrently while the fluid concrete is delivered into the void.

The diameter of a typical Franki pile varies from 300 mm to 700 mm, with a length up to 30 m and an allowable load between 35-200 tonnes (much lower than RBB piles) (GRV 2015). Franki piles with base volumes range from 0.14 m^3 to 0.85 m^3 (also much smaller than RBB piles), as it is difficult to make a larger base with small particles of gravel under small compact energy (Elkateb et al. 2003). According to Borg (2012), the use of Franki piles have dropped in the past decades due to the vibrations produced by the internal ram compaction and its comparatively high cost. Nevertheless, where site circumstances are appropriate, Franki piles are still attractive owing to their high bearing capacity. The construction method includes permanent steel tubes to avoid negative friction if predicted, or using precast pile shafts to form the Franki composite pile when the cast-in-place method is impractical (Borg 2012).

2.2.2 Under-reamed or belled piles

Under-reamed or belled piles have been reported by many researchers (Bu 2012; Curtin et al. 2006; Mainroads Western Australia 2011; Niroumand et al. 2012; Otieno, Hossain, and Shiau 2018; Singh 2016). To enhance the bearing resistance of the pile, the enlarged base can be fabricated using a mechanical reamer, to create an under-reamed pile as illustrated in Figure 2-15. After the tube reaches a defined depth, the drilling pole keeps penetrating the soil and the under-reamer is pushed open outward; the reamer blades stretch out to the designed diameters; the under-reamer is then spun to form the enlarged space while concrete is poured into the space to complete the bell-shape base. The most common belled base has a diameter of three times larger than the diameter of the tube. The extended under-reamer is then withdrawn with the drill rod from the hole. This technique is only generally used at sites with evidently stiff clayey soils, otherwise, the risk of collapse exists due to possibly unstable soil and the space formed by the under-reamer (Borg 2012; GRV 2015). Belled bearing

bases can improve the end-bearing capacity by up to 40% (Tomlinson and Woodward 2007).

Figure 2-15 Under-reamed piles: (a) single under-reamed pile; and (b) multiple under-reamed pile (National Programme on Technology Enhanced Learning India 2020).

The bearing capacity of under-reamed piles in clayey soils is calculated using the following equations (National Programme on Technology Enhanced Learning India 2020; Tomlinson and Woodward 2007):

$$P_u = P_{bu} + P_{su} \qquad \text{Equation 2-21}$$

P_{bu} = tip resistance calculated for a single under-reamed pile in clay as:

$$P_{bu} = n \times [\frac{\pi}{4} \times (D_u{}^2 - D^2) \times C_1 \times N_c] + [\frac{\pi}{4} \times (D^2 \times C_2 \times N_c] \qquad \text{Equation 2-22}$$

Whereas it is calculated for a single under-reamed pile in $c-\phi$ soils as:

$$P_{bu} = n \times [\frac{\pi}{4} \times (D_u{}^2 - D^2) \times (C_1 \times N_c + \sigma_1{}' \times N_q)] + [\frac{\pi}{4} \times D^2 \times (C_2 \times N_c + \sigma_2{}' \times N_q)]$$

Equation 2-23

P_{su} = skin resistance calculated as:

$$P_{su} = (\pi \times \Delta l_1 \times \alpha_1) + (\pi \times (D_u - D) \times l_2 \times C_2 \times \alpha_2) + \pi \times \Delta l_2 \times C_2 \times \alpha_3) \quad \text{Equation 2-24}$$

where: n = amount of bulbs/bases of one pile; σ_1' and σ_2' = effective vertical stress at the bulb base and stem base, respectively; α_1, α_2, α_3 = cohesion factors; N_c N_q = bearing capacity factors; D_u, D = diameter of the bulb and pile shaft, respectively; l_1, l_2 = bucket lengths; and C_1 , C_2 = constants.

The above equations for the Franki piles and belled piles involve a number of soils parameters (α_1, α_2, and α_3) and the bearing capacity factors N_c and N_q. The wide range of parameters in the equations above emphasizes the questionable reliability of the formulas if applied to RBB piles (Coyle and Sulaiman 1970). Thus, the design method of Franki piles and belled piles provides little assistance for the design of RBB piles.

2.2.3 Multiple bases and multiple bells piles

The enlarged base piles can be constructed with multi bases or bells with a single shaft to increase their vertical tensile and compressive capacity. A standard Franki pile has a working load of around 700 kN. A double based pile can be created where an upper base is formed (Mainroads Western Australia 2011). Installation of reamed bell piles requires special belling-out tools. For the RBB piling technology, the base can be created large enough to bear the upper load. No reports on its multiple base uses have been found.

Other enlarged base piles, such as the base-grouting piles (Fleming 1992), pedestal piles (Rao 2011), squeezed branch piles (Guo 2013; Qi et al. 2015) and bottom pressure injected footing piles (Paikowsky 2014) have similar installation methods and bearing mechanisms, and these are not discussed further in this thesis. The major enlarged base technologies are compared below in terms of their common features, differences and outstanding characteristics.

2.2.4 Characteristics of enlarged base piles

Enlarged-base piles have several advantages compared with conventional piles. These include much higher bearing capacity and better settlement performance, as well as lower noise and vibration owing to the bottom driving process of installation (Jaksa et al. 2002; Tchepak 1986). From the discussions in the previous sections, the similarities, pros and cons of enlarged base piles are summarised as follows:

Pros and Cons

- The common characteristic feature of the enlarged base piles is higher axial pile resistance compared to traditional piles in the comparable conditions (Johnson 2014). The load is carried more efficiently.
- An enlarged base enhances the use of the strength of the concrete shaft, and thus reduces material costs for the pile shaft (Johnson 2014). That is why the shafts of the enlarged base piles are always shorter and thinner than traditional piles.
- Compared with straight-sided piles, it is recognised that expanded base piles provide much higher resistance and perform better in both tensile uplift and compressive loading situations, not only in the field and model tests but also in numerical analyses (Qi et al. 2015; Tomlinson and Woodward 2007).
- Enlarged base piles have a small shaft diameter from 300 to 700 mm and a short shaft average length of less than 10 m in the range of 3-15 m (William 1991).
- The shape of the enlarged base is approximated to a sphere or a half ellipsoid with a cylinder above it (Paikowsky 2014).
- Most enlarged base piles have similar installation processes comprising driving the casing into position, creating the expanded base, and eventually constructing the shaft.
- Expanded-base piles provide such high bearing capacity that very limited reports have been found on failure cases in field tests (Neely 1990). In this circumstance, the determination of the ultimate bearing capacity, Q_u, needs a definition of failure. This will be discussed in Section 3.1.3.
- Spacing between adjacent enlarged-base piles must be larger than a certain value to avoid the inter-influence between the neighbouring piles (Tomlinson and

Woodward 2007). Details of the effect of construction tolerances and interaction were discussed previously for the RBB piles.

Limitations

- In the construction of an enlarged based pile, the compaction vibration may cause noise and shaking to affect the environment, especially in buildings and residents adjacent to the sites. To mitigate the reverse environmental impacts created by compaction, several new developments have been reported, such as the Franki VB piles; it integrates the strengths of bored piles and normal enlarged base piling to spin and thrust a steel tube into the ground instead of ramming compaction (GRV 2015). It is similar to RBB pile's application of the drilling method used in the complex strata with boulders where the ram compaction is unable to penetrate through. According to GeoForum (2012), the Franki VB piling is carried out without noise and vibration, and it is, therefore, suitable for use in specific sites, such as the CBD areas (cited by Borg (2012)).
- In RBB piling, due to the high ram weight and long free drop distance, the vibration and noise may be higher than the Franki piling. The silent jacking-in piling method has been considered to replace ram compaction. Some measures to mitigate the vibration and noise may be considered:
    - Allow minimum distances between piling location and buildings/services (Chang and Markides 2016);
    - Use vibration reduction and separation technology (Yang 2011);
    - Lower drop distance; and
    - Use silent driven machine.
- Each enlarged base technology has its limitation in the installation; the reamed bell piles with enlarged bases can be constructed only in soils or weak rocks with a minimum strength to allow the space to be created. RBB piles are difficult to construct in saturated clays. Driven piles are difficult to install in soils with boulders or other large obstacles, and the ground prone to heave (Tomlinson and Woodward 2007).
- Due to the characteristics of enlarged base piles, the construction often utilises high strength concrete to make the best use of materials and pile resistance.

- The base enlargement should not exceed the maximum size (Johnson 2014).

2.2.5 Comparison of RBB piles and Franki piles

Even though the application of Franki piles has diminished because of some environmental and cost concerns, this technology is still widely and competitively utilised at suitable sites (Fellenius 2006; GRV 2015). Franki piles technology was adopted in China in the 1970s but was named as the Gravel Piles. Based on the Gravel Piles, Mr Wang invented the RBB piles in the 1990s. Shen (2004) pointed out that RBB piling technology is the new pile type developed based on the Franki piles, but avoided the Franki piles problems. Therefore, RBB piles have significant similarities and differences with the Franki piles.

Similarities:

- Both have an enlarged bearing base.
- Bearing bases provide most of the total load capacity.
- Bearing layer can have a lower stiffness than in traditional piles.
- Pile shaft is shorter and thinner than in traditional piles.
- Installation procedures are similar.

Differences:

Beijing Puissant published the main differences between Franki piles and RBB piles, as follows (Beijing Puissant Group 2020):

- Different composition of the base materials: Franki piles use the same material – concrete or gravel to form the entire piles, including the pile shaft and pile base. However, RBB piles consist of three materials, i.e., rubble for the base, concrete and reinforcement cage for the shaft and dry concrete connecting the shaft and base. The base dimension of the RBB piles is generally much larger than Franki piles (Beijing Puissant Group 2020).

- Different construction refusals: The refusal of Franki piles uses the volume of the concrete and segment lift of the casing to determine the diameter and height of bases, but RBB piles use the three-drive-penetrations.
- Different bearing capacity calculation equations: Franki piles use Equation 2-20 as used for traditional concrete piles (Beijing Puissant Group 2020); however, the bearing capacity of RBB piles is calculated using Equation 2-15, by regarding the RBB base as an equivalent extended footing ignoring the shaft friction.
- Different influence extent of compaction in forming the bearing bases: Franki piles use less filling materials (concrete) to form the base with generally less than 1 metre in diameter. Yet RBB piles use rubble materials to construct the base with a volume ranging from 0.5 m^3 up to 1.8 m^3; the extent is up to 2-3 m horizontally and 3-5 m vertically, much larger than Franki piles.

Compared with Franki piles, RBB piles, therefore, have the following advantages (Wang 2008):

- RBB piles use demolition waste for constructing the bearing bases. The cost is therefore much lower and the resultant protection of the environment is promising. Franki piles use concrete/engineering gravels resulting in a much higher cost, and Franki piles don't make use of demolition waste.
- Bearing capacity of RBB piles is generally much higher than Franki piles. The larger particle diameters of the demolition waste under high compaction energy make it easier to create a larger diameter of bearing base in the horizontal and vertical directions. A wide horizontal cross-section of the bearing base is the key factor in providing a much higher bearing capacity for the RBB piles.
- RBB piles can provide more stable bearing capacity. Thus, RBB pile foundations can better mitigate large settlement and reduce differential settlement.
- When installed in liquefaction-prone soils, the whole RBB pile bearing base under one foundation works together to mitigate/eliminate the liquefaction

potential in three ways: displace the liquefaction soil away and consolidate/densify soils surrounding the foundation at depth when driving the liquefaction layer away from beneath the building, and separate the possible lower liquefaction layers below this spatial base.

2.3 Summary

Firstly, RBB piling technology is one of the typical enlarged base pile solutions, which has exclusive characteristics. It is unique in using demolition wastes as the major material to construct the bearing bases. Accordingly, the cost of RBB pile foundations is relatively low in comparable conditions. Secondly, the used demolition wastes have large and irregular particle size; this helps RBB piles create a much larger base sphere under high-energy compaction than other enlarged base piling technologies. The design methods of Franki piles and other enlarged base piles are based on empirical equations with various assumptions. A wide range of parameters/factors/coefficients are not suitable for predicting an accurate bearing capacity for RBB piles, and new design equations are sought and developed in the following chapters.

CHAPTER 3 DEVELOPMENT OF NUMERICAL MODELLING

This chapter mainly presents the research methodology and implementation used in this research, by utilising the finite element (FE) numerical modelling for RBB piles. A comprehensive parametric study is then carried out using the established FE models to produce output datasets from a series of hypothetical RBB piling inputs from which design equations for RBB piles are derived in Chapter 4 for use by practitioners.

3.1 Numerical modelling for RBB piles

Numerical modelling is one of three major techniques (i.e. experimental, analytical and numerical) used by researchers to assess the behaviour and stress-strain development of pile foundations. Numerical modelling methods is a technique that integrates arithmetic and software engineering that executes calculations for tackling numerically the issues of science and engineering. Currently, numerical modelling has become one of the most widespread methods in geotechnical studies, including pile foundations, as it provides better predictions than experimental and analytical techniques, with consideration of the interface between the soil and pile body (Gowthaman, Nasvi, and Krishnya 2017). Coyle and Sulaiman (1970) believe that numerical modelling takes the advantages of the use of nonlinear soil properties, hence, providing promising predictions. The literature on numerical modelling of RBB piling foundations revealed that a total of ten HDR theses and four technical papers are published in Mandarin using the finite element method. They all used the "wished-in-place" modelling approach, with predefined base profile and dimensions. None of the studies used rigorous modelling to determine the correlation between the bearing capacity and soil parameters or covered multi-batches insertion and compaction at depth.

In the use of numerical modelling for the design of RBB piles, the following items need to be decided: (1) constitutive model of soil and the corresponding soil properties; (2) parameters known and unknown in simulation of RBB piles; and (3) determination of the ultimate pile load capacity from load-settlement curve obtained from the numerical modelling. These issues are addressed below.

3.1.1 Constitutive model of soil and corresponding soil properties

Zhang (2014) pointed out that researchers have proposed many constitutive models for materials in geotechnical engineering; however, none of them can represent all the behaviours of all the materials. There is a trade-off in determining a certain constitutive model between its accuracy, reliability and applicability. Then the material model should be presenting the primary characteristics of the materials, but also the property parameters should be easy to obtain from the tests, experiments, and observations. A soil constitutive model is Mohr-Coulomb, which is extensively used in FE modelling of geotechnical engineering, due to its sufficient accuracy and simplicity. This constitutive model requires five of the most popular soil properties accepted widely in geotechnical engineering. These include the Young's Modulus (E), friction angle (ϕ), Poisson's ratio (v), dilatancy angle (ψ) and cohesion (c). Although this constitutive model does not include a full range of the non-linear features of soil properties, it has been found to provide the best load-settlement development of a single pile, even with its simple nonlinearity under working load up to approximately 13 MN (Gowthaman et al. 2017). As discussed in Chapter 2, bearing load of RBB piles are normally no more than this threshold. Therefore, the Mohr-Coulomb material model is selected for the RBB pile modelling implemented in this research.

3.1.2 Parameters known and unknown in numerical modelling

As discussed in Chapter 2, the current design approach of RBB piles is primarily based on empirical relationships and experience, with the densified zone soil properties and dimensions being estimated from historic empirical data (Chinese Ministry of Construction 2007). The various parameters and properties required for the design are shown in Figure 3-1. As indicated, the design requires details of the RBB pile (i.e., pile diameter and length), soil properties of the in-situ soil unaffected by compaction, and the volume and properties of the rubble and dry concrete zone, which can all be easily and relatively accurately determined. The applied load and the corresponding settlements are also required for the design and can be determined by conducting a static loading test on an installed RBB pile (Coyle and Sulaiman 1970); these known

details are indicated by the "✓" in Figure 3-1. The base diameter is approximated from the total volume of the base formation materials assuming a spherical base shape and correcting with a compaction factor of 0.8, as per Fellenius (1975) (cited by Kulhawy and Hirany (1988)). However, there remain two unknowns that limit the ability of the current design method to accurately represent the scenario – the extent or dimensions of the densified soil zone and the ultimate soil properties due to the compaction effect; these are indicated by the "?" in Figure 3-1.

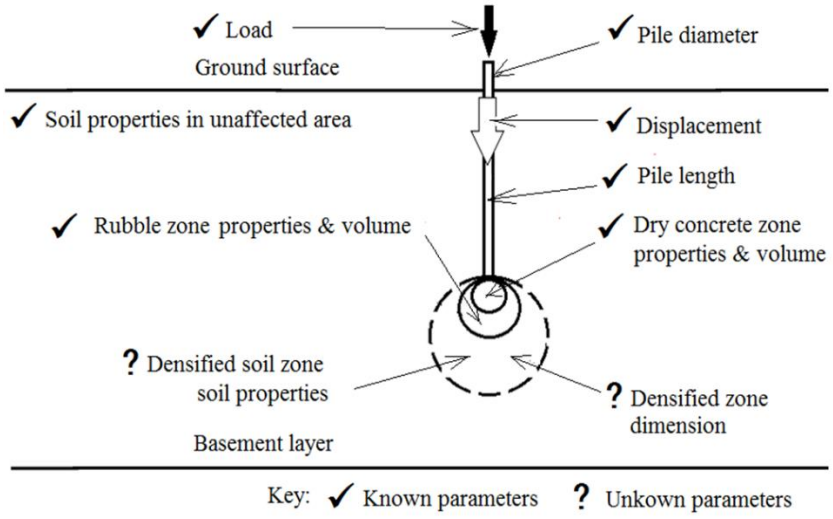

Figure 3-1 Sketch of RBB pile after installation with known and unknown parameters of soil and pile.

Owing to these limitations of the current design approach, this study investigates the ability of FE numerical modelling to accurately simulate the behaviour of RBB piles. In the current FE approach, the RBB structure was modelled using a wished-in-place or predefined pile structure with a spherical rubble base, with the surrounding soil represented by the Mohr-Coulomb elastic-perfectly plastic constitutive model. The unknown dimensions and properties of the densified zone can be dealt with by either: (1) assuming an increase of soil properties (i.e. 20% to 50% increase of density and Young's Modulus depending on the field test data as discussed in Section 2.1.3) of the densified zone, in excess of the in-situ material in the strengthened/bearing layer, before the RBB pile installation such as undertaken in Yu (2007); or (2) ignoring the effect of compaction on the densified soil zone, and instead increasing the rubble zone dimension to account for the strength increase of the soil such as used in some other researchers e.g. (Jin 2011; Luo 2010; Zhang 2012). In this study, the effect of ground

densification on the load test results is included using an increased coefficient in the design equation instead of those two methods above. According to Wang et al. (2006), a coefficient can be used to minimise or eliminate the difference between the predicted and measured Q_u values, a general equation for the pile ultimate bearing capacity, Q_u, measured at settlement, S, equal to the value predicted at S times a constant and can be represented as follows:

$$Q_{M@S} \approx Q_{P@S} \times (1+\theta) \qquad \text{Equation 3-1}$$

Where: $Q_{P@S}$ = predicted pile bearing capacity at settlement S; $Q_{M@S}$ = measured pile bearing capacity at settlement S; S = settlement and θ = soil improvement coefficient. The increased coefficient method initially proposed herein is presented and applied in Chapter 4.

3.1.3 Determination of Q_u for design of RBB piles

This section explores the methods used to determine the pile ultimate bearing capacity, Q_u, obtained from load-settlement (Q-S) curves derived from RBB pile numerical modelling. The chosen approach should be easily applied to processing a large number of dataset outputs used for the development of the AI models of Chapter 4, and to avoid focusing on scrutinizing each (Q-S) curve, such as, the tangent-tangent method which requires drawing tangent lines on each (Q-S) curve; that is impossible to attempt for over 1000 datasets in this research.

In Section 2.1.4.3, the three types of (Q-S) curves have been discussed (see Figure 2-12), and curve C (without sudden plunge fails) is the dominantly encountered type for the enlarged base piles. This section, therefore, focuses on the determination method used for the enlarged base piles, particularly RBB piles. Overall, no single criterion has been reported to delineate a "failure load" or "bearing capacity" of an enlarged base pile (Zein and Ayoub 2016). Many researchers in the past proposed different methods for assessment of pile ultimate capacity (Birid 2017), so the resulting Q_u values interpreted may be different (Elsamee 2013).

Generally, the maximum displacement reached during the test load ranged from about 3 to 5 % of the pile diameter for a traditional pile (Zergoun and Harris 2004). For an enlarged base pile, the percentage may be different. Even curve C (Figure 2-12) exhibits differing shapes and can result in different conclusions. Per curve, there is only a single value of load that can be selected and termed "capacity" from the entire curve. There are nearly 50 different approaches available in the literature for determining the "axial ultimate pile capacity" (Kulhawy and Hirany 1988; Wrana 2015). Although a few formulas were consistently among the best in practice, no one stood out as the formula of choice for every situation, as the local soil conditions and pile type affect the accuracy of each formula greatly (Fragaszy et al. 1989).

In general, the pile is usually tested to a maximum load equal to twice the assumed working stress (design capacity), instead of being tested to failure of the pile. If the pile head displacement was less than a certain displacement, the pile load test is thus considered satisfactory and the foundation installation could proceed. Increased reliability in the estimate of the ultimate pile capacity could be achieved by carrying out the test load to a higher gross pile head displacement. According to the study carried out by Borel et al. (2004), the ultimate pile capacity can be estimated with an accuracy of ±17% for pile head displacements exceeding 5% of the pile diameter (cited by Zergoun and Harris (2004)).

Some researchers proposed the 5% *D* (where *D* is the pile diameter) method to interpret the failure load ultimate capacity of a pile from the load-settlement (*Q*-*S*) curve of field load test without achieving a failure, such as the Alsamman-Reese-O'Neill method (Shahin 2015). This criterion is related to the diameter of the expanded bearing base of Franki type piles. The base diameter is approximated from the total volume of the base formation materials assuming a spherical base shape and correcting with a compaction factor of 0.8, as per Fellenius (1975) (cited by Kulhawy and Hirany (1988)). The base materials consist of zero-slump concrete or gravels.

Both Tomlinson and Woodward (2007) and Wrana (2015) discussed some of the known criteria and analysed common advantages and disadvantages of pile tests. Some of these criteria include the Hansen ultimate load, Davisson offset limit, Chin-

Kondner extrapolation, DeBeer yield limit, Mazurkiewicz graphical method and Decourt method, as shown in Figure 3-2. Tomlinson and Woodward (2007) recommended that the major failure loads interpreted to correspond to displacements the same as 0.1 *d*, and *d* is the equivalent diameter of pile (Tomlinson and Woodward 2007; Wrana 2015). Furthermore, commentary warned that extrapolation methods should be avoided in the determination of the Q_u values (Birid 2017).

Neely (1990) used a total settlement at 5% *D* of the expanded bearing base to extract the load assumed where the failure is to take place, which is approximately equal to 10% of the shaft diameter. In Neely's study, the diameter of the base is also estimated on the total volume of materials (gravel or zero-slump concrete) used in base construction with a compaction factor (again 0.8 for zero-slump concrete), as described earlier (Kulhawy and Hirany 1988; Neely 1990).

Figure 3-2 Comparison of pile capacity determination criteria from axial pile static load tests (Wrana 2015).

Curtin et al. (2006) proposed an approximate criterion for defining the ultimate pile capacity of (*Q*-*S*) type C curve where 10% of the pile diameter is generated under loading. Moreover, Singh (2016) stressed that the ultimate load is determined once the displacement caused more than 10% *D* of settlement, which is also supported by Engelbrecht and Kgole (2016). Details of the methods above are beyond the scope of this thesis and can be found elsewhere. A summary of the pile capacity determination methods is provided in Table 3-1, which is adapted from Elkateb et al. (2003).

Table 3-1 Determination methods of ultimate pile bearing capacity from the load-settlement tests.

Method name	Failure load definition	Comments	References
Hansen (1963) 80% criterion	The load that causes four times settlement of the pile head as measured at 80% of that load.	Not suitable for processing large datasets	(Alkroosh 2011; Tomlinson and Woodward 2007)
Hansen method	The square root of each displacement reading from (Q-S) data divided by resultant load reading.	Not suitable for processing large datasets	(Elsamee 2013)
Chin-Kondner extrapolation	A curve is drawn between settlement divided by corresponding load and the settlement. The ultimate load is read from the inverse slope of the straight-line.	Not suitable for processing large datasets	(Elsamee 2013)
Davission (1972) criterion /offset limit load	The load at the settlement exceeding the elastic strain of the pile by a factor equal to D/120 plus 4 mm (D is the pile diameter).	Not suitable for processing large datasets	(Alkroosh 2011; Birid 2017; Tomlinson and Woodward 2007)
Decourt extrapolation	Similar to that used in the Chin-Kondner and Hansen methods.	Not suitable for processing large datasets	(Alkroosh 2011; Elsamee 2013)
Egyptian code	Load determination uses following Equation $S_2/S_1 \geq 1.5$, S = displacement of pile; S_1 = displacement of pile at Q_{all}; S_2 = pile displacement at $1.25Q_{all}$; Q_{all} = allowable load.	Not suitable for processing large datasets	(Elsamee 2013)
D-over-30 method	The elastic compression line is plotted on (Q-S) curve, a second line parallel to the elastic compression line, with a y-axis (settlement axis) intercept equal to the pile diameter divided by 30, is also drawn on the graph. The interception of this line gives the predicted pile capacity.	Not suitable for processing large datasets	(Fragaszy et al. 1989)
Elastic tangent method	The elastic compression line and tangent to the load-settlement curve are drawn. A second line with a slope of 0.05 inch/ton is drawn tangent to the plunging portion of the load-displacement curve. The point where these two lines meet is the predicted pile capacity.	Not suitable for processing large datasets	(Fragaszy et al. 1989)
Plunging point method	The load at which point displacement continues to increase without any further escalation of the load.	Not suitable for processing large datasets	(Alkroosh 2011; Tomlinson and Woodward 2007)
Double tangent method	Two tangent lines, each parallel to the initial portion and the plunging portion of the (Q-S) curve. The intersection of these two lines is the predicted pile capacity.	Not suitable for processing large datasets	(Elsamee 2013; Fragaszy et al. 1989)

Chinese standards method (2007)	When the load-settlement (*Q*-*S*) curve line increases slowly and smoothly, the ultimate load is read from the point at the settlement of 60 mm, regardless of the variation of the shaft diameter and base diameter.	Suitable for processing large datasets	(Chinese Ministry of Construction 2007)
Alsamman-Reese-O'Neill 5% *D* method	The axial load taken read at a settlement equal to 5%*D* plus elastic deformation of the pile is used for drilled shafts under compression.	Suitable for processing large datasets	(Shahin 2015b)
LCPC 10% method/10% method	The load generating an overall displacement of 10% of the least pile width, or equal to one-tenth of pile diameter.	Suitable for processing large datasets	(Alkroosh 2011; Engelbrecht and Kgole 2016; Tomlinson and Woodward 2007; Wrana 2015); (Curtin et al. 2006)
Pusztai (2004) method	A failure below the bulbs of Franki piles occurs at the settlement of 1.5% to 4% of the Franki pile trunk diameter (smaller settlements than for bored piles at generally 10%*D*).	Suitable for processing large datasets	(Pusztai 2005)

From the discussion and table above, it can be seen that the three approaches: Alsamman-Reese-O'Neill 5% *D* method, LCPC 10% method and the Chinese Standards 60 mm method are potentially suitable for the large dataset used in the interpretation to determine Q_u from (*Q*-*S*) curves of the FE modelling for use in the development of the AI model in Chapter 4. According to data collected from over some ten thousands of RBB pile load tests, Qiu et al (2002) found that all (*Q*-*S*) curves resemble the type C curve (Figure 2-12), with no sudden drop (failure) occurrence since the RBB pile is an end-bearing pile with a solid enlarged base, no shear failure or thrust failure occurs. Considering the typical RBB shaft diameter to be 400 mm or a little larger, and the 60 mm settlement criterion required by the Chinese Standard JGJ135-2007, thus, in this research, the settlements used for determining the Q_u are suggested best falling between 10% to 15% of the shaft diameter, which varies from 40 to 60 mm. The two values of 40 mm and 60 mm are initially selected for the bearing capacity analysis in Chapters 3 and 4.

3.1.4 Mitigating difference of Q_u between FE predicted and field test results

As pointed out in Section 2.1, the current empirical methods for the design of pile foundations have two major problems: (a) design results are inconsistent and

inaccurate with a large variation of Q_u ranging from overestimated to underestimated because the empirical equations are based on non-typical soil properties and back-calculated historic data; and (b) most designs are over-conservative. The new AI equations developed in Chapter 4 can provide a consistent design because they are developed from FE models based on significant and typical soil properties. However, all of Q_u values predicted this way are anticipated to be smaller than the measured Q_u values of the pile loading tests once a pile is installed because Q_u predicted does not contain the compaction effect as the tested Q_u value does. Therefore, the new Q_u predicted will be consistently lower than the Q_u tested; the gap ΔQ_u is caused by the compaction effect as indicated in Figure 3-3 as follows:

$$\Delta Q_u = Q_M - Q_P \qquad \text{Equation 3-2}$$

where: ΔQ_u = difference of pile capacities between the measured value, Q_M, from the load test and predicted value, Q_P, from numerical modelling; this difference is caused by the compaction effect that is included in the load test results, but excluded in the preliminary prediction equations derived from modelling or equations.

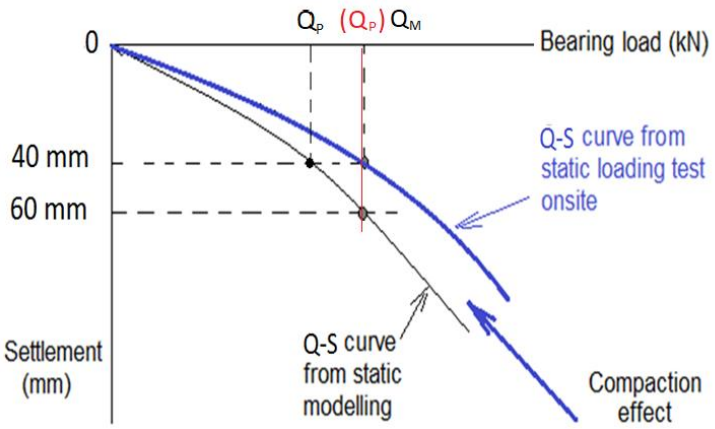

Figure 3-3 Schematic diagram to show how to reduce the gap of Q_u between FE modelling and field loading test, here 40 mm and 60 mm are just samples.

To reduce the gap ΔQ_u obtained from the AI new design equations developed in Chapter 4, an increase of the settlement value of Q_u over the 1008 datasets obtained from the parametric study of FE modelling explained later is used for the AI models to achieve a higher Q_u output, leading to decrease or eliminate the gap. As an example from Figure 3-3, it can be seen that if the settlement of 60 mm is used to determine the Q_u in the FE modelled (*Q*-*S*) curve, once this designed pile is installed, the Q_u reads at 40 mm settlement in the field test curve is expected to be very close to the Q_u designed, i.e. the compaction effect can be compensated by increasing the settlement in extracting the Q_u value from the predicted (*Q*-*S*) curve.

Regarding the Chinese Standards 60 mm method, the settlement (*S*) over the pile shaft diameter (*D*) ratio *S/D* is 15% as the RBB shaft diameter is normally chosen in practice at 400 mm, the ratio will drop to 10% once the shaft diameter increases to 600 mm. As the current design method of the RBB piles has proved too conservative, properly increasing *S/D* ratio (i.e., the *S* value when the *D* value is certain) in determining Q_u from the FE modelling will help extract a larger load value from the *Q*-*S* curve as the design value of Q_u, thus, decrease the conservativeness of Q_u.

According to Bruce (1986) and Cooke & Whitaker (1961), the end bearing component requires a displacement in the range of 10-15% *D* to fully develop its capacity. Now that the constant shaft diameter of 400 mm is usually used in the RBB piles, the matched settlement will be 40 mm to 60 mm; thus, the chosen settlements used to define the Q_u of RBB piles should range from 40 mm to 60 mm.

Cooke and Whitaker (1961) found in tests that the resistance of the pile shaft starts to be activated at a slight shaft displacement (about 0.5% *D*); however, the full development of the ultimate pile bearing capacity necessitates the displacement of at least 10-15% of the diameter of the pile enlarged bearing base, i.e. 20-30% of the diameter of the shaft assuming that the base diameter is roughly equal to twice the shaft diameter. This certifies that the settlement criterion of 60 mm still has a space to increase if necessary, in the Chinese Standards for RBB pile design.

The RBB piles are generally seating in the same geological layer at similar lengths. The shaft diameter is also fixed at 400 mm. The major varying factor of the pile profile is only the base diameter; each RBB pile may have a different base diameter on site. If the settlement criterion used to determine Q_u is based on a percentage of the base diameters, this settlement value varies extensively on one site, which is against the design principle that the allowable settlement of all kinds of piles under any one foundation should be unique in the pile design to achieve a unique settlement of a foundation.

In conclusion, the load-displacement (*Q*-*S*) curves for the enlarged base piles, especially the RBB pile resembles the shape of the C type cure (Figure 2-12) showing a gradually dropping rate without a sudden bend in the curve. The determination of settlement criteria for the Q_u values vary from 10-15% times the pile shaft diameter for the RBB piles. To reduce the value of ΔQ_u obtained from the new design equations derived from FE modelling, an increase of the settlement criterion value in the determination of Q_u over 1008 datasets used to develop the AI equations in Chapter 4 to achieve a higher Q_u output will decrease or eliminate the gap ΔQ_u. This method will be used in the following sections.

3.2 Basic FE-RBB pile numerical model development

This section carries out the basic FE-RBB pile numerical modelling development; it introduces the model configurations, properties of soils, pile and strata, and undertakes comparisons of RBB piles with conventional piles. The basic model is then validated for providing a platform with optimised model establishment and configurations for conducting a parametric study in the following sections.

3.2.1 Model profile and configurations

Based on the previous introduction of RBB pile profiles in Chapter 2, the RBB pile shaft is cylindrical and the base is spherical in shape and loaded in the axial direction only; therefore, the FE mesh of the pile and the surrounding soils can take advantage

of the axisymmetric condition that is one simplified 3D type model (Helwany 2007). Figure 3-4 shows a fully drawn model representing the whole profile of the RBB pile foundation (Wang 2014).

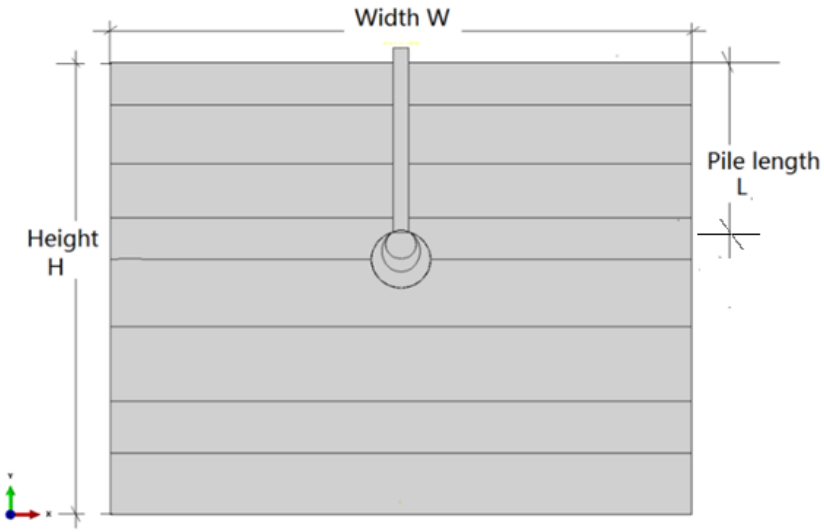

Figure 3-4 RBB pile model with predefined profile (washed-in-place) (the horizontal lines are the model partition lines used for improving the modelling performance).

There are a few commercial software packages that can be used in numerical modelling the RBB pile, such as ABAQUS, ANSYS, PlAXIS and FLAC. The most popular package is ABAQUS, and according to the literature reviewed in Chapters 2 and 3, based on the availability and the required advanced capacity for RBB pile modelling, ABAQUS (Dassault Systèmes Simulia 2014) software was used for this research.

The general model dimensions were chosen to minimise the boundary effects on the RBB pile performance (Helwany 2007; Ma 2013; Qiu 2014; Zhang 2014). To fulfil this, the full model width was set to at least 10 times greater than the bearing base diameter or 25 times of the shaft diameter, and the full model height was set to at least twice the length of the RBB pile. Contact pairs and interface elements were applied between the RBB pile shaft surface and the surrounding soils and between the RBB bearing base and underneath soils to simulate the pile skin frictional interactions (Han 2013; Helwany 2007).

There were two main soil constitutive models reported in RBB foundation modelling, including Mohr-Coulomb elastic-perfectly plastic model (here simply called the Mohr-Coulomb model in this study) and Drucker-Prager model. According to the availability of soil properties, Mohr-Coulomb model was chosen as the main soil constitutive model to simulate the soil behaviour, while the various elements of the RBB pile were modelled using the linear elastic Hooke's law model (Dassault Systèmes Simulia 2014).

Most literature reviewed on RBB pile modelling used the soil strata properties without groundwater condition. For simplicity, this preliminary RBB modelling ignores the presence of groundwater, and thus zero pore pressure was set throughout the model. In a subsequent phase of the current work, the presence of groundwater and its impact on the modelling results will be investigated. The boundary conditions of the model were such that the lower boundary was restrained in both the horizontal and vertical directions and axisymmetric around the left vertical boundary, while the right model boundary was restrained in the horizontal direction only. It should be noted that the FE mesh of soil–pile system must include interface elements that are capable of simulating the frictional interaction between the pile surface and the soil, and between the base and soils. The pile shaft and its base are presumed to be embedded in perfect contact with the soil before applying pile loads.

In the early stage of modelling, the mesh size varied throughout the model; a fine mesh was used in the region of high-stress gradients of the surrounding area of the pile shaft and the bearing bases, and a coarse mesh was used elsewhere. The fine mesh element size varies from 0.01m to 0.05 m; the coarse element size varies from 0.5 m to 1 m. Later work found that the unified mesh size can save a lot of meshing time and also provide accurate outputs. The initial model and mesh configurations are listed in Table 3-2.

Table 3-2 Model and mesh configurations.

Model Size	Strata Width	20-30 times of pile shaft diameter
	Strata Depth (height)	2 times of pile length
Mesh Configuration for Pile Shaft	Element Shape	Quad for Axisymmetric Model
	Element Size	Seeds: 0.2m
	Element Library	Standard-Quadric
	Element Family	Axisymmetric stress
Mesh Configuration for Soil Layers Dry Concrete and Rubble	Element Shape	Quad for Axisymmetric Model
	Element Size	Seeds bias control: Maximum:1 m, Minimium: 0.01m to 0.05m
	Element LIbrary	Standard-Quadric
	Element Family	Pore Fluid/Stress

After several trial-and-error runs, the step type was chosen: *Soils* step is found to be capable of solving the RBB modelling problem and make the simulation running efficiently and easily. This finding was also validated by all of the general geotechnical modelling samples from Helwany (2007). A summary of the FE modelling step configurations is provided in Table 3-3. The initial geostatic condition was applied by the *Predefined Field* method in the *Initial Step*. The gravity load was applied in Step 1 to establish equilibrium under gravity, and the step type *Soils* was used throughout the modelling.

Table 3-3 Step configuration of FE modelling.

Step	Step type	Step application	Step time
Initial step	Initial	Predefined field parameters, Geostress	Default
Step 1	Soils	Strata equilibrium of gravity	0.01s
Step 2	Soils	Loading (applying load)	1s
Step 3	Soils	Unloading	1s

The initial geostatic stress is used in most geotechnical modelling problems and is one of the important factors in controlling the RBB numerical modelling (Li 2007; Yang 2004; Yu 2007). However, due to the complexity of the RBB pile foundation in terms of its varying materials, profiles and the existence of the contact pairs, the GRAVITY Step application of the Geostress often causes simulation abortion. To solve this problem, applying Geostress in Predefined Field option is a pertinent approach (Table

3-3). The element type for the *Soils* step and the element family of *Pore Fluid*/*Stress* were CAX8P (Helwany 2007). This model configuration was found to reliably achieve convergence. The *Soils* step combined with the Element Family of *Pore Fluid*/*Stress* and other configurations aforementioned have successfully simulated RBB historic cases promptly and relatively accurately.

3.2.2 Model validation

Below are two typical examples to show the efficient use of the developed RBB numerical model with the optimised configurations aforementioned. The case studies will reveal that the FE model configurations are suitable for modelling the RBB pile loading tests. The FE numerical modelling with the optimal configurations in Tables 3-2 and 3-3 will thus be used for comparisons of the bearing resistance of RBB piles and conventional piles in Section 3.2.3, and will also be used for the parametric study carried out in Section 3.3.

3.2.2.1 Historic Case by Han (2013)

To validate the FE model, the case study presented by Han (2013) was firstly used with geometry as shown in Figure 3-5.The FE model configurations were established, as described previously in Tables 3-2 and 3-3. The first layer from the surface is a 6 m thick fill, and the second layer is silty clay with a thickness of 9 m, underlain by a 12 m sandy clay soil as the strengthened and bearing layers. The basement layer is a well-weathered rock stratum with a thickness of 6 m (Han 2013). The properties of the four layers are detailed in Table 3-4; both the bearing and strengthened layers were located in the sandy clay horizon.

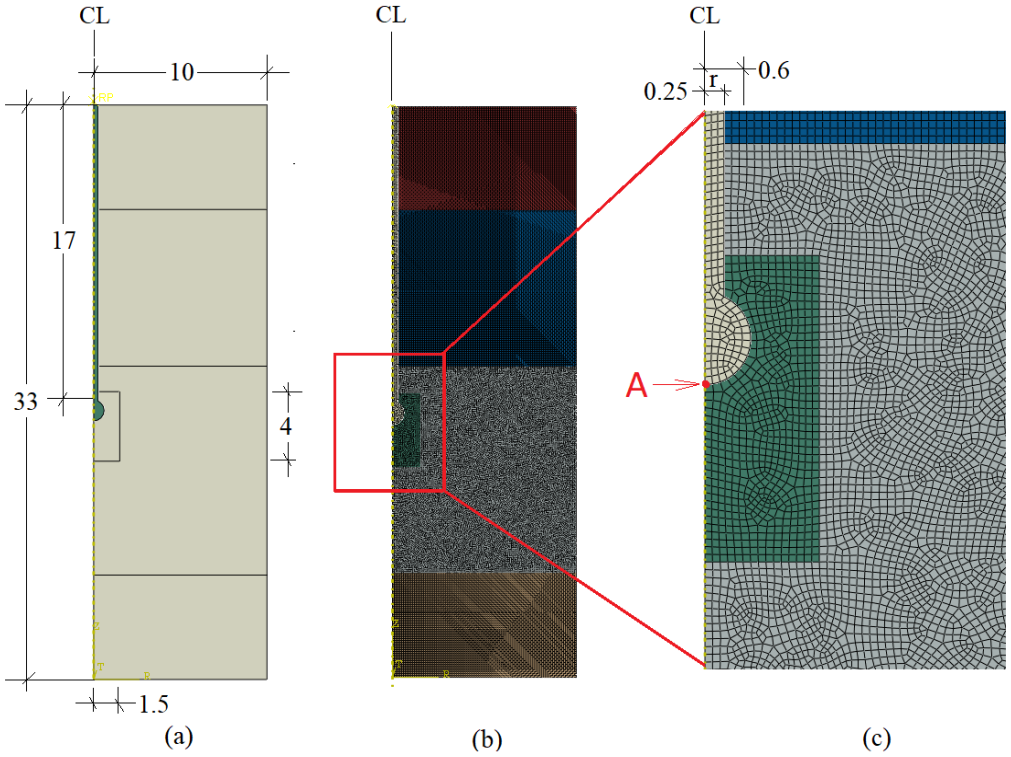

Figure 3-5 RBB pile axisymmetric FE model: (a) model geometry (dimensions in m) and soil strata from top – fill, silty clay, sandy clay, and weathered rock; (b) FE mesh discretization; and (c) enlargement of model near the RBB bearing (r = 0.25 m).

Table 3-4 Soil properties for case history by Han (2013).

Soil properties	Fill	Silty clay	Sandy clay	Weathered rock	Densified zone
Density (kg/m^3)	1700	1800	1900	2400	2280
Young's Modulus (MPa)	30.6	4.8	26.6	2600	39.9
Friction angle (°)	6.4	16.5	17.2	28.8	25.5
Dilation angle (°)	3.0	8.0	8.5	0.0	10.2
Cohesion (kPa)	25.3	19.6	24.3	82	29.2
Poisson's ratio	0.3	0.3	0.3	0.2	0.3

According to Han (2013), there was a densified zone around the bearing base, the zone dimensions were estimated to be 2-3 m in the horizontal diameter and 3-5 m in the vertical thickness. The improved soil properties in the densified zone were not provided; however, are estimated herein based on the literature reviewed in Sections 2.1.3, the density and dilation angle are increased by 20%; Young's modulus, friction angle and cohesion are increased by 50%, as listed in Table 3-4.

The mesh elements were chosen as the 8-node axisymmetric quadrilateral with bilinear pore pressure property (CAX8P). However, all the four soil layers had a pore water pressure of zero kPa, as mentioned earlier. The bottom edge of the model is clamped in both the horizontal and vertical directions. The left vertical boundary was a symmetry line, which was constrained in the *x*-axis direction. The right side of the model boundary in *y*-axis was restrained by rollers. To save the computer modelling resource, only the soil mesh adjacent to the pile shaft and pile base is finer, as this is the region of stress concentration.

The concrete pile shaft and dry concrete zone have a density of 2440 kg/m^3, Young's Modulus of 23.6 GPa and Poisson's ratio of 0.23. A single zone was used to represent the rubble base, which was modelled with the Mohr-Coulomb elastic-perfectly plastic model. The contact between the RBB shaft, the RBB bearing base and the soil is modelled by the use of a penalty-type interaction. The average coefficient of friction between the pile shaft and soil interface was given at 0.2, which was calculated by using the formula: $\mu = \tan(0.75\phi)$, here μ= coefficient of friction, ϕ = angle of internal friction. This type of contact pair can represent the frictional interface between the RBB pile and its surrounding soil (Han 2013).

A mesh refinement analysis was initially undertaken to ensure that the results achieved convergence with appropriate accuracy. The base radius was 0.6 m, requiring the element seed size to be no larger than 0.1 m. Five different mesh sizes (ranging from 0.005-0.15 m) were considered to assess the influence of the mesh size on the RBB pile displacement, vertical stress at the bottom of the RBB base (point "A" in Figure 3-5) and modelling computational time. The results, summarised in Table 3-5, showed a reduction in both the pile displacement and vertical stress with reducing the seed size, yet an increase in the model computational time. The convergences of these results, normalised by the predicted coarse mesh values, are shown in Figure 3-6. Herein, the last three datasets are suitably consistent for both the displacement and vertical stress; thus a seed size of 0.03 m was chosen.

Table 3-5 Results of mesh refinement study.

Seed size	Displacement of pile top	Vertical stress at base bottom	Modelling time
m	mm	MPa	sec.
0.15	19.41	0.544	56
0.1	19.41	0.466	107
0.03	19.23	0.431	1111
0.01	19.2	0.415	10799
0.005	19.19	0.411	47022

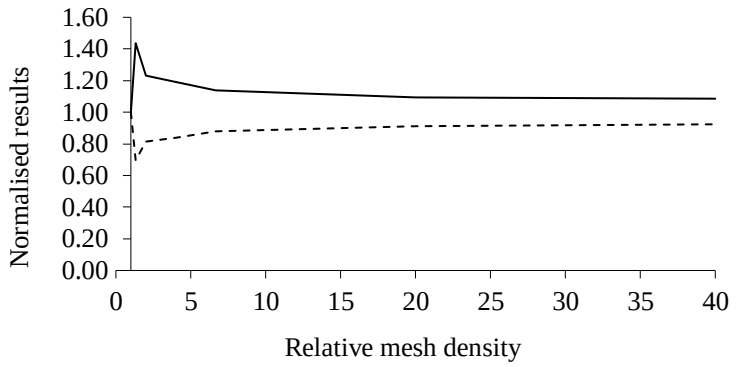

Figure 3-6 Convergence of results of mesh refinement study.

The simulation of the RBB pile model with new configurations was completed in about 18.5 minutes and has output accurate results compared to the site testing data. Table 3-6 shows that the results from the new RBB model are in good agreement with the site test data, although at the lower force loading stage the prediction errors were still large, i.e., 51% at 1000 kN. The load-settlement simulation results of the developed FE model are shown in Figure 3-7, demonstrating an improved accuracy in matching site testing data.

Table 3-6 Comparison of FE modelling results with site test data from Han (2013).

Maximum static load, kN	0	1000	2000	3000
Settlement of pile from site test, mm	0	4.63	20.38	46.55
FE modelled, mm	0	7.0	18.60	49.30
FE modelled accuracy %	0	51%	-8.7%	5.9%

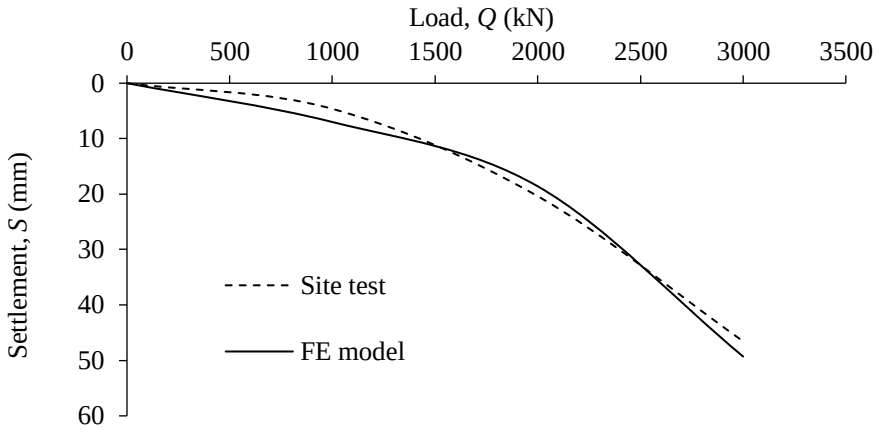

Figure 3-7 Pile load and settlement plot of FE model result and site testing data.

3.2.2.2 Historic Case by Guo (2015)

A historic case by Guo (2015) also presented here to validate the developed model using the geometry, as shown in Figure 3-8. Similar to the first historic case, the mesh elements were chosen as the 8-node axisymmetric quadrilateral with bilinear pore pressure property. However, all the three soil layers had a pore water pressure of zero kPa. The coefficient of friction between the shaft and soil interface, the bearing base and soil contact was directly given at 0.30. The model bottom edge was clamped in both the horizontal and vertical directions. The left boundary was a vertical symmetry line, which used a roller support boundary condition. The right boundary of the model was restrained with rollers. It was found that using the same seeding size can save a lot of time in mesh configuring and modelling simulation, thus save overall modelling time.

The silt layer of 1 m thickness overlays 1.5 m of clayey sand stratum. The basement layer underlying the clayey sand consists of 15.5 m round gravel. Guo (2015) defined a 4 m times 1.8 m densified zone; however, he did not provide the soil properties of this zone. According to the literature in Chapter 2 and the soil type of round gravel in the strengthened/bearing layer, an increase of 10% for soil properties was used to calculate the compacted soil parameters of this zone. All of the soil properties used

are listed in Table 3-7 for the three strata, and both the bearing and strengthened layers were located in a round gravel layer.

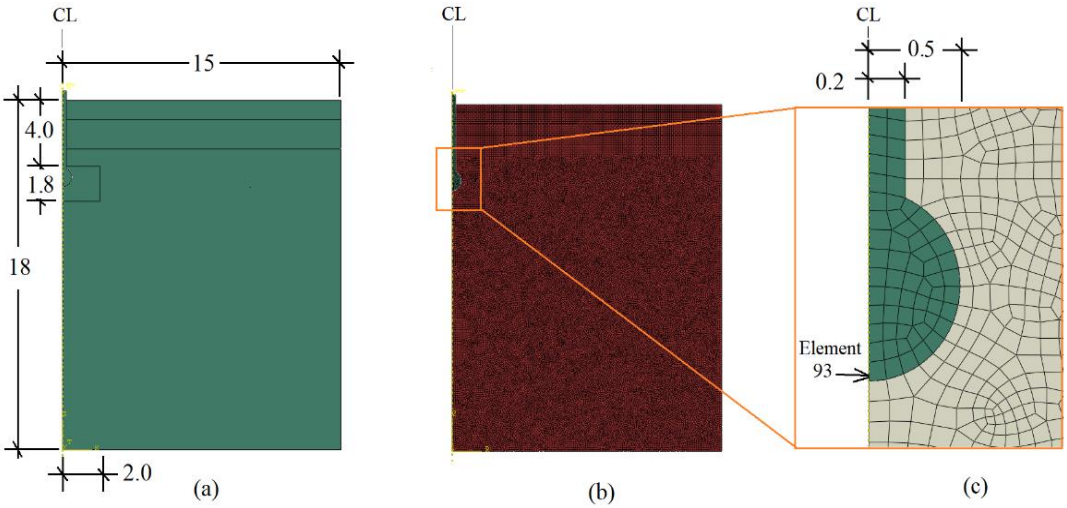

Figure 3-8 RBB pile testing axisymmetric FE model: (a) model geometry (in metre); (b) mesh discretization; (c) enlargement of mesh near the RBB bearing base.

Table 3-7 Strata soil properties (Guo 2015).

Layer	Density ρ	Young's Modulus, E	Friction angle, ϕ	Dilation angle, ψ	Cohesion c	Poisson's ratio, v
	(kg/m^3)	(MPa)	(°)	(°)	(kPa)	
Silt	1940	7.9	22.3	11	62.0	0.3
Clayey sand	2000	23.0	27	13	28.0	0.25
Round gravel	2500	75.0	34	17	5.0	0.2
Densified zone	2750	82.5	37.4	18.7	5.5	0.22

During the simulation, the mesh refinement analysis was undertaken to ensure that the results are satisfactory. The influence of the mesh density on three specific results from this model is considered:

- Displacement of the top of the RBB pile.
- Mises stress of Element 93 at the bottom of the base (Figure 3-8c).
- Model runtime.

The results for each of the eight mesh densities are compared in Table 3-8, along with each model run time. The mesh refinement analysis was carried out with varying size from 30 mm up to 250 mm. Table 3-8 shows that the numerical results are relatively consistent for both the displacement and the stress readings. The displacement curve is relatively flat and consistent. The coarse mesh gave a slightly larger displacement value of 34.0-34.2 mm, the finer mesh presented a slightly smaller displacement of 33.6 mm. The stress curve fluctuated relatively dramatically comparing with the displacement curve; it reached the peak on the right end.

Table 3-8 Results of mesh refinement study.

Seed size	Displacement (at 2,200 kN)	Mises stress	Model run time
(mm)	(mm)	(MPa)	(s)
250	34.08	2291	300
200	34.20	1935	480
150	34.14	1850	1020
120	34.19	1834	1700
100	33.97	1849	5100
80	33.75	1885	7200
50	32.56	1854	10800
30	32.56	1798	15800

The results, summarised in Tables 3-8 and 3-9, also showed a reduction in both the pile displacement and vertical stress with reducing seed size, yet an increase in the model computational time. The convergences of these results, normalised by the predicted coarse mesh values, are shown in Figure 3-9. Herein, the middle four datasets are suitably consistent for both the displacement and stress; thus a seed size of 100 mm was chosen.

Table 3-9 Analysis of the results of mesh refinement study.

Mesh size (mm)	30	50	80	100	120	150	200	250
Mesh size ratio	1.0	1.7	2.7	3.3	4.0	5.0	6.7	8.3
Mises stress (MPa)	1798	1854	1885	1849	1834	1850	1935	2291
Mises stress ratio	1	1.03	1.05	1.03	1.02	1.03	1.08	1.27
Displacement at 2200 KN	32.56	32.56	33.75	33.97	34.19	34.14	34.20	34.08
Displacement change (%)		0.00%	3.64%	4.34%	4.99%	4.85%	5.04%	4.68%
Displacement ratio	1.00	1.00	1.04	1.04	1.05	1.05	1.05	1.05

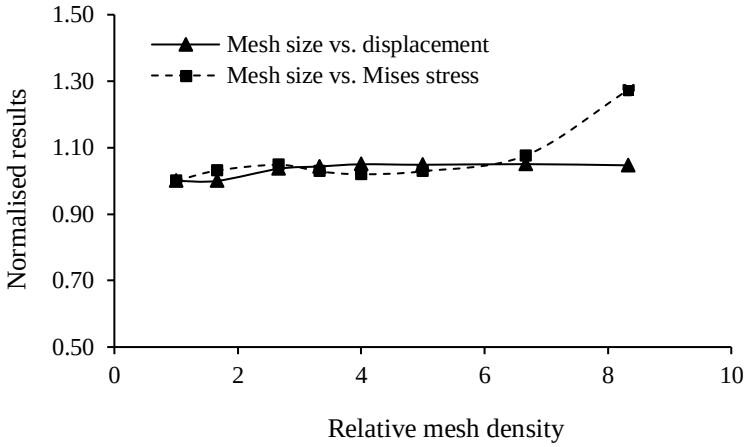

Figure 3-9 Convergence of results of mesh refinement study.

Simulation of the model established with new configurations was completed in about 85 minutes and provided accurate results compared to the site testing data. Table 3-10 shows that the modelling results with new configurations were close to the site pile test data, though at the low load stage (600 kN) the prediction errors were still large with an error of 33%. Within the load range from 1000 kN to 2200 kN, the modelling result errors were all less than 30 %, agreeing reasonably well with the data obtained from the site test. Figure 3-10 is the plot of the comparison of the results showing the FE modelling results were close to the curve line of the site test data (Guo 2015).

Table 3-10 Modelled results and comparison with site test data in Jin (2011).

RBB pile top settlement reading & accuracy	Static load test, applied load (kN)					
	0	600	1000	1400	1800	2200
Site test (mm)	0	6	10.2	15.5	21.5	28
FE modelled (mm)	0	4	10	17.6	25.5	34.1
FE modelled error (%)		33%	2%	-14%	-19%	-22%

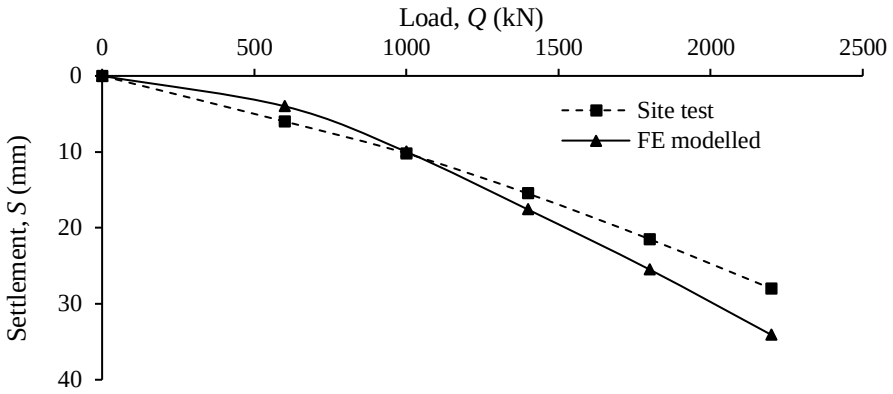

Figure 3-10 Plot of the result comparison showing results from FE model and site tests.

3.2.3 Comparisons of *bearing resistance* for RBB and conventional piles

To assess the bearing resistance of RBB piles compared with conventional piles, the developed FE-RBB model was used in comparable situations (i.e., geometry and material type) with a conventional pile.

3.2.3.1 Comparable model situations

The RBB piles and conventional piles were modelled in the comparable (or similar) situations. Here the conventional piles mean a normal concrete pile installed by the boring or driving method. Except that the RBB pile model has a bearing base under the pile shaft, other model configurations, strata structures and soil properties are the same in each scenario, as shown in Figure 3-11, where full-width (W = 10 m), height (H = 33 m) and pile shaft length (L = 17 m). The top three layers from the surface include a 6 m thick fill, a clay layer with a thickness of 9 m, underlain by a 12 m silty clay soil as the strengthened layer and the bearing layer. The basement layer (4^{th} layer)

is a well-weathered gravel stratum with a thickness of 6 m (Han 2013). The RBB bearing base has a diameter (D = 0.8 m). The two pile types are each installed in the same soil layers, where the strengthened layer and bearing layer are in the same geological stratum.

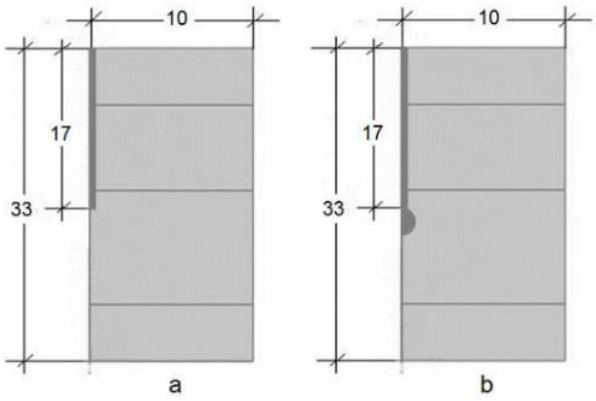

Figure 3-11 Cases used for comparison (dimensions in metre): (a) traditional pile; and (b) RBB pile.

The bearing base provides over 90% of the bearing capacity of the whole RBB pile, and also its magnitude is mostly controlled by the soil properties of the bearing layer (Qiu et al. 2002; Yang and Wang 2011). Therefore, this comparison is conducted by only changing the bearing layer material (the third layer). The soil properties of the third stratum are listed in Table 3-11, showing an increase in the soil Young's Modulus from sandy clay, fine sand, gravel, weathered rock to bedrock (Han 2013; Jin 2011). The properties of the other three layers are detailed in Table 3-4 in Section 3.2.2.1.

Table 3-11 Soil properties of the third stratum (i.e. the basement layer).

Soil properties	Sandy clay	Fine sand	Gravel	Weathered rock	Bedrock
Density (kg/m^3)	1900	2000	2100	2400	2450
Young's Modulus (MPa)	26.6	30	55	2600	5500
Friction angle (°)	17.2	24	38	28.8	–
Dilation angle (°)	8.5	12	26	0	–
Cohesion (kPa)	24.3	20	1	35	–
Interface friction	0.2	0.2	0.2	0.2	–
Poisson's ratio	0.3	0.3	0.17	0.2	–

3.2.3.2 Modelling results and bearing capacity analysis

The bearing load (applied load) of a single pile and the corresponding pile displacement comprise a pile load-displacement (*Q*-*S*) plot. The bearing load for the conventional and RBB piles are referred to as Q_c and Q_r, respectively. For each settlement reading, the ratio *R* was determined and averaged over the entire load increase times interval; the *R* values are calculated by the following equation:

$$R = Q_r / Q_c \qquad \text{Equation 3-3}$$

Comparative modelling work has been undertaken with four different bearing layers: sandy clay, clayey sand, gravel, and weathered rock. Load-settlement (Q–S) plots with piles installed in five different strata are provided in Figure 3-12. Then the bearing capacity ratio *R* in Table 3-12 was computed from the modelled results. It can be seen from Table 3-12 and Figure 3-12 that, in all cases, the RBB pile has an increased bearing resistance compared to the conventional pile.

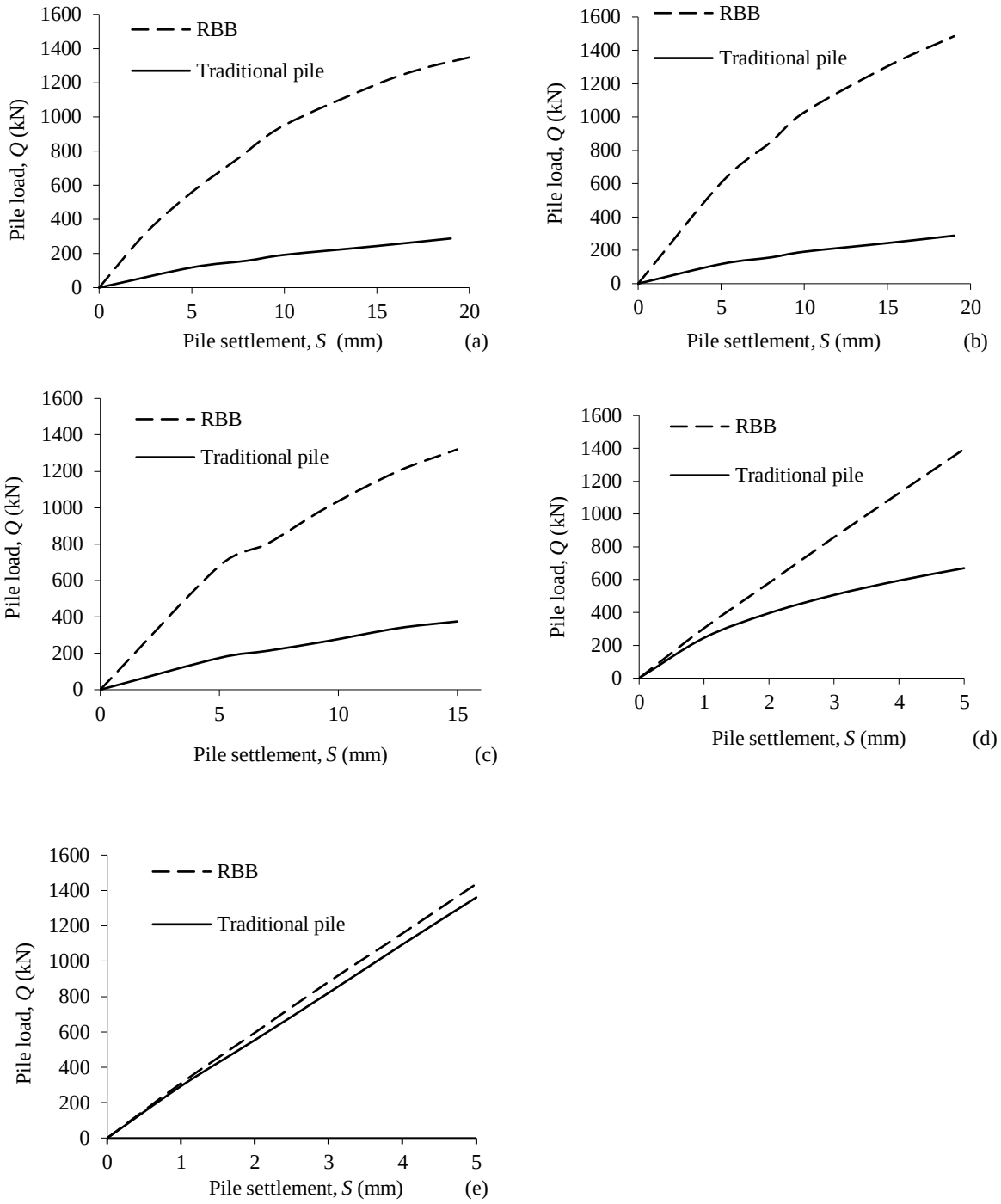

Figure 3-12 Load-settlement (Q–S) plots with piles installed in five different strata of: (a) sandy clay, (b) fine sand, (c) gravel, (d) weathered rock and (e) bedrock (the test load Q was applied and the settlement S is read from the top of the pile).

Table 3-12 Values of the bearing load ratio R in a different bearing layer.

Bearing layer soil	Bearing load ratio, $R = Q_r / Q_c$	Average ratio
Sandy clay	5.8 to 7.4	6.9
Clayey sand	5.1 to 5.4	5.3
Gravel	3.5 to 3.9	3.7
Weathered rock	1.6 to 3.3	2.5
Bedrock	1.105 to 1.108	1.1

Figure 3-12a indicates an improved RBB pile bearing resistance of *R* of almost 7 times more than traditional pile resistance in sandy clay soil. As discussed by Yu (2007) and Jin (2004), this can be attributed to the bearing base expanding faster horizontally than vertically in clay soil, while the bearing area of the base can be up to 10 times larger than the end of the RBB pile shaft (or indeed a conventional pile) (Jin 2004; Yu 2007).

The results presented herein show that in fine sand, the average bearing load ratio was 5.3 (Figure 3-12b) and 3.7 in gravel (Figure 3-12c). In weathered rock (Figure 3-12d), the RBB piles only provide 2.5 times with the bearing load over a traditional pile. Interestingly, when both the RBB and conventional piles directly seat in the bedrock, the average bearing capacity ratio varied at 1.0~1.1 (Figure 3-12e), showing a very limited increase of the bearing capacity of the RBB pile compared with the traditional pile. This finding agrees well with the introduced variable range of the bearing capacity in the literature. It was understood that when the bearing layer in Figure 3-11 has the same properties as the compacted rubble, the RBB pile shaft interacts with the bearing soil in the same way as a traditional pile does.

The above ranges of bearing resistance ratios and increasing trends agree reasonably well with those previously published in the literature (Jin 2011; Yang 2011; Yang and Wang 2011). Therefore, the RBB piles have much greater strength in soft soil than the conventional piles, in terms of the provision of bearing capacity. This advantage is limited in stiff bearing soil. The above results matches well with the finding by Tomlinson and Woodward (2007) that provision of an enlarged base adds considerably to the end-bearing resistance of piles in loose to medium dense sands and gravels.

It can also be observed from Figures 3-12a to 3-12e that regardless of the strengthened layer material, the RBB pile capacity (upper lines, dotted line) increases at a much faster rate than that of traditional piles (lower, flatter solid line). The concrete shafts of both the RBB and traditional piles have the same dimensions and shape, installed in the same soil, so would provide the same pile skin friction resistance. At the beginning stage of loading, the skin friction resistance is gradually enabled, until fully mobilised, where the ratios of *R* were small. Once the shaft begins to settle, the shaft resistance reaches its maximum and both the bearing ends of the traditional and RBB piles would take the increasing load. It is at this point that the RBB pile will present its advantage due to the much larger base and bearing area.

On Figure 3-12, the first three diagrams (a-c) show a step of varied scale in the mid-section of the Q-S curves. The steps are more pronounced in the diagram (c). No such steps are given in diagram (d-e). It may imply something new of the RBB piling mechanism in weak and medium stiff soils, which has not been scrutinised yet. This phenomenon is recommended for the subsequent phase of future work.

3.3 Parametric study using FE-RBB pile modelling

3.3.1 Configurations of FE-RBB model used in the parametric analysis

Section 3.2 presented the basic 3D axisymmetric FE model with the preliminary model structure and configurations. The FE model used for the parametric study herein is more sophisticated than that the basic model in terms of the wider variation of soil properties, more complex RBB base structure and strata profiles. Figure 3-13 illustrates the FE loading model utilised in the parametric study. The model consists of three strata and one RBB pile. The three strata include the first layer on top as the weak soil layer (in dark blue), the second layer in the middle as the strengthened and bearing layer (in dark red), and the third layer at the bottom as the basement layer (in dark grey), which are noted in Figure 3-13a.

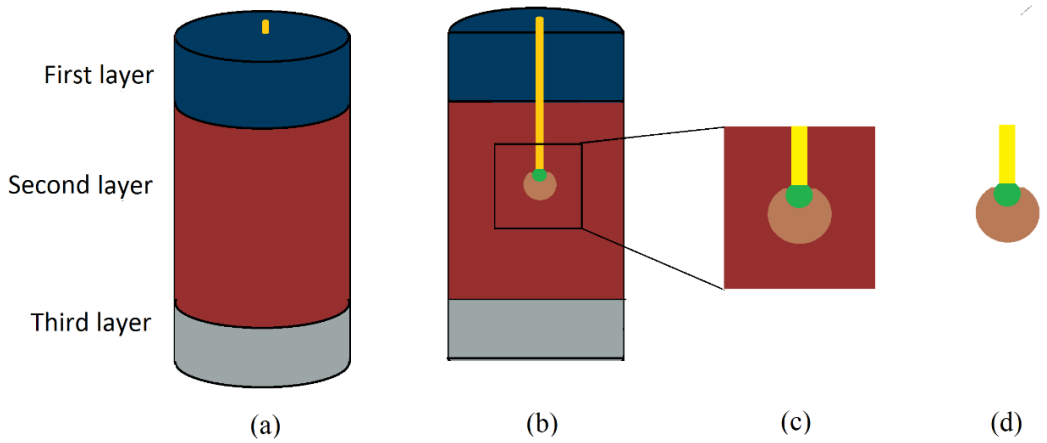

Figure 3-13 A typical sketch of the 3D FE axisymmetric model of a single RBB pile used in the parametric study: (a) complete model; (b) semi-model (vertical cross-section); (c) enlargement of RBB bearing base area; and (d) RBB pile.

The RBB pile consists of (from top) the concrete shaft (in dark yellow) and the bearing base at the bottom (Figure 3-13b). Here the bearing base is composed of two zones: the upper dry concrete zone (in green) and the lower compacted rubble zone (in orange) (Figures 3-13c and d). Using the same principles as discussed in Section 3.2.1, the model dimensions consist of a normal full width of 40 m, a normal full thickness (height) of 30 m throughout the parametric study, except where noted specifically. Details of the model configurations are listed in Table 3-13. The profile details such as soil parameters, layer thickness and other parameters used in the parametric study were listed in Table 3-14.

Table 3-13 Model and mesh configurations.

Model Dimensions	Strata Width Strata Depth (height)	40 m 30 m
Mesh Configuration for Pile Shaft	Element Shape Element Size Element Library Element Family	Quad for Axisymmetric Model Seeds: 0.2 m Standard-Quadric Axisymmetric stress
Mesh Configuration for Dry Concrete and Rubble	Element Shape Element Size Element Library Element Family	Quad for Axisymmetric Model Uniform size is chosen from 0.06m to 0.1m Standard-Quadric Axisymmetric stress
Mesh Configuration for Soil Layers	Element Shape Element Size Element LIbrary Element Family	Quad for Axisymmetric Model Uniform size is chosen from 0.06m to 0.1m Standard-Quadric Pore Fluid/Stress

Table 3-14 RBB piling parametric analysis and selection of model configurations.

Strata		Value Type	Soil Properties						Coef. of Friction		Pile			Material Model	Data Sources
Name	Thick-ness		Density ρ	Young's Modulus E	Cohesion c	Internal Friction ϕ	Dilation Angle ψ[a]	Poisson's Ratio v	Shaft to Soil μ	Base to Soil μ	Shaft Length L	Shaft dia. D	Base dia. d		
	(m)		(kg/m^3)	(MPa)	(kPa)	(°)	(°)				(m)	(m)	(m)		
Weak layer	4	Typical values	1882	18	15	24	1	0.28						Mohr Coulomb	(Zhang 2014)
Bearing/strengthen layer (Clayey sand)	21		2000	40	30	30	10	0.3						Mohr Coulomb	GD[c]
Base layer (Gravel)	5		2100	120	0	38	5	0.3	0.35	0.35				Mohr Coulomb	GD[c]
Shaft concrete			2500	42000				0.25				0.4		Elastic	(Yang 2004)
Dry concrete			2500	40500				0.23						Elastic	(Yang 2004)
Compacted rubble			2000	1260	0	35	3.5	0.29						Mohr Coulomb	(Yang 2004)
Modelling inputs of varying significant parameters of soils in bearing layer		Lower Upper		5 90	0 75	20 50					5[b] 15[b]		0.6[b] 1.5[b]		GD[c] GD[c]
		Value range		5, 15, 30, 45 60, 75, 90	0, 25, 50 75	20, 30, 40 50					5, 10, 15		0.6, 1, 1.5		
Variable Amount				7	4	4					3		3		
Combination	7x4x4x3x3= 1008 (datasets)														

[a] Data ranges refer to SCHANZ & VERMEER (1996) and Vermeer & de Borst (1984) (Schanz and Vermeer 1996; Vermeer and de Borst 1984).

[b] Data refer to Ministry of Chinese Construction (2007) about the RBB Standards, page 6 (diameter), p32 (length), p34 (length) (Chinese Ministry of Construction 2007).

[c] GD refers to the web page: http://www.geotechdata.info/parameter/angle-of-friction, 2020.

Comparison of the mesh refining work has shown that using the same size of model meshes can ensure a significant reduction of model runtime while yielding accurate outputs. The mesh size was chosen from 0.05 m to 0.1 m. The previous methods using the fine mesh in the region of the surrounding area of the pile shaft and the bearing bases, and a coarse mesh used elsewhere were time-consuming during both optimising mesh structure and model simulation. The Soils Step combined with the Element Family of Pore Fluid/Stress and other configurations aforementioned have successfully ensured the completion of the parametric analysis modelling

3.3.2 Significance of parameters

The previous discussions showed that most of the Q_u prediction methods use several coefficients and factors with a few assumptions and restrictions; thus, most of these equations do not produce consistent and accurate Q_u predictions. Hence, the design process of a pile foundation, especially RBB piles, is not yet entirely comprehensible and there is a lack of an equation that can be universally applied to all soil conditions with surety (Suman 2015). The second outstanding feature of those equations is that none of them correlates the bearing capacity Q_u with the typical soil properties. This may be the root cause of inaccurate and unreliable design results even for those equations equipped with substantial coefficients and factors.

Section 2.1 has initially discussed the importance of typical design parameters. Section 3.1 listed some typical soil properties as inputs in general FE numerical modelling. This section determines the specific parameters of soil properties and pile profiles for the preliminary parametric analysis validated in Section 3.2.2. The parameters determined are to be used as inputs into the RBB-FE modelling for the parametric study in the following sections.

As required by the FE modelling package of ABAQUS code (Dassault Systèmes Simulia 2012), the significant parameters can be chosen based on the following categories:

- Physical and mechanical properties of soils in the strengthened/bearing layer: soil density, cohesion, friction angle at pile tip, dilation angle of soil, Young's Modulus, Poisson's ratio, at-rest coefficient of lateral earth pressure, coefficient of international friction.
- RBB pile profile feature: pile shaft length, shaft diameter and rubble base diameter.

The ranges of parameters used in the parametric analysis below were selected according to the reviewed literature. Significance analyses of the parameters of soils, pile features and strata profiles are carried out as follows.

3.3.2.1 Impact of pile length on pile bearing capacity

The impact of RBB pile shaft length L on pile bearing capacity Q_u is deliberated first. Figure 3-14 illustrates the relationships between Q_u with three varying L values of 5 m, 10 m and 15 m. It can be seen that, when the pile length increases by 100% from 5m to 10m, the bearing load only improved by about 24% from 2,550 to 3,200 kN (extracted at 40 mm settlement). However, the concrete used for the shaft increased by 100% from 0.63m^3 to 1.26 m^3; consequently, the installation cost will increase by at least 100% considering the construction difficulty escalation. Contrary to a normal frictional pile, once the length increases by 100%, the bearing capacity will increase approximately by 100% in a comparable situation. Therefore, the RBB piles have an outstanding strength when used in a short length, generally less than 10 m, to achieve savings of material cost and to avoid installation difficulties associated with the depth increase. The equal gaps between the three curves indicate the impact of pile length on Q_u is constant.

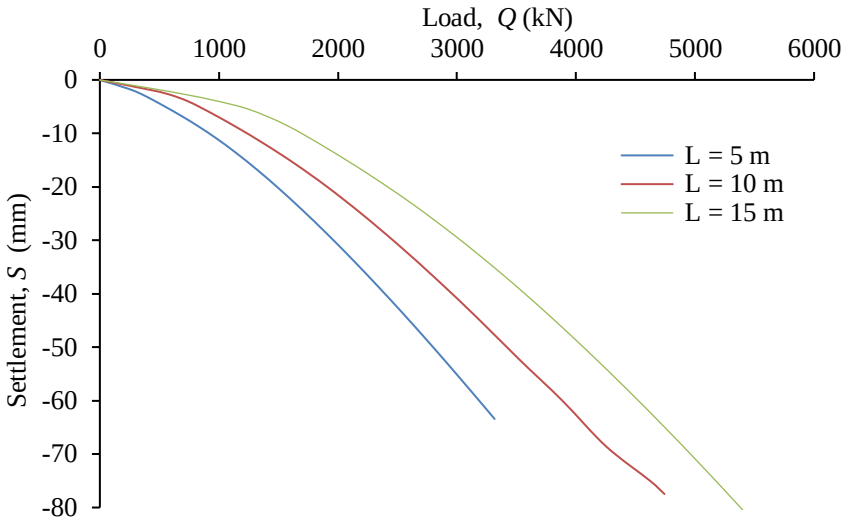

Figure 3-14 RBB pile (*Q*-*S*) curves at three pile lengths *L* = 5, 10 and 15m, with shaft *d* = 400 mm, *D* = 1 m, friction angle ϕ = 30 degrees and soil Young's Modulus *E* = 45 MPa.

3.3.2.2 Impact of pile shaft diameter on pile bearing capacity

The impact of RBB pile shaft diameter *d* on pile bearing capacity Q_u is considered with four typical values varying from 300, 400, 500 and 600 mm. Figure 3-15 illustrates the relationship between the varying *d* with Q_u and shows that when the pile shaft diameter rises by 25% from 400 mm to 500 mm the bearing load only increased about by 10% from 3,000 to 3,300 kN (extracted at 40 mm settlement). However, the concrete volume used for the shaft grows by 54% from 1.3 m^3 to 2 m^3. Apparently, enlarging the shaft diameter to obtain higher bearing capacity is an uneconomic and inefficient approach. That is why most RBB piles use the common shaft diameter of 400 mm once the shaft stiffness meets the strength criteria. The equal gaps between the curves indicate that the impact of shaft diameter on Q_u is constant.

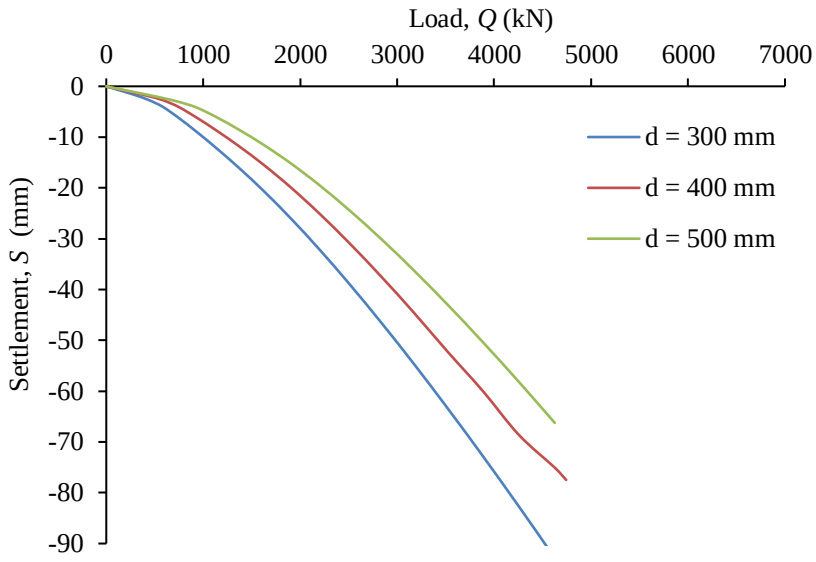

Figure 3-15 RBB pile (Q-S) curves at four shaft diameters d of 300, 400, 500 and 600 mm, with shaft L = 10 m, D = 1 m, friction angle ϕ = 30 degrees, cohesion c = 50 kPa and soil Young's Modulus E = 45 MPa.

3.3.2.3 Impact of pile base diameter on pile bearing capacity

The impact of RBB base diameter D on pile bearing capacity Q_u is investigated with three typical values varying from 0.6 m, 1.0 m and 1.5 m. Figure 3-16 illustrates the relationship between the varying D with Q_u. The significant data included in Figure 3-16 were extracted and analysed in Table 3-15. It can be observed that when the pile base diameter rises from 0.6 m to 1.5 m the bearing area increases by 5.25 times from 0.28 m^2 to 1.77 m^2, and the bearing load has approximately doubled from 2,552 kN to 5,100 kN (extracted at 60 mm settlement). However, the rubble used for constructing the base increases by 14.6 times from 0.11 m^3 to 1.77 m^3. Even though the rubble cost is very low and can be neglected, the 14.6 times rubble compaction generates much more labour and equipment costs. Obviously, relying solely on enlarging the base size to increase the bearing capacity per single RBB pile is not an economical and efficient option. Meanwhile, too large base requires large pile spacing, causing a significant increase in the costs for the larger cap and beam structure above. This conclusion agrees well with the finding by Zhang (2014) in Section 2.1.3.5, thus, the Standards require that the optimal base volume ranges from 0.5 m^3 to 1.5 m^3 (Chinese Ministry of Construction 2007). Also, interestingly, the

three (*Q*-*S*) curves show varying slopes with different rates indicating varying settlement manners. The *D* = 0.6 m curve decreased much more quickly than the other two curves, indicating a fast strain-stress development. The *D* = 1.5 m curve developed in an inclined straight line approximately. The *D* = 1.0 m curve fell between the other two curves. Moreover, the curve gaps varied over depth, designating the impact of base diameter on Q_u is changing over pile displacement.

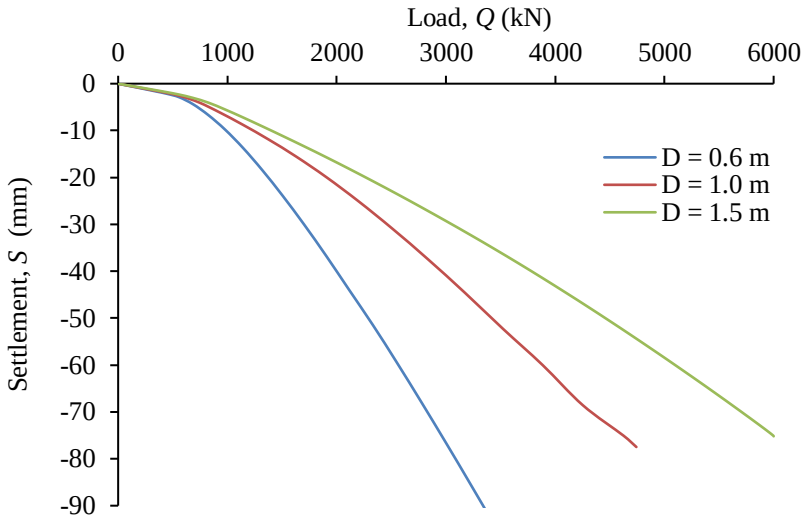

Figure 3-16 RBB pile (*Q*-*S*) curves at base diameters *D* of 0.6, 1.0, and 1.5 m, with shaft *d* = 400 mm, length *L* = 10 m, friction angle ϕ = 30 degrees, cohesion *c* = 50 kPa and soil Young's Modulus *E* = 45 MPa.

Table 3-15 Relationship between base dimensions and bearing capacity.

Base diameter (m)	0.6	1	1.5
Base bearing area (m^2)	0.28	0.79	1.77
Bearing area increase by (%) (per increase)	–	1.78	1.25
Bearing area increase by (%) (*D*1.5/*D*0.6)	–	–	5.25
Base volume (m^3)	0.11	0.52	1.77
Base volume increases by (%) (per increase)	–	1.78	1.25
Base volume increases by (%) (*D*1.5/*D*0.6)	–	–	14.63
Capacity at 60 mm (kN)	2552	3886	5100
Capacity increases by (%) (per increase)	–	0.52	0.31
Capacity increases by (%) (*D*1.5/*D*0.6)	–	–	1.00

3.3.2.4 Impact of soil cohesion on pile bearing capacity

The impact of soil cohesion *c* on pile bearing capacity Q_u is explored with four typical values varying from 0.0, 25, 50 and 75 kPa. Figure 3-17 illustrates the relationship of the *c* values with Q_u. In Figure 3-17, when the soil cohesion increases by 100% from 25 to 50 kPa, the bearing load has increased slightly, less than 3% (extracted at 60 mm settlement). Even when the cohesion has escalated to three times from 25 kPa to 75 kPa, the capacity only gained less than 10% (extracted at 60 mm settlement). Thus, soil cohesion is in fact not a significant parameter to influence the bearing load.

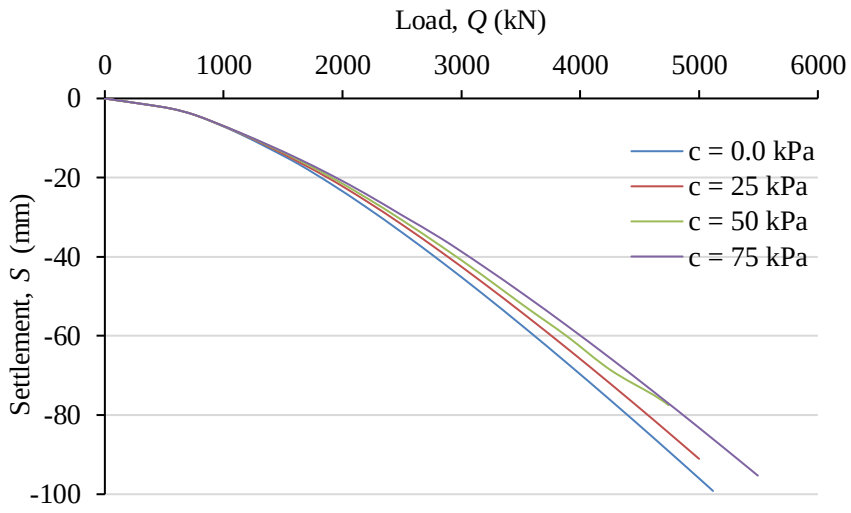

Figure 3-17 RBB pile (*Q*-*S*) curves at 4 soil cohesions of 0, 25, 50 and 75 kPa, with shaft *d* = 400 mm, length *L* = 10 m, friction angle ϕ = 30 degrees, base *D* = 1 m and soil Young's Modulus *E* = 45 MPa.

3.3.2.5 Impact of soil friction angle on pile bearing capacity

The impact of soil friction angle ϕ on pile bearing capacity Q_u is deliberated with four typical values varying from 10, 20, 30, 40 and 50 degrees. Figure 3-18 illustrates the relationship of ϕ with Q_u. In Figure 3-18, when the soil friction angle increases by 50% from 20 to 30 degrees the bearing capacity only increases by 11% from 2,700 kN to 3,000 kN (extracted at 40 mm settlement). Following the friction angle increase, the curve intervals decrease dramatically; demonstrating that the impact of friction

angle on Q_u descends over its increase; especially the two curves of 40 degrees and 50 degrees are very close.

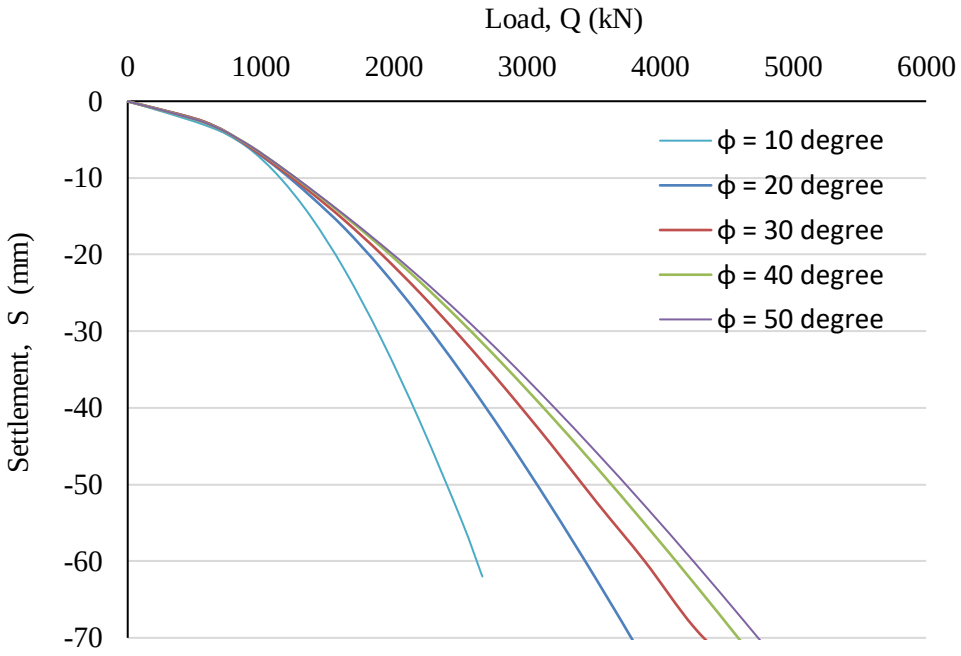

Figure 3-18 RBB pile (*Q*-*S*) curves at four friction angles ϕ of 20, 30, 40, 50 degrees, with shaft d = 400 mm, length L = 10 m, soil cohesion c = 50 kPa, base D = 1 m, and soil Young's Modulus E = 45 MPa.

3.3.2.6 Impact of soil Young's Modulus on pile bearing capacity

The impact of soil Young's Modulus E on pile bearing capacity Q_u is analysed with seven typical values varying from 5.0 MPa to 90 MPa. Figure 3-19 illustrates the relationship of the E values with Q_u. In Figure 3-19, when the soil Young's Modulus E increases by 100% from 15 to 30 MPa, the pile bearing capacity increases by 40% from 1,800 to 2,550 kN (extracted at 40 mm settlement). Following the Young's Modulus increase, the curve intervals decrease remarkably, representing that the impact of Young's Modulus descends over its increase. This analysis agrees well with the finding in Section 3.2.3.2 that RBB piles have much greater strength in soft soil, in terms of provision of the bearing capacity and the provision of an enlarged base

adds considerably to the end-bearing resistance of these piles in loose to medium-dense soils.

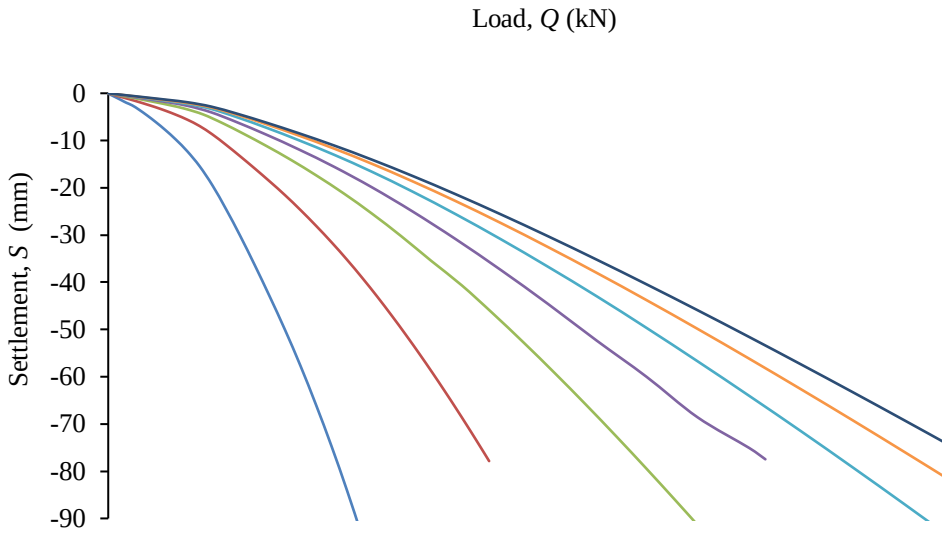

Figure 3-19 RBB pile *Q-S* chart at 7 soil Young's Modulus of 5, 15, 30, 45, 60, 75, and 90 MPa, cohesion c = 50 kPa with shaft d = 400 mm, length L = 10 m, friction angle ϕ = 30^{O}, base D = 1 m.

3.3.2.7 Impact of coefficient of earth pressure at rest K_0 on pile bearing capacity

The coefficient of earth pressure at rest K_0 is one of the parameters used in ABAQUS FE modelling. In this research, the values of K_0 were calculated by the Jaky (1944) simplified solution: $K_0 = (1-\sin\phi)$, where ϕ is the internal friction angle of the soil (Helwany 2007). Figure 3-20 shows the interaction of the pile bearing capacity with the coefficient of earth pressure at rest with a slowly rising near straight line. Overall, the pile bearing capacity has an approximately positive proportional correlation with the soil lateral coefficient K_0. However, when K_0 has risen by 367% from 0.3 to 1.4, the capacity has only grown from 2,891 to 3,611 kN (outputs at 60 mm settlement) , increased by 29%. An average 10% increase of K_0 only results in a 0.8% growth of the bearing capacity. Consequently, the significance of K_0 to Q_u is very limited, with impact on the bearing capacity being minor, and therefore $K_0 = 1$ is used throughout this research for simplicity.

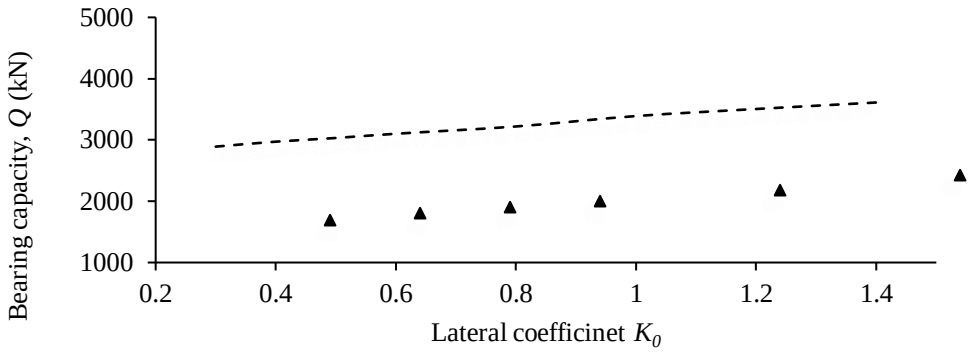

Figure 3-20 RBB pile bearing capacity at a varying coefficient of earth pressure at rest K_o, with shaft d = 400 mm, length L = 10 m, base D = 1 m, soil friction angle ϕ = 30^{O}, and cohesion c = 50kPa.

3.3.2.8 Impact of coefficient of friction on pile bearing capacity

Figure 3-21 presents the variations of the pile bearing capacity with the coefficient of the friction μ with a slowly rising curve. The pile bearing capacity started from 4,310 kN (extracted at 60 mm settlement) at $\mu = 0$, gradually increased to around 4,740 kN at $\mu = 0.9$. The Q_u value kept stable at around 4,805 kN after $\mu > 1.0$. From Figure 3-21, it can also reveal that the side friction is the difference of the Q_u values measure at $\mu = 0$ and $\mu = 1.0$, i.e., F = 4,805 – 4300 = 490 kN. Therefore, the maximum ratio of the friction in the total capacity is calculated, as follows: Maximum friction ratio = 495/4805 = 10.3% in this case. Considering that the actual μ value is mostly less than 1.0 (refer to Section 2.1.4), and the above friction contains both components of the shaft friction and the base friction, so the shaft friction is generally lower than 10% of the total bearing capacity of RBB pile. This agrees well with the findings discussed in Section 2.1.4.1.

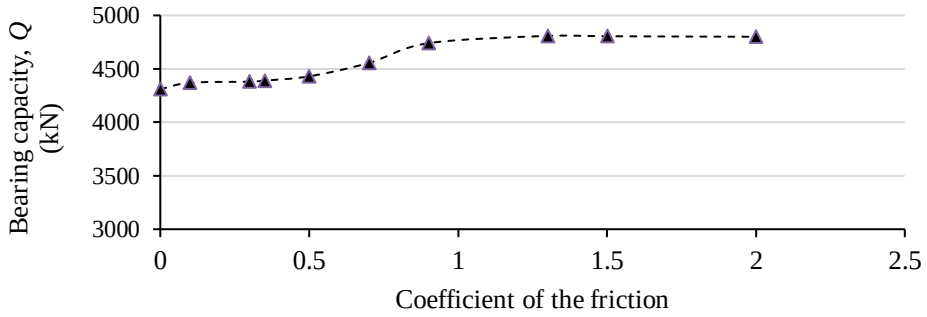

Figure 3-21 RBB pile capacity at varying coefficient of friction μ, with shaft d = 400 mm, length L = 10 m, friction angle ϕ = 30 degrees, base D = 1 m and soil cohesion c = 50 kPa.

3.3.2.9 Impact of lower layer distance on pile bearing capacity

A lower layer is the layer underlying the bearing layer. If a weak basement layer (a lower layer) underlies the bearing layer, it may affect the overall settlement of the RBB piling foundation. Analysis of the impact of the lower basement layer distance on the variations of the pile bearing capacity is one of the important requirements of the RBB Standards, especially when the lower basement is weaker than the overlaying bearing/strengthened layer. The soil properties for the third layer are listed in Table 3-16, and the interface distance *z* varying from 0-9 m is displayed in Figure 3-22.

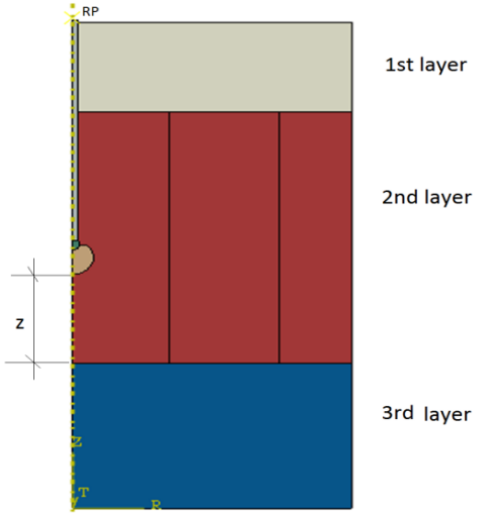

Figure 3-22 RBB pile showing bearing base is located at a distance *z* (0-9 m) to the layer interface of the second and the basement layer with shaft d = 400 mm, length L = 10 m, base D = 1 m; soil friction angle ϕ = 30°, Young's Modulus E = 45 MPa and cohesion c = 50 kPa of the second layer.

Table 3-16 Properties of soil in the weak basement layer.

Name	Density, ρ	Young's Modulus, E	Cohesion, c	Internal Friction angle, ϕ	Dilation Angle, ψ	Poisson's Ratio, v
	(kg/m^3)	(MPa)	(kPa)	(degree)	(degree)	
Basement layer	1800	15	5	20	5	0.3

Figure 3-23 presents the variations of the pile bearing capacity versus the lower layer distance z. The pile bearing capacity started from 3,165 kN at $z = 0$, and gradually decreased to around 3,150 kN at z = 2-3 m, then slowing rises to 3,195 kN. The Q_u

value remained stable after z ≥ 5 m. In the case, all the values of Q_u were extracted at 60 mm settlement.

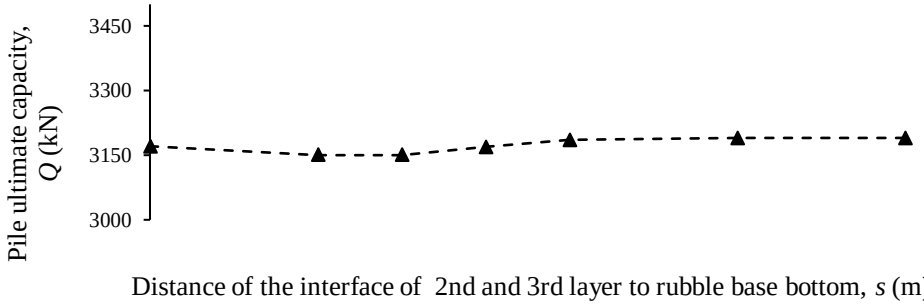

Figure 3-23 RBB pile (Q-z) chart at varying distance of z (0-9 m) to the layer interface of the 2nd and 3rd layers, with shaft d = 400 mm, length L = 10 m, friction angle ϕ = 30 degrees, base D = 1 m, soil cohesion c = 50 kPa and E = 45 MPa for the bearing layer soil.

Figure 3-23 reveals that when the weaker layer is further from the rubble base bottom, the pile bearing capacity increases by 40 kN from 3150 kN at around 2 m to 3190 kN at around 5 m away. This increase is insignificant. It is pointed out that the Q_u at zero distance should have been slightly less than all of the other readings measured from other distances; some error may have arisen during the simulation for z = 0 scenarios. It is initially estimated that the interference effect of the interface to the pile bearing base behaviour at z = 0 m may cause this simulation error; further inspection is required to solve this issue. Overall speaking, the impact of lower layer distance on bearing capacity Q_u is insignificant.

3.3.2.10 Impact of soil dilation angle on pile bearing capacity

The impact of soil dilation angle ψ on the pile capacity Q_u is analysed with three typical values varying from 0.0, 10 and 20 degrees. Figure 3-24 illustrates the relationship between the E values with Q_u. It can be seen that, when the soil dilation angle increases by 100% from 10 to 20 degrees, the bearing load increases by 7.3% from 2,750 to 2,950 kN at 40 mm settlement. When the dilation angle increases the gaps of the curves decrease, indicating the influence of the dilation angle of soil to the bearing capacity declines. Thus, the soil dilation angle is not a significant parameter to influence the Q_u of RBB piles.

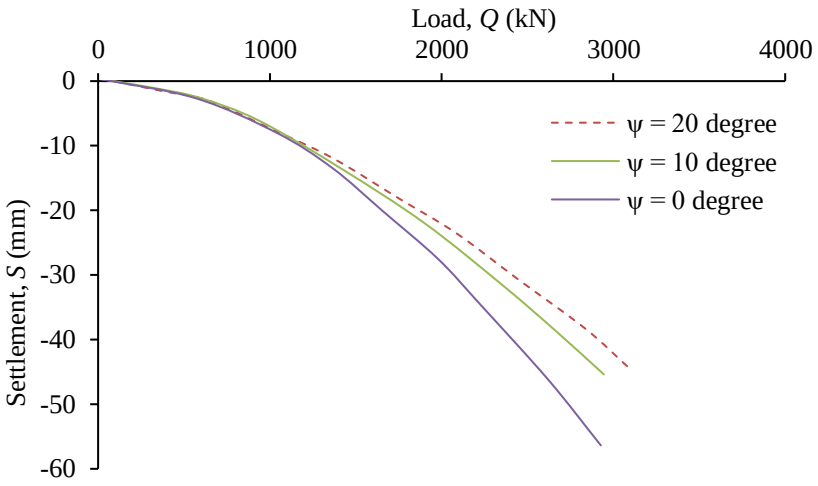

Figure 3-24 Parametric significance analysis on dilation angle of soil, showing insignificance to the RBB pile bearing capacity, where shaft d = 400 mm, length L = 10 m, friction angle ϕ = 30 degrees, base D = 1 m, soil cohesion c = 50 kPa, Young's modulus E = 45 MPa for the bearing layer soil.

3.3.2.11 Impact of Poisson's ratio on pile bearing capacity

The impact of soil Poisson's ratio v on the pile bearing capacity Q_u is analysed with four typical values varying from 0.2, 0.25, 0.35 and 0.4. Figure 3-25 illustrates the relationship between the v values with Q_u. It can be clearly seen that Poisson's ratio of soil is not a significant parameter to influence the bearing load of RBB piles.

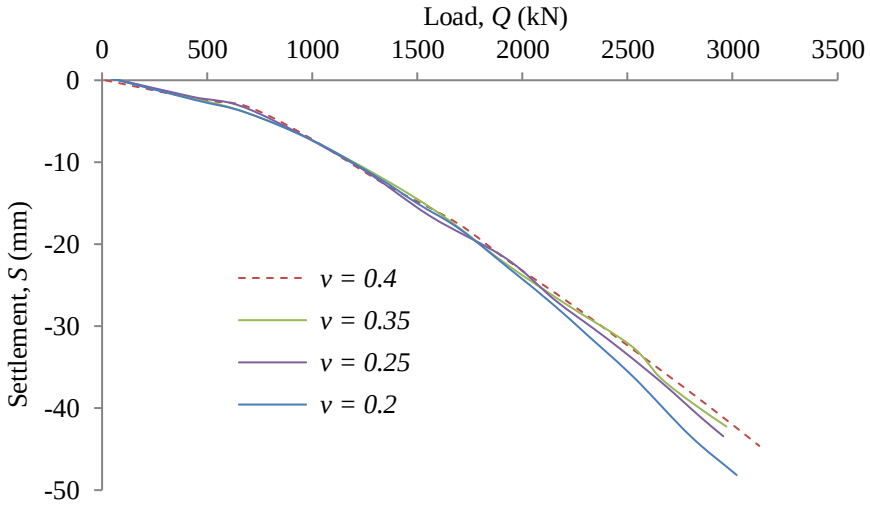

Figure 3-25 Parametric significance analysis of Poisson's ratio of soil v, showing insignificance to the RBB pile bearing capacity, where shaft d = 400 mm, length L = 10 m, friction angle ϕ = 30 degrees, base D = 1 m, soil cohesion c = 50 kPa, Young's modulus E = 45 MPa for the bearing layer soil.

3.3.2.12 Impact of soil density on pile bearing capacity

The impact of soil density ρ on the pile bearing capacity Q_u is analysed with three typical values varying from 1,800, 2,000, and 2,200 kg/m^3. Figure 3-26 illustrates the relationship between the ρ values with Q_u. It can be evidently seen that soil density is not a significant parameter to influence the bearing capacity of RBB piles.

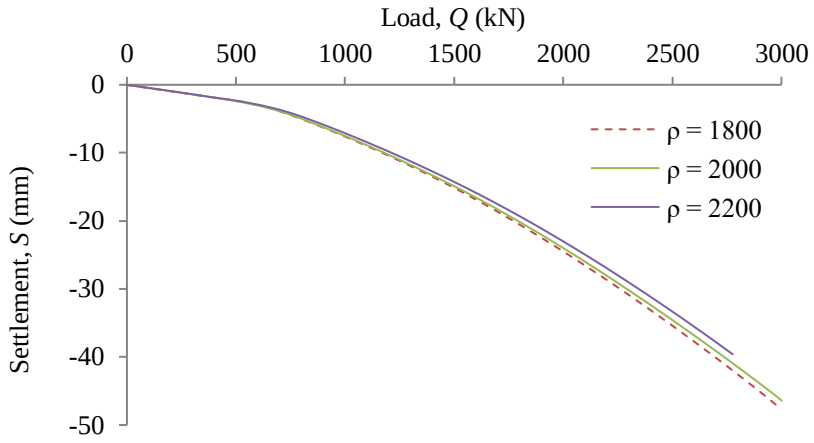

Figure 3-26 Parametric significance analysis of soil density ρ, showing insignificance to the RBB pile capacity, where shaft d = 400 mm, length L = 10 m, friction angle ϕ = 30 degrees, base D = 1 m, soil cohesion c = 50 kPa, Young's modulus E = 45 MPa for the bearing layer soil.

3.3.3 Parameters significance and ranges

Section 3.3.2 discussed the key parameters of soil properties and pile profiles, and confirmed that the Poisson's ratio, mass density, dilation angle and pile shaft diameter were insignificant in the estimation of the RBB pile bearing capacity. On the contrary, the study showed that other parameters including the pile shaft length, rubble base diameter, soil Young's Modulus, friction angle are significant to the prediction of the RBB pile capacity. The cohesion was initially evaluated as a significant parameter to the pile bearing capacity in the early stage of the research, but the later rigorous analysis in previous section showed that this parameter is insignificant to the RBB pile bearing capacity. However, soil cohesion is still included into the five typical parameters affecting the pile bearing capacity as inputs into the FE numerical modelling and the corresponding equations developed in Chapter 4. This inclusion does not compromise the equations accuracy and integration.

The ranges of values of the significant parameters of the soils, pile and strata as input variables were determined according to the literature review, as listed in Table 3-17. Thus, there were 1008 combinations of these parameters, indicating 1008 simulations to be carried out (i.e., $7 \times 4 \times 4 \times 3 \times 3 = 1008$). Part of the input combinations used is shown in Table 3-18 as samples, and other parameters used in the parametric study were fixed as constants, as listed in Table 3-14.

Table 3-17 Value range of significant parameters used for parametric study.

Parameters/Input variables	Values used	Amount of values
Range of parameters of the 2nd layer soil used		
Young's Modulus, *E* (MPa)	5, 15, 30, 45 60, 75, 90	7
Cohesion, *c* (kPa)	0, 25, 50 75	4
Internal Friction Angle, ϕ (degree)	20, 30, 40 50	4
Range of pile parameters used		
Shaft Length, *L* (m)	5, 10, 15	3
Rubble Base Diameter, *D* (m)	0.6, 1, 1.5	3

Table 3-18 Part of model inputs of five significant parameters used for parametric study.

Model input				
Pile Profile		Bearing/Strengthening Layer Soil		
Shaft length, *L*	Rubble diameter, *d*	Friction angle, ϕ	Young's Modulus, *E*	Cohesion, *c*
(m)	(m)	(degree)	(MPa)	(kPa)
5	0.6	20	5	0
5	0.6	20	5	25
5	0.6	20	5	50
5	0.6	20	5	75

To conclude, the significant soil parameters used as input variables in developing the AI equations in Chapter 4 are the soil cohesion, friction angle and Young's Modulus in the bearing/strengthened layer. The significant pile parameters include the pile shaft length and the rubble base diameter. Other parameters are treated as fixed constants as detailed in Table 3-14 throughout the modelling except were specified separately.

3.4 Model outputs for development of new design equations

Each of the 1008 simulations carried out for the parametric study yielded one load-settlement (Q-S) curve; the one as an example modelled with L = 10 m, E = 30 MPa, c = 50 kPa, ϕ = 30^0 and D = 1 m is shown in Figure 3-27. According to the discussion in Section 3.1.4, the ultimate bearing capacity Q_u can be read out as 2,524 kN and 3,251 kN at two settlement values of 40 mm and 60 mm, respectively, for developing the new prediction equations in this thesis.

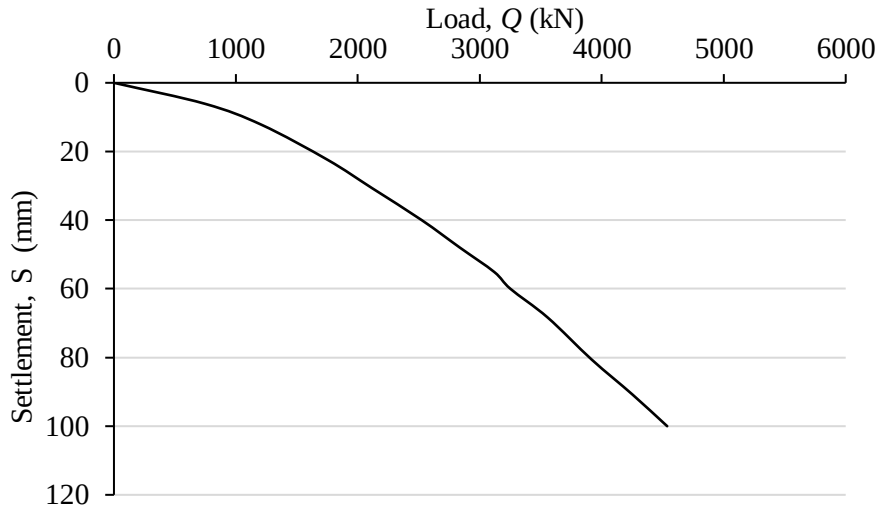

Figure 3-27 Example of FE model output (Q-S) curve for L = 10 m, E = 30 MPa, c = 50 kPa, ϕ = 30^0 and D = 1 m.

Samples of the output datasets at 60 mm are presented in Table 3-19. Each dataset consists of one output of pile ultimate bearing capacity Q_u and five significant variables as inputs of shaft length, rubble diameter, soil friction angle, Young's Modulus and soil cohesion. In the 1008 output datasets, the Q_u varied from 337 kN to 5492 kN at 40 mm settlement criterion, and from 404 kN to 7358 kN at 60 mm settlement criterion.

Table 3-19 Samples of output datasets at 60 mm.

Model input					Model output
Pile Profile		Bearing/strengthening layer soil			Ultimate capacity, Q_u
Shaft length, *L*	Rubble diameter, *d*	Friction angle, ϕ	Young's Modulus, *E*	Cohesion, *c*	Q_{60} at 60 mm settlement
(m)	(m)	(degree)	(MPa)	(kPa)	(kN)
5	0.6	20	5	0	404
5	0.6	20	5	25	470
5	0.6	20	5	50	520
5	0.6	20	5	75	564
5	0.6	20	15	0	734
5	0.6	20	15	25	824
5	0.6	20	15	50	907
5	0.6	20	15	75	981

3.5 Conclusions

Chapter 3 mainly presented the research methodology and implementation used in this research, by utilising the finite element (FE) numerical modelling. This chapter analysed the methods used to determine the bearing capacity of a single pile to choose the appropriate approaches and prepare for the basics of the RBB design undertaken in the following chapters. The load-displacement (*Q*-*S*) curves for the enlarged base piles, especially the RBB pile, showed a gradually dropping rate without a sudden bend in the curve. The determination settlement criteria for the Q_u values vary from 10% to 15% times the RBB pile shaft diameter.

The basic FE model was built with the optimised configurations and then was calibrated with several historic RBB piling cases. The calibrated model was then used to undertake comparisons of RBB piles with conventional piles. In the soft soil, the RBB piles provided much higher bearing capacity than in the hard soil. When the bearing layer was replaced by the bedrock, the RBB pile shaft was similar to directly seating on the bedrock. Therefore, the RBB piles provided much greater strength in soft soil than the conventional piles, in terms of the provision of bearing capacity. This advantage is limited in the very stiff bearing soil.

A parametric study was also carried out using the established sophisticated three-dimensional FE models to evaluate the impact of the parameters of soil properties, pile profiles and strata features on the RBB pile bearing capacity. Consequently, five significant parameters of soils, pile and strata were selected from the parametric analysis: soil cohesion (c), friction angle of soil at pile tip (ϕ) and soil Young's Modulus (E). The significant pile parameters are the pile shaft length (L) and the rubble base diameter (D). Other parameters are treated as fixed parameters throughout the parametric study except were specified separately. Then the FE validated model was used to produce 1008 datasets from which design equations for RBB piles will be derived in Chapter 4 for use by practitioners.

CHAPTER 4 NEW DESIGN EQUATIONS: DEVELOPMENT AND APPLICATIONS

This chapter mainly focuses on the development and applications of the new design equations based on artificial intelligence (AI). Firstly, the chapter introduces the option of suitable AI technique using evolutionary polynomial regression (EPR) to process the results acquired from the parametric study carried out in Chapter 3 to develop simple design equations for RBB piles suitable for use by practitioners. This chapter also presents the soil improvement due to the settlement criterion increase, and its use in enhancing the accuracy of the new design method of RBB piles. To the end, four applications of the new design equations are performed to confirm the new design method, its conservatism and accuracy.

4.1 Artificial Intelligence techniques

This section covers a brief discussion on the option of the suitable AI techniques to process the results acquired from the parametric study to develop new design equations for RBB piles. From the previous sections, it has been determined that the new RBB design equations will be developed from the FE numerical models developed for the parametric study of Chapter 3. The AI method is then used to integrate over one thousand datasets into relationship equations between the RBB pile inputs of significant parameters of soil, pile and strata and the RBB pile bearing capacity.

In several sections of Chapters 2 and 3, it has been demonstrated that the excessively variable behaviour of soil and the application of different pile installation methods introduce various factors and coefficients to tackle the uncertainties and assumptions in the prediction of load-settlement development of piles. No definite formula has been reported which can predict the pile capacity precisely and overall consider all the piling scenarios systematically. The effective calculation by these (semi-) empirical methods is largely based on the statistical and theoretical techniques selected to integrate the inputs and output and the approaches to define the parameters used in modelling (Das and Basudhar 2006; Suman 2015). To mitigate the issues

caused by empirical methods, AI techniques may be the ideal alternative. AI methods are recognised by effectively developing accurate prediction equations by integrating the datasets of inputs and outputs derived from field tests, laboratory tests and/or numerical modelling (Alkroosh 2011; Suman 2015). To achieve this aim in this research, it is essential to determine one suitable AI method to develop the formulas for prediction of pile capacity; the equation development is based on numerous datasets available from RBB-FE numerical modelling in this research.

Artificial intelligence techniques have been used widely to simulate various complex civil engineering problems such as design of foundations and are found extensively in the literature (e.g. Gandomi, Alavi, and Ryan 2015; Huang et al. 2004; Ismail and Shahin 2012; Shahin 2015; Shahin 2009, 2013). The broadly used AI techniques consist include: genetic programming (GP), evolutionary polynomial regression (EPR), backpropagation (BP) nerve network, artificial neural networks (ANNs) and support vector machines (SVM) (Shahin 2013). The advantage of ANNs and GP over conventional methods is their capability in the investigation of the complex nonlinear correlation between the problem and parameters. Also, ANNs and GP methods can define the model configurations and the unidentified parameters of the model, to avoid the constraints of the traditional methods (Alkroosh 2011). However, genetic programming (GP) methods involve more previous information on the problems being resolved (Alkroosh 2011). ANNs have been used for over half a century for a wide range of problems in engineering. However, ANNs are deemed to be a “black box” technique (Giustolisi et al. 2007; Shahin 2015; Shahin and Jaksa 2008) and the network configurations of ANNs are complex in terms of weights and biases inaccessible to the users (Suman 2015). There were limited cases reported on the development of RBB design models using the AI techniques, such as (Chen, Zhimin; Jia 2002; Li 2010). Li (2010) researched predictions of the RBB bearing base pile using BP nerve network based on 40 datasets of the RBB pile tests, achieving accurate results. However, those results were based on very narrow datasets – 40 data from 13 sites in Handan City, China, indicating limited representativeness (Li 2010). Similar problems of limited datasets have been found in Chen, Zhimin, and Jia (2002).

Evolutionary polynomial regression (EPR) has been recently preferably utilised in many research areas, especially in geotechnical engineering problems (Shams 2019), due to the outstanding provision of its 'simple symbolic forms' of equations from trained data; this is the exact function expected by this research to correlate the typical parameters of soils, pile and strata with the RBB pile capacity. The next section focuses on the introduction of the ERP; other AI technologies are not discussed further.

4.1.1 Evolutionary Polynomial Regression (EPR)

Evolutionary Polynomial Regression (EPR) is a hybrid regression method used for data mining purposes. It is based on evolutionary computing, developed by Giustolisi and Savic in the early 2000s (cited by Shahin (2015)). This technique builds symbolic models by combining the most comprehensive features of numerical regression, with inherent algorithms and symbolic regression. The EPR regression includes two major steps showing its fundamental features: (1) choose exponents for polynomial terms utilising an evolutionary searching approach associated with genetic algorithms; (2) carry out numerical regression with the least square approach to acquire the parameters of the polynomial terms previously selected (Shams, Shahin, and Ismail 2019). EPR equation is generally shown as follows (Gandomi et al. 2015; Giustolisi and Savic 2006):

$$y = \sum_{j=1}^{m} F\left(X, f(X), a_j\right) + a_o \qquad \text{Equation 4-1}$$

where: y = vector of regression output; m = number of terms of the expression as target; F = function created by the regression process; X = matrix of variables as inputs; f = user-defined function; and a_j = constant; a_0 = an optional bias.

A typical sample of EPR pseudo-polynomial model structure that corresponds to Equation (4-1) is presented in the vector form, as follows (Gandomi et al. 2015; Giustolisi and Savic 2006):

$$\hat{Y} = a_0 + \sum_{j=i}^{m}\left(a_j.(X_i)^{ES(j,1)}.....(X_k)^{ES(j,k)}.f\left[(X_i)^{ES(j,k+1)}.....(X_k)^{ES(j,2k)}\right]\right)$$

Equation 4-2

where: $\hat{Y}$ = vector of output values; m = expression length; a_j = constants; X_i = vector(s) of the (k) variables as inputs; *ES* = matrix of exponents; and *f* = user-defined function.

EPR inherits two functions for simulating realistic problems: (1) introduction of prior facts about the physical problems and its process that are to be simulated at three defined times (i.e. before, during and after calibration of EPR modelling); and (2) formation of symbolic equations, starting data mining to examine patterns that represent the preferred parameters (Shahin 2015). In EPR function (1), the modeller determines the relevant parameters as inputs and organizes them in an appropriate arrangement based on their physical denotation before configuring the EPR model. During EPR model formation, the model configurations are determined according to a number of user-defined settings, e.g., a certain polynomial structure, user-defined functions (such as exponentials, natural logarithms, and tangential hyperbolics), including exploring strategic parameters.

EPR approach starts from true polynomials and launches the development of non-polynomial expressions integrating user-defined functions, such as the natural logarithms. The user engineering judgement and physical intuition can also be combined into the EPR model; this is achieved by making postulations on the selection of structure and elements for the independent functions, allowing for refinement of the modelling. After the returned EPR models are calibrated, an optimal one can be chosen from the series of models based on the modeller's decision and the regression performance indicators. The performance indicators include the coefficient of determination, R^2; the coefficient of correlation, *r;* mean absolute error, *MAE;* root mean squared error, *RMSE*; and the ratio of average measured to predicted outputs, μ. The strategies used here for judging the optimal regression equations out of a number

of returned models are: (1) the model is validated and reveals promising performance indicators; (2) the performance of the model in the validation set is as consistent as that in the training set; and (3) the model configurations are simple with a minimum amount of parameters.

In this research, EPR formulas were developed using the EPR TOOLBOX Version 2.0 software package (Shahnazari, Shahin, and Tutunchian 2014). The modelling was conducted in the following steps:

- The datasets divided for two purposes of training and validation should be numerically consistent to correctly denote the same numerical population. Accordingly, these two sets opted should be very close in terms of mean (average) and standard deviation. The appropriate values, e.g., lower bound (minimum) and upper bound (maximum) of the input parameters should be carefully chosen in compiling the training datasets to elude extrapolation during modelling and application of the model results as warned by Birid (2017).
- The dataset obtained from the parametric analysis in Chapter 3 was divided into two groups: a large training set helps avoid over-fit, so 90% of the data was used for training the model, whereas 10% of the data was assigned for validation of the trained model. Altogether 1008 datasets were collected from the parametric analysis modelling covering a wide variation of RBB piling scenarios that include the comprehensive combinations of most soil types, usual pile dimensions and strata profile.
- The inputs of the EPR method include five variants in this research: rubble base diameter (D); pile embedment length (L); Young's Modulus of soil in the bearing/strengthened layer (E); Cohesion of soil in the bearing/strengthened layer (c); internal friction angle of soil in the bearing/strengthened layer (ϕ). The major output is the pile ultimate bearing capacity (Q_u).

It should be noted that the EPR modelling was conducted individually for each of the abovementioned outputs at the settlement criteria of 40 mm and 60 mm using the same

inputs, leading to two derived equations in the new design method. This will be detailed afterwards in the thesis.

If the AI method relies on the data collected from laboratories and site tests, the data are generally limited and specific to sites; its representativeness is questionable due to limitation and biases. However, in this research, the datasets for regression are derived from FE numerical modelling where simulations are based on a wide and comprehensive range of the typical parameters of soil properties, pile profile and strata features, especially, the variation of soils covering all the combinations of the typical soil properties. Therefore, the new equations obtained from EPR are representative of all the soil types without the limitation to specific sites and data scale.

4.1.2 Developed EPR Equations

Based on the EPR method discussed in Section 4.1.1, the 1008 datasets extracted from the FE parametric study of Chapter 3 are randomly divided into two statistically consistent sets: 901 datasets as the training set for model calibration and an independent validation set of 107 datasets as model performance verification. Once the training phase is accomplished successfully, the performance of the trained models is verified using the validation set. The performance of the EPR model equations in the training and validation sets were evaluated using five analytical standard measures including the coefficient of correlation, r; coefficient of determination, R^2; root mean squared error, RMSE; mean absolute error, MAE; and the ratio of average measured to predicted outputs, μ.

The EPR analysis returned two models for each output parameter Q_u at 40 mm and 60 mm settlement. The model performance representations are indicated in Figures 4-1 and 4-2, and the optimal models are expressed as follows:

For 40mm settlement criterion:

$$Q_u = (0.23676 \times \frac{E^2}{L \times D} \times \sqrt{\frac{c}{\phi}}) - (328.1371 \times \frac{E}{\sqrt{L \times \phi}}) + (571.1302 \times \sqrt{D \times E}) + (2.809 \times L^2 / \sqrt{D}) - 434.6191$$

Equation 4-3

For 60mm settlement criterion:

$$Q_u = [-0.3895208 \times \sqrt{E / (L \times \phi)}] + (712.5371 \times \sqrt{D \times E}) + (0.49852 \times L \times \sqrt{c \times E}) + 366.1439$$

Equation 4-4

Here: E = Young's Modulus (MPa), c = cohesion (kPa) and ϕ = Internal friction angle (degree) are three properties of soil in the bearing/strengthened layer; L = pile shaft length (m) and D = rubble base diameter (m), are the dimensions of the RBB pile. Q_u = pile ultimate bearing capacity (kN).

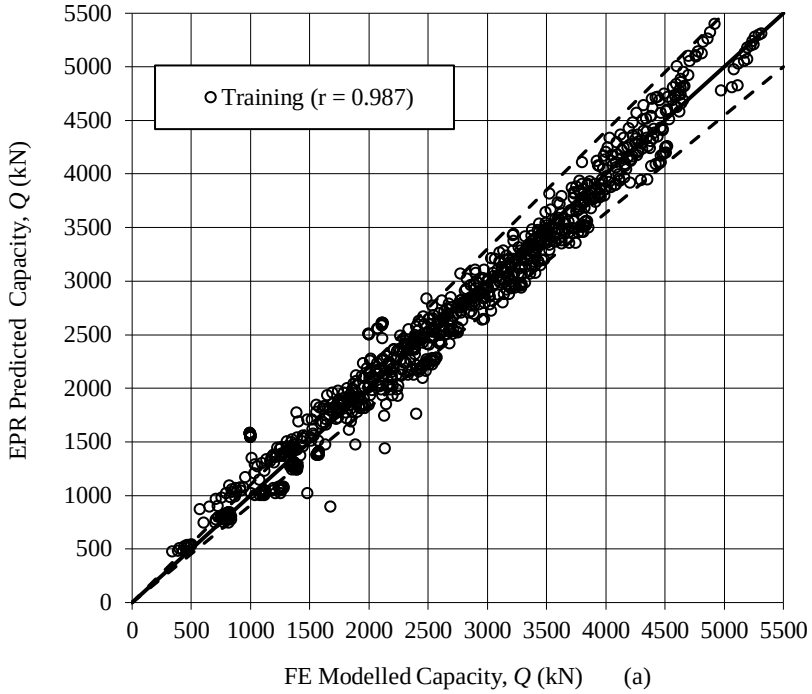

(a)

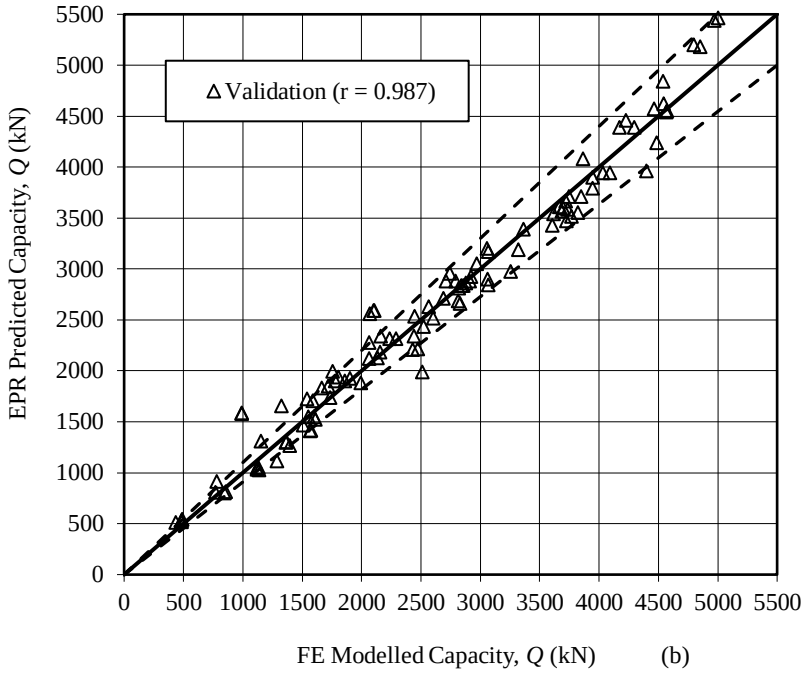

(b)

Figure 4-1 Graphical performance of the EPR model of Equation 4-3 for Q_u at 40 mm settlement criterion: (a) training set; and (b) validation set.

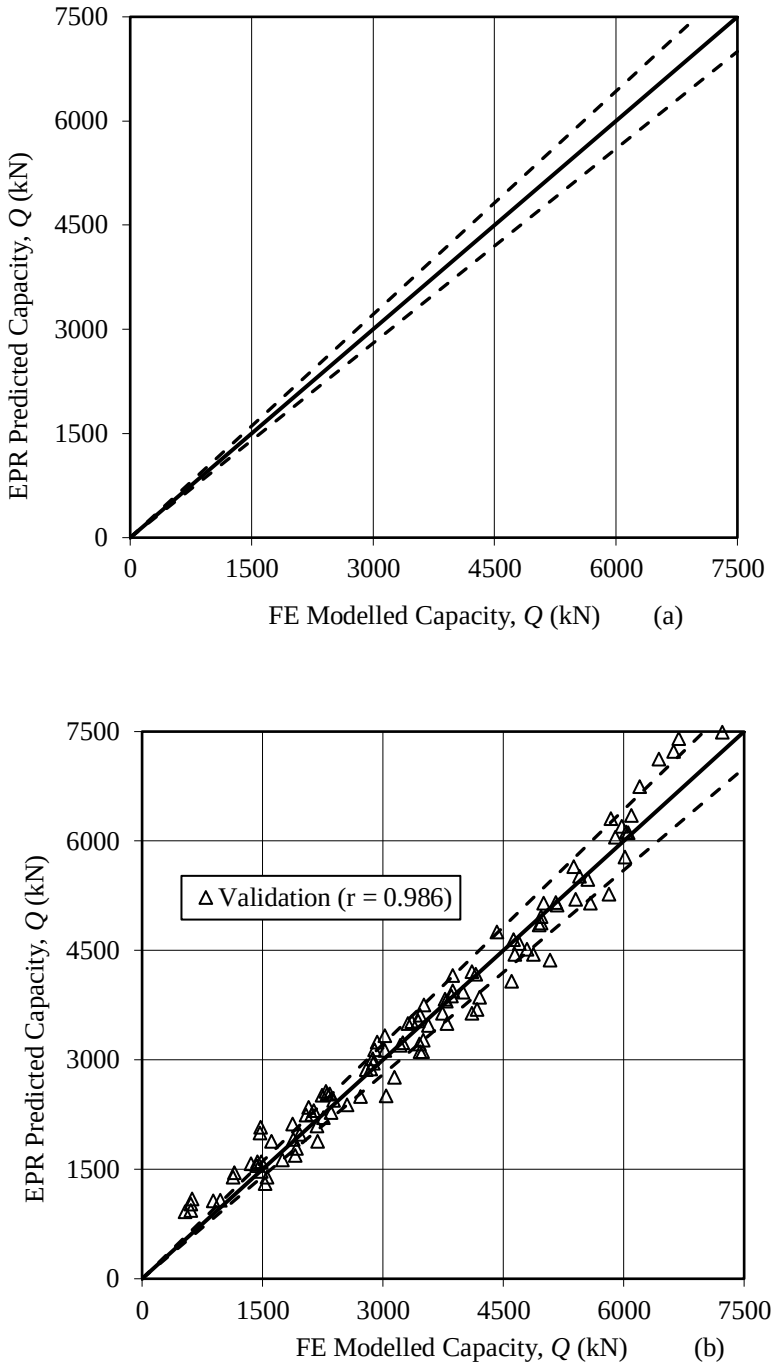

Figure 4-2 Graphical performance of the EPR model of Equation 4-4 for Q_u at 60 mm settlement criterion: (a) training set; and (b) validation set.

The performance measures for Equation 4-3 are listed in Table 4-1. According to Evans & Feltz (1996) for the absolute value of *r* and the scatter charts in Figure 4-1, the associations between EPR predicted Q_u and FE modelled Q_u are very strong ($r >$ 0.8) for both the training and validation sets, regarding Q_u at 40 mm settlement criterion. Therefore, there is a strong correlation between the predicted RBB pile

ultimate capacity Q_u and soil parameters: Young's Modulus, E; cohesion, c; internal friction angle, ϕ; and shaft length, L; and rubble base diameter, D in Equation 4-3.

Table 4-1 Performance measures of the EPR model of Equation 4-3 for Q_u in training and validation.

Statistics	Training	Validation
r	0.987	0.987
RMSE (kN)	188.9	202.5
MAE (kN)	145.5	151.6
R^2	0.975	0.974
μ	1.00	0.99

The performance measures for the new Equation 4-4 are listed in Table 4-2. According to Evans & Feltz (1996) for the absolute value of r, and the scatter charts in Figure 4-2, the associations between predicted pile capacity and measured capacity are also very strong (r > 0.8) for both the training set and validation set, regarding Q_u at 60 mm settlement criterion. Therefore, there is a strong correlation between the predicted RBB capacity Q_u and the parameters of Young's Modulus E; Cohesion c; internal friction angle ϕ; Shaft length L; and rubble base diameter D in Equation 4-4.

Table 4-2 Performance measures of the EPR model of Equation 4-4 for Q_u in training and validation.

Statistics	Training	Validation
R	0.987	0.986
RMSE (kN)	263.1	292.4
MAE (kN)	210.3	231.4
R^2	0.973	0.970
μ	0.99	0.98

4.2 Bearing capacity improvement obtained from settlement increase

The bearing resistance (Q_u) increases over the settlement increase, as indicated in Figure 3-27. In FE modelling, regarding each (Q-S) curve, the Q_u value determined

at 60 mm is larger than that defined at 40 mm. If the increase of Q_u (i.e. ΔQ_u) is approximately stable, i.e. its variation falls in a narrow envelope; a constant can be used for adjusting the newly developed equations to include the compaction effect, as proposed earlier in Sections 3.1.3 and 3.1.4. Here, $\Delta Q_u = Q_{u-60mm} - Q_{u-40mm}$. Therefore, the increase ratio of the pile bearing capacity defined from 40 mm to 60 mm can be estimated as follows:

$$\Delta Q_u\% = \frac{Q_{u-60mm} - Q_{u-40mm}}{Q_{u-40mm}} \times 100\% \qquad \text{Equation 4-5}$$

Figure 4-3 illustrates the scatter plot of the FE modelled 1008 Q_u values obtained at 40 mm (*x*-axis) versus at 60 mm (*y*-axis); it shows that over 95% of 1008 Q_u, a hollow circles falling in a narrow envelope (outlined in two dotted lines), indicating firstly, that all the values of Q_u values modelled at 60 mm are larger than those at 40 mm; secondly, the increase of Q_u in RBB piling seems stable and consistent.

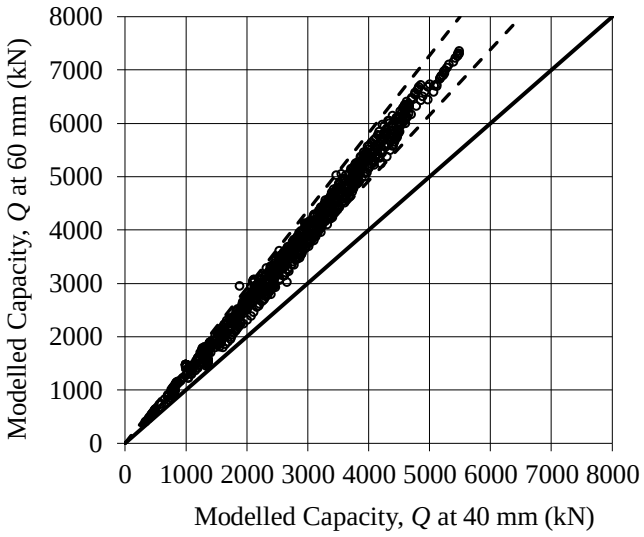

Figure 4-3 Graphical performance of 1008 modelled Q_u values at 40 mm versus at 60 mm.

Figure 4-4 illustrates the scatter plot of the 1008 $\Delta Q_u\%$ values calculated from Equation 4-5 with those modelled at 40 mm (*x*-axis) versus the increase ratio of Q_u modelled at 60 mm (*y*-axis); it shows that over 95% of 1008 Q_u, hollow circles falling

in a narrow envelope outlined in two dotted lines with upper envelope value of 40%, and lower envelope value of 20%, averaging at 30%. According to Equations 3-1 and 3-2, and discussion in Section 3.1.3 (Wang et al. 2006), the Q_u modelled at settlement criterion S_2 = 60 mm equals to the value at S_1 = 40 mm times a factor (1+ θ), θ = 30%, as follows:

$$Q_{u-60mm} \approx Q_{u-40mm} + Q_{u-40mm} \times \theta = 1.3 \times Q_{u-40mm} \qquad \text{Equation 4-6}$$

Therefore, the above comparison has testified that firstly, all of Q_u values modelled at 60 mm are larger than those at 40 mm; furthermore, the increase of Q_u in RBB piling was primarily stable and consistent with an average ratio of 30% as the settlement increases from 40 to 60 mm.

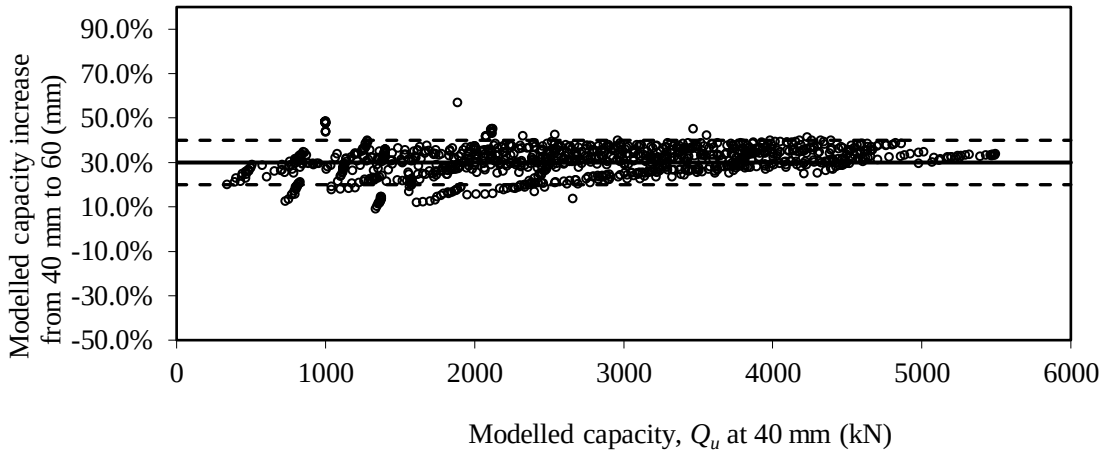

Figure 4-4 1008 Q_u hollow circles falling into an envelope of 20% to 40% with an average of 30%.

The accuracy of Equation 4-6 can be assessed by comparing the Q_u values modelled at 60 mm with the newly calculated Q_u values at 60 mm using Equation 4-6. Figure 4-5 illustrates the comparison in the scatter plot of 1008 Q_u values. The high r value (r = 0.996) confirms that the correlation between the new value calculated with Equation 4-6 and the modelled value is strong.

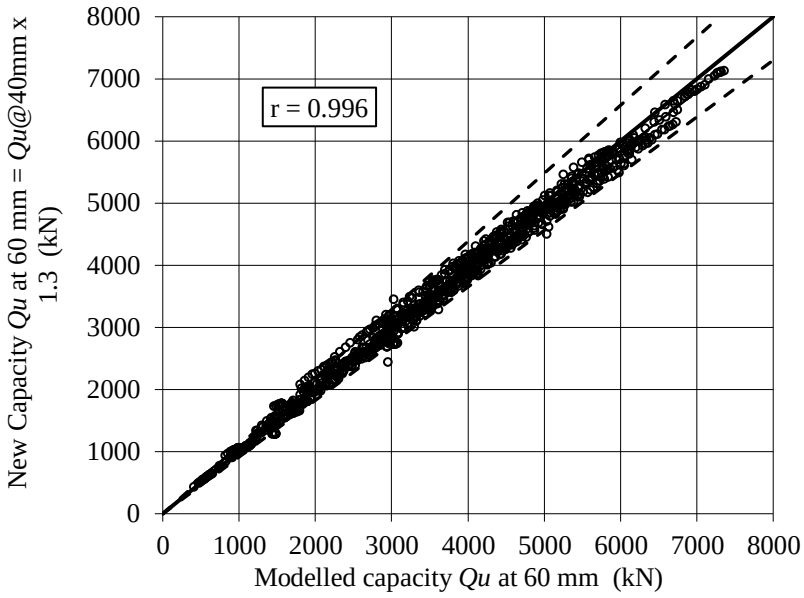

Figure 4-5 Graphical performance of 1008 Q_u values modelled at 60 mm versus Q_u calculated at 60 mm by Equation 4-6.

Figure 4-6 explores the prediction accuracy of the 1008 Q_u at 60 mm calculated from Equation 4-6 with the modelled at 60 mm; it shows that over 95% of 1008 Q_u, hollow circles falling in a narrow envelope outlined in two dotted lines with upper envelope value of 7% and lower envelope value of -7%. According to the accuracy definition by Corson (1989), as cited in Section 2.1.4.1, the range of ±7% falls well within the 30% criterion; thus, Equation 4-6 is deemed to be reliable and accurate.

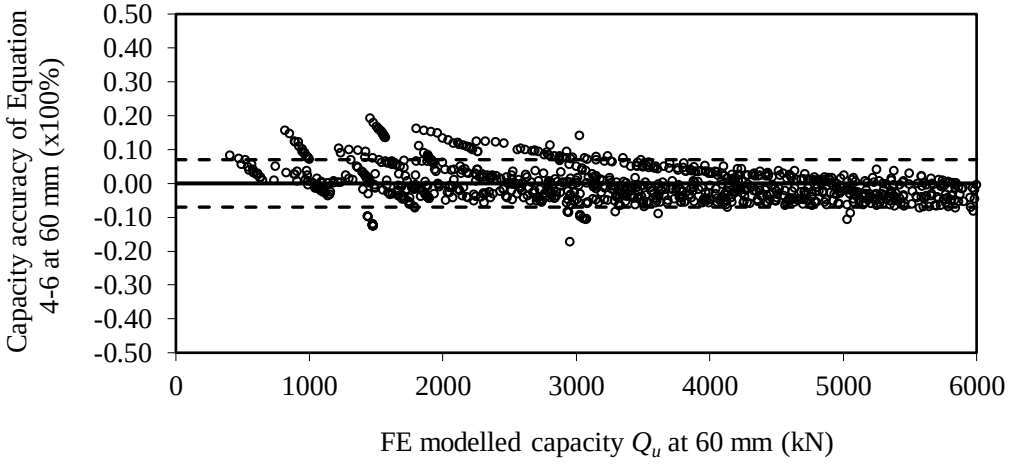

Figure 4-6 Capacity accuracy of Equation 4-6 at 60 mm, 1008 Q_u, hollow circles falling into a narrow envelope of 0.07 to -0.07.

4.3 Application of new developed equations against historic cases

This section validates the new RBB pile design Equations 4-3 and 4-4 developed in the previous section against the historic cases, meanwhile demonstrates how the new equations apply in the new RBB design. As mentioned in Section 2.1.4.1, most of the load tests reviewed terminated before reaching 60 mm after the load applied reached the designed ultimate value. Therefore, it is difficult to obtain full load-settlement (*Q*-*S*) curves with settlements at 60 mm from the reviewed literature. Below are several samples for prediction of the RBB pile bearing capacity using the newly developed equations.

4.3.1 Application to historic case by Wang (2014)

Wang (2014) studied the application of the RBB pile with a bearing base in a dense sand stratum of a site with a number of site load tests in Antai, China. All pile load tests stopped with settlements less than 45 mm, while the measured pile bearing capacity met the design purposes (refer to Figure 4-7, No. D04 RBB pile was loaded to settlement of approximately 45 mm).

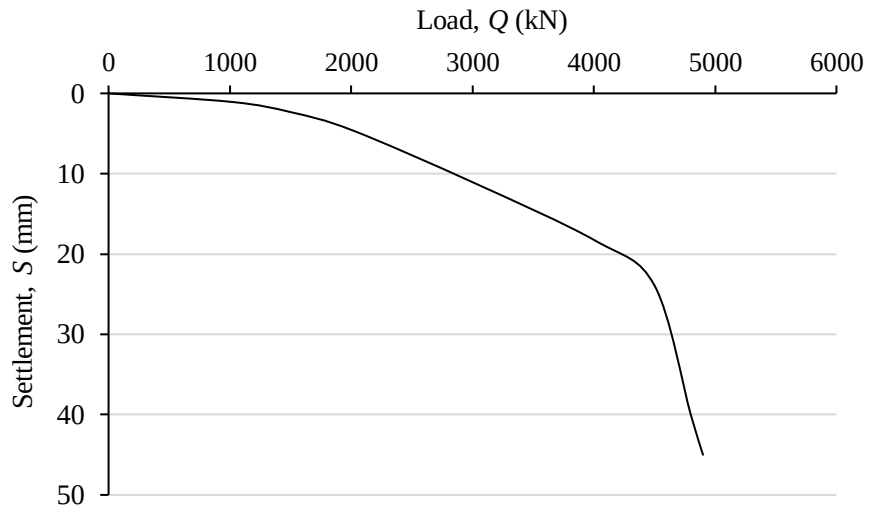

Figure 4-7 Load-settlement (*Q*-*S*) curve of No. D04 pile from the historic case by Wang (2014).

The soil properties in the bearing/strengthened layer (fine sand) included the typical soils Young's Modulus of 80 MPa (calculated from the provided Compression

Modulus value), friction angle of 28.5°, and cohesion of 0.0 kPa. The cohesion herein was taken as 1 instead of zero for consistence in calculation by the equations below, in accordance with the modelling requirement for avoiding early abortion when zero cohesion was used in the FE simulations (Table 4-3). The RBB pile shaft was designed with a length of 6 m and the bearing base was constructed to a diameter of 1.58 m. Thus, the five typical parameters used as inputs into the new RBB pile design Equation 4-3 are L = 6 m, D = 1.58 m, E = 80 MPa, c = 1.0 kPa, ϕ = 28.5^0. In modelling, other parameters of soil properties, pile profiles and stratum features of the site cited by Wang (2014) falling into the normal variation ranges outlined in Table 3-14 and are not repeated herein.

Table 4-3 Soil properties in historic case by Wang (2014).

Layer	Compression Modulus E_s	Young's Modulus E*	Friction angle ϕ	Density ρ	Cohesion c	Poisson's ratio ν
	(MPa)	(MPa)	(°)	(kg/m^3)	(kPa)	
Silt	9.3	37.2	24.3	1920	14.3	0.25
Silty clay	6.5	26	14.5	1990	25.4	0.32
Fine sand	20	80	28.5	2020	0	0.23

*Only Compression Modulus data were given in Wang (2014), so Young's Modulus (E) values were estimated using equation: $E = C_e \times E_s$, C_e = 2~5.0, here C_e = 4.0 (Wang 2014).

The pile load test for No. D04 pile was carried out up to 45 mm settlement. Thus, the five typical parameters were just input into Equations 4-3; the predicted pile bearing capacity Q_u at 40 mm settlement is computed as follows:

$$Q_u = (0.23676 \times \frac{80^2}{6 \times 1.58} \times \sqrt{\frac{1}{28.5}}) - (328.1371 \times \frac{80}{\sqrt{6 \times 28.5}}) + (571.1302 \times \sqrt{1.58 \times 80}) + (2.809 \times \frac{6^2}{\sqrt{1.58}}) - 434.6191$$

= 4,089 (kN)

Figure 4-7 shows that the Q_u reading at 40 mm was 4800 (kN). Then the underestimation of the prediction of Q_u from the new design Equation 4-3 can be calculated using Equation 2-17 as follows:

Underestimation ratio = $(Q_M - Q_P)/Q_P$ = (4,800-4,089)/4,089×100% = 17% (at 40 mm settlement)

This ratio is lower than the 50% as defined in Table 2-8; therefore, the prediction result using the new Equation 4-3 indicates an economic design; and the underestimation ratio is less than 30%, which means that the prediction can be considered as accurate.

4.3.2 Application to historic case by Zhang (2014)

Zhang (2014) reported a number of site static load tests. The investigation data measured from the soil in the bearing/strengthened layer (No. 4 layer) showed that the typical soils Young's Modulus was 38 MPa, friction angle was 29^0 and cohesion was 19 kPa. The No. H5 RBB pile was designed with a length of 7 m and the bearing base was constructed to a diameter of 1.4 m. The five typical parameters used as inputs into the new RBB design Equations 4-3 and 4-4 are L = 7 m, D = 1.4 m, E = 38 MPa, c = 19 kPa and ϕ = 29^0. Other parameters of soil properties (except the data in Table 4-4), pile profiles and stratum features of the site cited by Zhang (2014) falling into the normal variation ranges outlined in Table 3-14 and are not repeated herein.

Table 4-4 Soil properties for historic case by Zhang (2014).

Layer Number	Density ρ	Young's Modulus E	Friction angle ϕ	Cohesion c	Poisson ratio v
	(kg/m^3)	(MPa)	(°)	(kPa)	
1	1882	18	24	15	0.28
2	1977	31	28	18	0.3
3	2044	22	25	13	0.3
4	1956	38	29	19	0.3
5	2022	19	23	25	0.3

The five parameters are input into the Equations 4-3; the predicted pile bearing capacity Q_u at 40 mm settlement is calculated as follows:

$$Q_u = (0.23676 \times \frac{38^2}{7 \times 1.4} \times \sqrt{\frac{19}{29}}) - (328.1371 \times \frac{38}{\sqrt{7 \times 29}}) + (571.1302 \times \sqrt{1.4 \times 38}) + (2.809 \times \frac{7^2}{\sqrt{1.4}}) - 434.6191$$

= 3,000.5 (kN)

The five parameters are input into the Equations 4-4; the predicted bearing capacity Q_u at 60 mm settlement is calculated as follows:

$$Q_u = (-0.3895208 \times \sqrt{\frac{38}{7 \times 29}}) + (712.5371 \times \sqrt{1.4 \times 38}) + (0.49852 \times 7 \times \sqrt{19 \times 38}) + 366.1439$$

= 3,971.75 (kN).

The load-settlement (*Q*-*S*) curve provided by Zhang (2014) is presented in Figure 4-8; the Q_u readings at 40 mm and 60 mm are 3,750 (kN) and 4,420 (kN), respectively. Then the underestimation ratios of the prediction of Q_u using the new Equations 4-3 and 4-4 can be calculated using Equation 2-17, as follows:

Underestimation ratio $= (Q_M - Q_P) / Q_P =$ (3,750-3,000.5)/3,000.5 $\times$100% = 25% (at 40 mm settlement)

Underestimation ratio = $(Q_M - Q_P) / Q_P$ = = (4,460-3,971.75)/3,971.75 $\times$ 100% = 12% (at 60 mm settlement)

Both ratios are lower than 50% as defined in Table 2-8; therefore, the two prediction results indicate an economic design and as the two underestimation ratios are both less than 30%, the predictions can be considered as accurate.

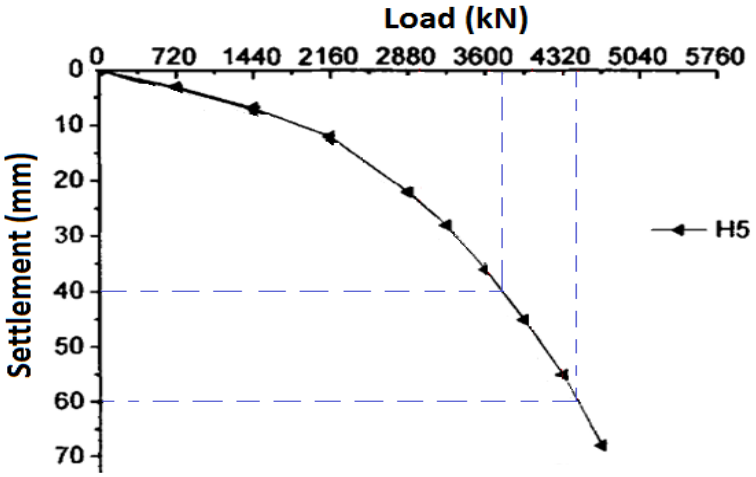

Figure 4-8 Load-settlement (*Q*-*S*) curve of No H5 RBB pile from historic case by Zhang (2014).

The second pile in Zhang (2014), No. H3 RBB pile was designed with a length of 7 m and the pile bearing base was constructed to a diameter of 1.0 m. The five typical parameters of L = 7 m, D = 1.0 m, E = 38 MPa, c = 19 kPa and ϕ = 29^0 are input into Equations 4-3; the predicted bearing capacity Q_u at 40 mm settlement is as follows:

$$Q_u = (0.23676 \times \frac{38^2}{7 \times 1} \times \sqrt{\frac{19}{29}}) - (328.1371 \times \frac{38}{\sqrt{7 \times 29}}) + (571.1302 \times \sqrt{1 \times 38}) + (2.809 \times \frac{7^2}{\sqrt{1}}) - 434.6191$$

= 2,388 (kN)

The five parameters are input into the Equations 4-4; the predicted bearing capacity Q_u at 60 mm settlement is as follows:

$$Q_u = (-0.3895208 \times \sqrt{\frac{38}{7 \times 29}}) + (712.5371 \times \sqrt{1 \times 38}) + (0.49852 \times 7 \times \sqrt{19 \times 38}) + 366.1439$$ =

3,167 (kN).

The load-settlement (*Q*-*S*) curve provided by Zhang (2014) is presented in Figure 4-9; the Q_u readings at 40 mm and 60 mm were 3,240 (kN) and 4,020 (kN), respectively. Then the underestimation ratios of the prediction of Q_u using the new Equations 4-3 and 4-4 can be calculated using Equation 2-17, as follows:

Underestimation ratio = $(Q_M - Q_P)/Q_P$ = = (3,240-2,388)/2,388 ×100% = 36% (at 40 mm settlement)

Underestimation ratio = $(Q_M - Q_P)/Q_P$ = = (4,020-3,167)/3,167 ×100% = 27% (at 60 mm settlement)

Both underestimation ratios are lower than the 50% as defined in Table 2-8; therefore, the two prediction results indicate an economic design and as the ratio at 40 mm is larger than 30%, the prediction is not that accurate; however, the ratio at 60 mm is less than 30%, so the prediction at 60 mm can be considered as accurate.

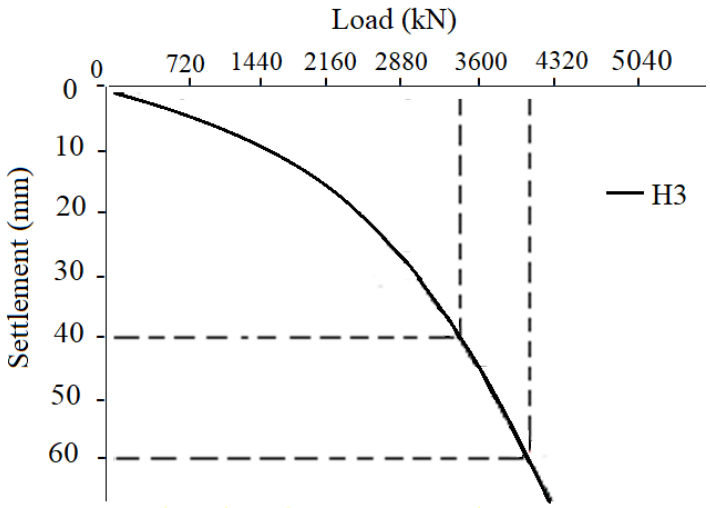

Figure 4-9 Load-settlement (*Q*-*S*) curve of No. H3 RBB pile from historic case by Zhang (2014).

4.3.3 Application to historic case by Jin (2011)

Jin (2011) studied the application of RBB piles on one site located in Sichuan. All the three tested piles Nos 4, 37 and 87 for pile load tests reached the design load when the pile settled to 15.56, 10.57 and 11.56 mm, respectively. Therefore, this analysis will use the reading of Q_u at 40 mm in the extrapolated curve of No. 4 pile. The soil parameters from investigation in the bearing/strengthened layer (Dense gravel I) showed that the typical soil's Young's Modulus was 45 MPa, friction angle was 38^0 and cohesion was 0.0 kPa in Table 4-5. The RBB pile was designed with a length of 3.5 m, and the bearing base was constructed to a diameter of 0.8 m. The five typical

parameters used as inputs into the new RBB design Equation 4-3 are L = 3.5 m, D = 0.8 m, E = 45 MPa, c = 1 kPa and ϕ =38^0. Other parameters of soil properties, pile profiles and stratum features of the site cited by Jin (2011) falling into the normal variation ranges outlined in Table 3-14 are not repeated herein. The layer thicknesses from top to bottom are 0.5, 1.0, 2.0, 2.0 and 4.5 m, respectively.

Table 4-5 Soil properties for historic case by Jin (2011).

Layer	Density	Deformation Modulus	Young's Modulus	Friction angle	Dilation angle	Cohesion	Poisson's ratio
	ρ	E_0	E	ϕ	ψ	c	v
	(kg/m^3)	(MPa)	(MPa)	(°)	(°)	(kPa)	
Fill	1910	15	40.4	17	15	20	0.3
Silty Clay	2000	9	27.7	15.51	5	31.35	0.34
Loose Gravel	2050	13	28.9	35	30	0	0.2
Dense Gravel I	2100	21	45.0	38	26	0	0.17
Dense Gravel II	2200	28	59.1	40	25	0	0.15

*Only Deformation Modulus values were given in Jin (2011), thus, Young's Modulus (E) values were estimated using the equation: $E = C_e \times E_s$, $C_e = (2.0 \sim 5.0)$, $E_0 = \beta \times E_s$ $\beta = 1 - 2 \times v^2 / (1 - v)$ here $C_e = 2.0$.

The five typical parameters of L = 3.5 m, D = 0.8 m, E = 45 MPa, c = 1 kPa and ϕ =38^0 are input into the Equations 4-3; the predicted bearing capacity Q_u at 40 mm settlement is as follows:

$$Q_u = (0.23676 \times \frac{45^2}{3.5 \times 0.8} \times \sqrt{\frac{1}{38}}) - (328.1371 \times \frac{45}{\sqrt{3.5 \times 38}}) + (571.1302 \times \sqrt{0.8 \times 45}) + (2.809 \times \frac{3.5^2}{\sqrt{0.8}}) - 434.6191$$

= 1,778 (kN)

The load-settlement (Q-S) curve provided by Jin (2011) is presented in Figure 4-10; the Q_u reading at 40 mm in the extended curve was read at 2,000 (kN). Then the underestimation ratio of the prediction of Q_u using the new Equation 4-3 can be calculated using Equation 2-17, as follows:

Underestimation ratio = $(Q_M - Q_P)/Q_P$ = = (2,000 – 1,778)/1,778 ×100% = 12% (at 40 mm settlement)

As the ratio is lower than the 50% as defined in Table 2-8, the prediction result indicates an economic design, and as the underestimation ratio is also less than 30%, the prediction can be considered as accurate. It is evident that the pile length in this case was 3.5 m lower than the lower bound of 5 m in the modelling; however, the new equation is still suitable, and the design prediction is still accurate and economic.

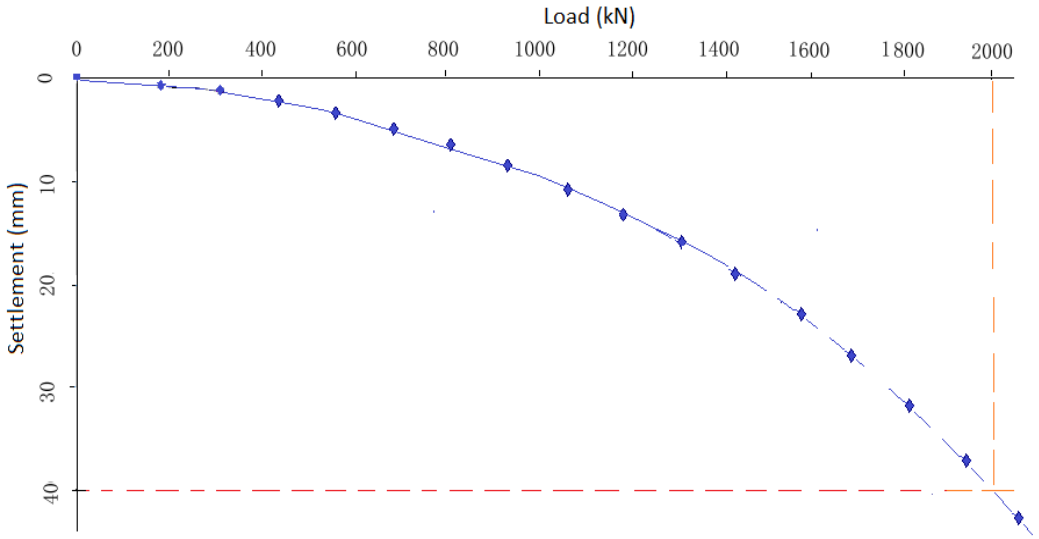

Figure 4-10 Load-settlement (*Q*-*S*) curve of No. 4 RBB pile from historic case by Jin (2011), the low part of the curve is dotted line as extension (Jin 2011).

4.3.4 Prediction improvement of new design equations using coefficient

From the four applications of Equations 4-3 and 4-4, it can be seen that the underestimation ratios of four predicted pile bearing capacity values were 17% (No. D04), 25% (No. H5), 36% (No. H3) and 12% (No. 4) at 40 mm, respectively. If a common improvement coefficient θ = 12% is introduced to the new design prediction method, then, based on Equation 4-6:

For case by Wang (2014) (No. D04 pile)

New prediction Q_{u-40mm} = 4,089 × (1 + 12%) = 4,579.7 kN

New underestimation ratio = $(Q_M - Q_P)/Q_P$ = = (4,800 – 4,569.7)/4,579.7×100% = 10% (at 40 mm settlement).

For case by Zhang (2014), No. H5 pile:

New prediction Q_{u-40mm} = 3,000.5 × (1 + 12%) = 3,360.7 kN

Underestimation ratio = $(Q_M - Q_P)/Q_P$ = = (3,750 – 3,360.7)/3,360.7 ×100% = 11.6% (at 40 mm settlement).

For case by Zhang (2014), No. H3 pile:

New prediction Q_{u-40mm} = 2,388 × (1 + 12%) = 2,674.6 kN

Underestimation ratio = $(Q_M - Q_P)/Q_P$ = = (3,240 – 2,674.6)/2,674.6 ×100% = 21.1% (at 40 mm settlement).

For case in Jin (2011) (No. 4 pile)

New prediction Q_{u-40mm} = 1,778 × (1+12%) = 1,991.4 kN

Underestimation ratio = $(Q_M - Q_P)/Q_P$ = = (2,000 – 1,991.4)/1,991.4 ×100% = 0% (at 40 mm settlement).

The above four applications have demonstrated the use of Equation 4-6, and the improvement coefficient herein implementing more accurate prediction by the new equations. After correction with θ = 12%, the underestimation ratios for the four cases were all smaller than the original ratios, and also less than 30%.

4.4 Summary and discussion

This chapter developed the RBB pile design equations based on the produced datasets by the parametric study carried out using the 3D finite element model established in Chapter 3. These equations were validated against historical field cases.

The scatter plot of the 1008 Q_u values indicated that all of the Q_u values modelled at 60 mm are larger than those modelled at 40 mm; and the increase of the pile bearing capacity Q_u in RBB piling was stable and consistent, falling in a narrow envelope with upper envelope value of 40% and lower envelope value of 20%, averaging at 30%.

The two new RBB pile design equations developed were applied to four historic cases; it has been testified that the prediction results using the new equations were economic and accurate. All of the four applications showcased how the new equations can be used in the future design, and indicated the new design method is simple, economic and straightforward.

CHAPTER 5 SUMMARY, CONCLUSIONS AND RECOMMENDATIONS

This chapter summarises the research carried out in this thesis and provides the research contributions and limitations. The chapter also concludes the presented research with recommendations for potential future work.

5.1 Summary and Conclusions

This thesis developed new artificial intelligence (AI) based design equations for predicting the ultimate bearing capacity of ram-compacted bearing base (RBB) piles installed in a stratum of a wide and comprehensive soil types, based on a robust 3D FE numerical modelling, associated with Mohr-Coulomb elasto-perfectly plastic soil constitutive model. The thesis comprised five main chapters, as follows.

Chapter 1 introduced the basic research background of the RBB piling technology, followed by a discussion of the research objectives and scopes. The research significance was then highlighted before the entire structure of the thesis was finally outlined. The current design procedures for RBB piles rely on semi-empirical equations that typically lead to over-conservative and inconsistent designs, often necessitating costly pilot pile installation and their loading tests before construction. This research aimed at developing a new design method to reduce the current design over-conservatism by providing accurate, consistent and economical predictions.

Chapter 2 carried out the literature review. Firstly, it reviewed the RBB pile installation, mechanism, strengths and weaknesses, and then discussed the available design methods and existing problems of the RBB piling. This chapter also provided suggestions to improve the existing design approaches. The literature showed that the 3.5-tonne ram compaction influenced the foundation soil down to a maximum depth of 2.3 m. The lateral extent of the influence of compaction was about 1 m from the edge of the spherical rubble base. The liquefaction risk was eliminated within about a 4 m thick layer including the rubble base layer and the lower improved soil layer at depth. Obviously, enlarging the base size can increase the bearing capacity per a single RBB pile; however, an excessively large base requires larger pile spacing, which may

further increase the cost of the cap beam. Three problems in the most commonly used current design method were identified in connection with determining the three values of f_a, A_e and R_a. (1) Majority of the data used to determine f_a do not represent the relatively deep soil affected by the RBB installation compaction; f_a value does not consider the deep densification of the soil. (2) The empirical data for determining A_e values were back-calculated from RBB piling cases, only relying on the soil liquidity index (I_L) for clays, void ratio (e) for silts and soil compactness. Moreover, the wide range of values in these options of the equivalent bearing areas A_e with varying three-drive-penetrations P_t emphasizes the questionable reliability of dynamic formulas**.** (3) Both the literature review and the over-conservative design during the 20 years of the RBB pile application confirm the unreliability of the three-drive-penetration method as a means to determine installation refusal. The three problems described above are responsible for the over-conservatism that is currently associated with the design of RBB piles. Therefore, an alternative design method excluding these problems is required for the RBB piles. In summary, the critical problem of the current RBB design method is that the equations and calculation procedures did not use the correct soils parameters. Accordingly, this research aims to improve the current design method by incorporating more relevant soil parameters into the correlation with the RBB pile bearing capacity.

Chapter 2 also reviewed a number of enlarged base piles and compared them with RBB piles. RBB is one of the typical enlarged base pile solutions and the new pile type developed based on the Franki pile but avoided the Franki pile problems. Therefore, the RBB piles have significant similarities and differences with the Franki piles. The RBB technology is unique in using demolition wastes as the major material to construct the bearing bases. Accordingly, the cost of the RBB pile foundation is evidently low in comparable conditions. Secondly, the used demolition wastes have large and irregular particle sizes; this helps RBB piles to create a much larger base sphere under high energy compaction than other enlarged base piling technologies.

Chapter 3 mainly presented the research methodology and implementation used in this research, by utilising the finite element (FE) numerical modelling. This chapter

analysed the methods used to determine the bearing capacity of a single pile to choose the appropriate approaches and prepare for the basics for the RBB design undertaken in the following chapters. The determination settlement criteria for the pile ultimate bearing capacity Q_u values were found varying from 10% to 15% times the pile shaft diameter for the RBB piles. The basic pile load test was modelled and built with the optimised configurations and then calibrated with several historic RBB piling cases. The calibrated model was then used to undertake comparisons of RBB piles with conventional piles. It was found that in the soft soil, the RBB piles provide much higher bearing capacity than in the hard soil. Therefore, the RBB piles have much greater strength in soft soil than conventional piles, in terms of provision of the bearing capacity. This advantage is limited in very stiff bearing soil.

This chapter developed the sophisticated three-dimensional FE numerical models which correctly simulated the performance and behaviour of RBB foundations using the commercial software package ABAQUS. The chapter also included validation of the developed FE models through comparisons with historic cases. A parametric study is also carried out using the established FE models to evaluate the impact of soil properties, pile profiles and strata features on the pile bearing capacity. Consequently, five significant parameters for soils, pile and strata were selected from the parametric analysis as the most significant including: soil cohesion (c), soil friction angle at pile tip (ϕ), soil Young's Modulus (E). The significant pile parameters are pile shaft length (L) and rubble base diameter (D). Other parameters are treated as fixed constants throughout the modelling except were specified separately. Then the validated model was then used to produce 1008 hypothetical datasets from which design equations for RBB piles were derived for use by practitioners.

Chapter 4 developed the RBB pile design equations based on the produced datasets of the parametric study carried out using the 3D finite element model in Chapter 3 and utilising artificial intelligence (AI), mainly Evolutionary Polynomial Regression (EPR) technique. These equations were validated against historical field cases. The scatter plot of the 1008 Q_u values indicated that all of the Q_u values modelled at 60 mm pile settlement are larger than those modelled at 40 mm; and, the increase of Q_u

in RBB piling was stable and consistent, falling in a narrow envelope with the upper envelope value of 40% and lower envelope value of 20%, averaging at 30%. The two new RBB pile design equations developed were applied to four historic cases; it has been testified that the prediction results using the new equations were economic and accurate. All the four applications showcased how the new equations can be used in the future design, and indicated that the new design method is simple and economic.

5.2 Discussion

The effects of installation in RBB piles should be considered at the design stage whether by dynamic formula or static equations. This will produce more realistic assessments of pile performance. Although the current RBB standards have implicitly contained some of the installation effects in the equivalent bearing area by using the increased area values; however, the back-calculated areas were inconsistent and inaccurate. The essential problems of the current mostly commonly used RBB design method are lacking the direct correlations expressed between the bearing capacity with the typical properties of soils, pile and strata. The new design Equations 4-3 and 4-4 developed in this thesis can be finally verified by field loading tests whenever possible even though in Chapter 4 it has initially been validated with four RBB piling historic cases. Regression equations generally are site or region-specific and have limited use if the data samples for regression are not sufficiently available. The new equations developed in this research; however, can be used without limitation of being site-specific or region-specific because all the datasets input in regression are derived from a parametric study based on FE numerical modelling, where the soil properties represent most typical soil physical and geotechnical properties, covering whole ranges that are widely used globally.

It should be noted that this research considered the design and developed new equations for a single RBB pile foundation only, which has provided a solid base for the design of RBB pile group. This is not the topic of concern in this research. The research provided a base for further RBB dynamic modelling, and also can assist the researchers of the RBB foundation or similar foundation in their modelling work. This thesis revealed the problem of the unknown soil properties and dimensions of the

densified soil zone in the RBB pile installation and its static load test simulation. The accurate soil properties and dimension of the densified zone may only be expected to be sought in a future dynamic modelling stage.

5.3 Original contributions of the thesis

This thesis made the following original contributions:

1- Development of a robust static loading FE numerical model capable of successfully simulating the complex interaction behaviour between the RBB pile and the surrounding soils.
2- Implementation of a comprehensive parametric study using the developed FE modelling procedure that included all the ranges theoretically covering the soil physical and geotechnical properties encountered in the RBB piling practice (except for pure clay).
3- A successful development of brand new RBB design equations through AI Evolutionary Polynomial Regression (EPR) method, which can be used widely without a location-specific limitation.
4- The first establishment of correlation of the bearing capacity of RBB piles with the typical soil properties, through the developed AI equations. This new straightforward design method is more realistic, accurate and economical than available methods since it mitigates many of the limitations, assumptions and shortcomings of those methods.
5- The method using a constant multiplying the static loading formula to represent an unsolved dynamic compaction solution in exploring the new RBB design method associated with the dynamic installation performance (refer to Equations 3-1 and 4-6).
6- It has been found that the improvement of the pile bearing capacity predictions during the settlement increase of RBB testing was approximately constant (e.g., 30% increase of Q_u determined from 40 mm to 60 mm).
7- First time having quantified the improvement of the bearing capacity of RBB piles compared to traditional piles. The research has found that improvement

of the bearing capacity by the RBB pile varies depending on different soil types. The improvement ratio is as low as 1.1 in bedrock and as high as 6.9 in soft and weak soils, i.e. clayey soils. The weaker the bearing layer soil, the higher the bearing capacity that the RBB piles can offer compared to conventional piles in comparable situations.

5.4 Recommendations for future work

This research firstly provided an efficient RBB-FE model with the optimal combination of configurations, which were validated with historical cases. The optimised new configurations included: the axisymmetric model type, SOIL step type, Pore Fluid/Stress element family, element type CAX8P, along with the appropriate model dimensions and proper mesh element size. New design equations were then derived from a comprehensive parametric study carried out using the developed FE modelling procedure. Despite the good performance of the new design equations, there are still more enhancements that can be made as explained below:

- The new models can ensure the RBB pile static loading simulation is faster, and the modelling results more accurate. However, the error of the predicted settlement is still relatively large for the low force loading test; this needs a further study.
- For simplicity, the preliminary RBB modelling developed in the current study ignores the presence of groundwater, and thus zero pore pressure was set throughout the FE models. In a subsequent phase of the future work, the presence of groundwater and its impact on the modelling results should be investigated.
- When RBB piles are designed with the new design equations developed in this research, more RBB pile static loading tests should be conducted to ultimately calibrate and validate the new equations against the load-settlement (*Q*-*S*) curve measured on the installed RBB piles. The possible gaps between the measured and predicted values of bearing capacity can be reduced or eliminated by multiplying a constant to compensate for the compaction effect.

- This research was undertaken for a single RBB design. The study for RBB pile group design is recommended based on the research outcome of the single RBB pile from this thesis.

REFERENCES

Alkroosh, Iyad Salim Jabor. 2011. "Modelling Pile Capacity and Load-Settlement Behaviour of Piles Embedded in Sand & Mixed Soils Using Artificial Intelligence."

Beijing Puissant Group. 2020. "The Ram-Compacted Piles with Bearing Bases." *Creative Technology* 5–8. Retrieved February 2, 2020 (www.puissant.com.cn/cxjs/ztzjs/).

Berry, A., A. T. Visser, and E. Rust. 2000. "State of the Art Review of the Prediction of Ground Improvement Using Impact Compaction Equipment." P. 11 in *South African Transport Conference, 'Action in Transport for the New Millennium' Conference Papers*.

Birid, Kedar. 2017. "Evaluation of Ultimate Pile Compression Capacity from Static Pile Load Test Results." P. 15 in *The 1st GeoMEast International Congress and Exhibition, EgyptAt: Egypt*.

Bo, M. W., Y. M. Na, a. Arulrajah, and M. F. Chang. 2009. "Densification of Granular Soil by Dynamic Compaction." *Proceedings of the ICE - Ground Improvement* 162(3):121–32. doi: 10.1680/grim.2009.162.3.121.

Borg, Thomas. 2012. "Alternative Foundation Techniques in Urban Environment - A Study of European Piling Techniques and Methods for Retaining Structures." Chalmers University of Technology.

Bottiau, M. 2006. "Recent Evolutions in Deep Foundation Technologies." P. 38 in *Proceedings of the 10th International Conference on Piling and Deep Foundations*.

Bruce, D. A. 1986. "Enhancing the Performance of Large Diameter Piles by Grouting 1 & 2." *Ground Engineering* May:16.

Bu, Johann. 2012. *Calculation and Graphical Representation of Piles to DIN 4014, DIN 1054, EC 7, EA-Pfähle and after Franke: GGU-AXPILE, Verson 6*.

Chang, H. N., and B. D. Markides. 2016. "Vibration Associated with Construction of DCIS Enlarged-Base Piles." Pp. 53–58 in *Proceedings of the fi rst Southern African Geotechnical Conference – Jacobsz (Ed.)*. Taylor & Francis Group, London.

Chen, Zhimin; Jia, Lihong. 2002. "BP Networks in the Forecast of Bearing Capacity of Composite Foundation with Rammed Expanded Piles." *Chinese Journal of*

Geotechnical Engineering 24(3):286–89.

Chen, Bin, Junneng Ye, Jianfeng Zhu, Ganbin Liu, and Bo Jia. 2013. "Determination of the Bearing Capacity of the Foundations in Typical Soils in Ningbo." *Journal of Enginering Geology* 21(4):493–500. doi: 10.1017/CBO9781107415324.004.

Cheng, Quan. 2006. "Determining the pile end bearing capacity eigenvalue of the compound carrier ramming extended pile in medium, coarse and gravely sand stratum." *Journal of Enginering Geology* Suppl:135–37.

Chinese Ministry of Construction. 2007. *JGJ 135-2007: Chinese Professional Standards: Design Specification of Ram- Compacted Piles with Base Bearing (in Mandarin)*. China.

Chinese Ministry of Construction. 2008. *JGJ 94-2008: Chinese Professional Standards: Technical Specification of Pile Foundation (in Mandarin)*. Beijing China.

Chinese Ministry of Construction. 2012. *GB50007-2011: Code for Design of Building Foundation (in Mandarin)*. China.

Chinese Ministry of Construction. 2018. *JGJ/T 135-2018: Technical Standard for Piles with Ram-Compacted Bearing Sphere (in Mandarin)*. 2018th ed. edited by Wang et al. Beijing China: China Construction Industry Press.

Chinese Ministry of Science & Technology. 2008. *Rebuild Technical Manual for Residential Buildings in Sichuan, China*. 1st ed. edited by C. M. of S. & Technology. Chinese Ministry of Science & Technology.

Civil-engg-world. 2011. "Foundation, Concrete and Earthquake Engineering." 1–5. Retrieved (http://civil-engg-world.blogspot.com.au/2011/12/different types of earth pressure cells_19.html).

Cooke, R. W., and Thomas Whitaker. 1961. "Experiments on Model Piles with Enlarged Bases." *Geotechnique* 11(1):1–13. doi: 10.1680/geot.1961.11.1.1.

Corson, Willian M. 1989. *Analysis: Prediction of Pile Capacity Using the Cone Penetration Test*. UNIVERSITY OF FLORIDA.

Coyle, Harry M., and Ibrahim H. Sulaiman. 1970. "Bearing Capacity of Foundation Piles : State of the Art." Pp. 87–103 in *49th Annual Meeting of the Highway Research Board*.

Curtin, W. G., G. Shaw, G. I. Parkinson, J. M. Golding, and N. J. Seward. 2006. *Structural Foundation Designers' Manual*. Singapore: Utopia Printers.

Das, Sarat Kumar, and Prabir Kumar Basudhar. 2006. “Undrained Lateral Load Capacity of Piles in Clay Using Artificial Neural Network.” *Computers and Geotechnics* 33(8):454–59. doi: 10.1016/j.compgeo.2006.08.006.

Dassault Systèmes Simulia. 2012. “Abaqus CAE User’s Manual.” *Abaqus 6.12* 1174.

Dassault Systèmes Simulia. 2014. “Abaqus 6.14 Scripting User’s Guide.” 324.

Department of Environment Australia. 2011. “Construction and Demolition Waste Status Report - Management of Construction and Demolition Waste in Australia.” 413. Retrieved February 20, 2016 (http://www.environment.gov.au/protection/national-waste-policy/publications/construction-and-demolition-waste-status-report).

Du, Z., M. A. Shahin, and Jethro Neeson. 2016. “Ram-Compacted Base Bearing (RBB) Piling Technology for Infrastructure Developments.” Pp. 1–8 in *The 2016 New Zealand Society for Earthquake Engineering (NZSEE) Annual Technical Conference*. Christchurch New Zealand: New Zealand Society for Earthquake Engineering (NZSEE).

Du, Z., M. Walske, M. A. Shahin, and B. Ghadimi. 2019. “Numerical Modelling of Ram-Compacted Bearing Base Piles.” Pp. 333–38 in *Proceedings of the 13th Australia New Zealand Conference on Geomechanics*.

Elkateb, Tamer, Don Law, and Robin Tweedie. 2003. “Underpinning of Franki Pile Foundations of A Mall in Spruce Grove , Alberta A Case Study.” in *56th canadian geotechnical conference; 4th joint iah-cnc/cgs conference; 2003 nags conference*.

Elsamee, Wael N. Abd. 2013. “New Method for Prediction Pile Capacity Executed by Continuous Flight Auger (CFA).” *Engineering, Scientific Research* 5(April):344–54. doi: 10.4236/eng.2013.54047.

Engelbrecht, J. H., and H. Kgole. 2016. “Capacity and Performance of Franki Enlarged-Base Piles.” Pp. 3–8 in *Proceedings of the first Southern African geotechnical conference – Jacobsz (Ed.)*.

Eslami, A., I. Tajvidi, and M. Karimpour-Fard. 2014. “Efficiency of Methods for Determining Pile Axial Capacity-Applied to 70 Cases Histories in Persian Gulf Northern Shore.” *International Journal of Civil Engineering* 12(1 B):45–54.

Evans, J. D., and Cl Feltz. 1996. “Straightforward Statistics for the Behavioral Sciences.” *Perceptual and Motor Skills* 81(1995):1391.

Fellenius, Bengt H. 2006. “Basics of Foundation Design f Basics of Foundation

Design.” (January):433.

Fleming, Ken, Austin Weltman, Mark Randolph, and Keith Elson. 2009. *Piling Engineering*.

Fleming, W. K. 1992. “New Method of Single Pile Settlement Prediction.Pdf.” 411–25.

Fragaszy, Richard J., Douglas Argo, and Jerry D. Higgins. 1989. “Comparison of Formula Predictions with Pile Load Tests.” *Transport Research Record* (No. 1219):1–12.

Gandomi, Amir H., Amir H. Alavi, and Conor Ryan. 2015. *Handbook of Genetic Programming Applications*.

Giustolisi, O., A. Doglioni, D. A. Savic, and B. W. Webb. 2007. “A Multi-Model Approach to Analysis of Environmental Phenomena.” *Environmental Modelling and Software* 22(5):674–82. doi: 10.1016/j.envsoft.2005.12.026.

Giustolisi, Orazio, and Dragan A. Savic. 2006. “A Symbolic Data-Driven Technique Based on Evolutionary Polynomial Regression.” *Journal of Hydroinformatics* 8(4):235–37. doi: 10.2166/hydro.2006.020.

Gowthaman, S., M. C. M. Nasvi, and S. Krishnya. 2017. “Numerical Study and Comparison of the Settlement Behaviours of Axially Loaded Piles Using Different Material Models.” *Engineer: Journal of the Institution of Engineers, Sri Lanka* 50(2):10. doi: 10.4038/engineer.v50i2.7247.

Grevtsev, A. A., and V. G. Fedorovskii. 2013. “Formula for Limiting Pressure of Cavity Expansion and Its Practical Application.” *Soil Mechanics and Foundation Engineering* 50(5):2–5.

GRV. 2015. “Franki Pile.” *Geoforum* 1–2. Retrieved October 20, 2015 (http://www.geoforum.com/info/pileinfo/view.asp?ID=15).

Guo, Bailiang. 2015. “Analysis and Study on Behavior of Ram-Compacted Piles with Bearing Base Composite Foundation.Pdf.” University of Science and Technology Liaoning.

Guo, Wei Dong. 2013. *Theory and Practice of Pile Foundations*. Boca Raton, FL: CRC Press Taylor & Francis Grroup.

GWIZDALA, KAZIMIERZ. 1984. *Large Diameter Bored Piles in Non-Cohesive Soils -Determination of the Bearing Capacity and Settlement from Results of Static Penetration Tests (CPT) and Standard Penetration Test (SPT)*.

Han, Xiangang. 2013. “Study on the Mexhanism and Design Method of Ram-Compacted Piles with Bearing Base (in Mandarin).” Eastnorth Univeristy of China.

Hannigan, P. J., G. G. Goble, G. E. Likins, and F. Rausche. 2006. *Design and Construction of Driven Pile Foundations Reference Manual – Volume I*. Vol. I. U.S. Department of Transportation Federal Highway Administration Publication.

Helwany, Sam. 2007. *Applied Soil Mechanics with Abaqus Applications*. Hoboken, New Jersey: John Wiley & Sons, Inc.

Huang, Wenxiong, D. Sheng, S. W. Sloan, and H. S. Yu. 2004. “Finite Element Analysis of Cone Penetration in Cohesionless Soil.” *Computers and Geotechnics* 31(7):517–28. doi: 10.1016/j.compgeo.2004.09.001.

Inner Mongolia Puissant Ltd. 2015. “The Excavation of the Ram-Compacted Bearing Base Pile at Jiangnan Huafu Site (in Mandarin).” 1. Retrieved (http://www.nmg-bst.com/html/gongchengyeji/gongchengyeji/2015/1104/124.html).

Ishihara, Kenji. 1985. “Stability of Natural Deposits during Earthquakes.” Pp. 321–76 in *Proceedings of the Eleventh International Conference on Soil Mechanics and Foundation Engineering*. San Francisco.

Ismail, Mostafa A., and Mohamed A. Shahin. 2012. “Numerical Modeling of Granular Pile-Anchor Foundations (GPAF) in Reactive Soils.” 6362(March):149–56. doi: 10.3328/IJGE.2012.06.02.149-156.

Jaksa, M. B., M. C. Griffith, and R. W. Grounds. 2002. “Ground Vibrations Associated with Installing Enlarged-Base Driven Cast-in-Situ Piles.” *Australian Geomechanics* 37(1):67–73.

Jin, Changlai. 2004. “Analysis and Applicaton of the New Compacton and Enlarged Base Piles (in Mandarin).” Tongji Univeristy.

Jin, Xiao. 2011. “The Application of the Ram-Compaction Piles with Composite Bearing Base (in Mandarin).” Chongqing University, Chongqing, China.

Johnson, Alan. 2014. *Recommendations on Piling (EA Pfähle)*. (Translato. edited by Geotechnik (Editor).

Kulhawy, F. H., and A. Hirany. 1988. *Conduct and Interpretation of Load Tests on Drilled Shaft Foundations Research Project Final*.

Li, Guangxin, and Kaibin Qiu. 2009. “Research on the influence extent of the ram-

compacted bearing base pile (in Mandarin).” *Geotechnical Investigation and Surveying* supplement(1):21–25.

Li, Guangxin, Kaibin Qiu, Yuxin Jie, and Wang Jizhong. 2002. “Study on Optimal Spacing for Rammed Enlargede Composite Bearing Piles.” *Industrial Construction* 32(1):29–31.

Li, Jiping. 2010. “Research on Pridiction of the Quality of Bearing Base Pile Using BP Nerve Network.” Hebei University of Engineering.

Li, Wei. 2007. “Numerical Analysis of Ultimate Bearing Capacity for Rammed-Expanding Pile (in Mandarin).” Nanchang University.

Likins, Garland E., Bengt H. Fellenius, and Robert .. D. Holtz. 2012. “Pile Driving Formulas — Past and Present Garland.” Pp. 737–53 in *Full-Scale Testing and Foundation Design*, edited by M. H. Hussein, K. R. Massarsch, G. E. Likins, and R. H. D. American Society of Civil Engineers.

Liu, Xiangyang, Chaoyang Xiao, and Xinjun Fu. 2008. “Applications of the RBB Pile on Different Project Sites.” *Western Drillling and Exploration* 9:12–13.

Long, JH, J. Hendrix, and D. Jaromin. 2009. “Comparison of Five Differente Methods for Determining Pile Bearing Capacities.” (217).

Luo, Hao. 2010. “Experiment on Site Investigating the Settlement of the Composite Foundation with the Ram-Compacted Bearing Base Piles, and the Construction Techniques on the Foundations of the High-Speed Highway (in Mandarin).” Xinan Univeristy of Transports, China.

Ma, Cheng. 2013. “Analysis on the Bearing Capacity of the Ram-Compacted Pile with Bearing Base and Its Control of the Engineering Quality (in Mandarin).”

Mainroads Western Australia. 2011. *Structures Engineering Design Manual*. WA Australia.

Mayne, P., and J. Jones. 1983. “Impact Stresses During Dynamic Compaction.” *Journal of Geotechnical Engineering* 109(10):1342–46. doi: doi:10.1061/(ASCE)0733-9410(1983)109:10(1342).

Mayne, Paul W., and Jones S. Jones. 1983. “Impact Stresses during Dynamic Compaction.” *Journal of Geotechnical Engineering* 109(10):1342–46. doi: 10.1061/(ASCE)0733-9410(1983)109:10(1342).

Meyerhof, G. G. 1951. “THE ULTIMATE BEARING CAPACITY OF FOUNDATIONS.” *Géotechnique* 2(4):301–32.

Ministry for the Environment New Zealand. 2002. *A Guide to the Management of Cleanfills*. New Zealand: Prepared by Beca Carter Hollings & Ferner Ltd.

Ministry of Housing and Building of China. 2014. *Technical Code for Testing of Building Foundtion Piles - JGJ106-2014*. China.

National Programme on Technology Enhanced Learning India. 2020. "Module 5 : Design of Deep Foundations." *Lecture 24 : Under Reamed Pile* 8. Retrieved (https://nptel.ac.in/content/storage2/courses/105101083/download/lec24.pdf).

Nazhat, YAHYA. 2013. "Behaviour of Sandy Soil Subjected to Dynamic Loading." University of Sydney.

Neely, By William J. 1990. "Bearing Capacity of Expanded-Base Piles in Sand." *Journal of Geotechnical Engineering* 116(1):73–87.

Niazi, Fawad S., and Paul W. Mayne. 2013. "Cone Penetration Test Based Direct Methods for Evaluating Static Axial Capacity of Single Piles." *Acta Geotechnica* 31:979–1009. doi: 10.1007/s10706-013-9662-2.

Niroumand, Hamed, Khairul Anuar Kassim, Amin Ghafooripour, and Ramli Nazir. 2012. "Uplift Capacity of Enlarged Base Piles in Sand." *Electronic Journal of Geotechnical Engineering* 17 R:2721–37.

Otieno, Owino Alex, Zakaria Hossain, and Jim Shiau. 2018. "Pull-out Resistance of Single Piles and Parametric Study Using the Finite Difference Method (FDM)." *American Journal of Civil Engineering and Architecture* 6(5):193–98. doi: 10.12691/ajcea-6-5-4.

Paikowsky, Samuel G. 2014. "Lecture 1 – Introduction to Deep Foundations Class Notes." 45.

Pusztai, József. 2005. "Contributioin to Determing the Load Bearing Capacity of Franki Piles." *Periodica Polytechnica Ser. Civ . Eng.* 48(1):47–52.

Qi, Chang-guang, Gan-bin Liu, Yan Wang, and Yue-bao Deng. 2015. "Theoretical Study on Setup of Expanded-Base Pile Considering Cavity Contraction." *Journal of Central South University* 22(11):4355–65. doi: 10.1007/s11771-015-2984-x.

Qiu, Feng. 2014. "Study on Bearing Capacity and Influence Factor of Pedestal Bored Pile Compacted Column-Hammer (in Mandarin)." Hebei University of Industries.

Qiu, Kaibin, Yuxin Jie, Guangxin Li, and Jizhong Wang. 2002. "Finite Element

Analysis of Bearing Capacity Properties for Rammed Enlarged Composite Bearer Piles." *Engineering Mechanics* 19(3):90–94.

Rao, N. S. V. Kameswara. 2011. "Deep Foundations – Piles, Drilled Piers, Caissons and Pile-Raft Systems 9.1." P. 42 in *Foundation Design: Theory and Practice*. © 2011 John Wiley & Sons (Asia) Pte Ltd. ISBN: 978-0-470-82534-1.

Rogers, J. David. 2009. "Fundamentals of Cone Penetometer Test (CPT) Soundings." *Missouri Univerity of Science and Technology: USA*.

Shah, By D. L., and A. V. Shroff. 2003. *Soil Mechanics and Geotechnical Engineering*. Lisse : Balkema.

Shahin, Mohamed. 2015a. "A Review of Artificial Intelligence Applications in Shallow Foundations." *International Journal of Geotechnical Engineering* 9(1):49–60. doi: 10.1179/1939787914Y.0000000058.

Shahin, Mohamed. 2015b. "Use of Evolutionary Computing for Modelling Some Complex Problems in Geotechnical Engineering." 10(2):109–25. doi: 10.1080/17486025.2014.921333.

Shahin, Mohamed A. 2009. "Intelligent Computing for Modeling Axial Capacity of Pile Foundations." (2008):230–43. doi: 10.1139/T09-094.

Shahin, Mohamed a. 2013. "Artificial Intelligence for Modeling Load-Settlement Response of Axially Loaded (Steel) Driven Piles." *Proceedings of the 16th International Conference on Soil Mechanics and Geotechnical Engineering: Geotechnology in Harmony with the Global Environment* 491–95.

Shahin, Mohamed a, and Mark B. Jaksa. 2008. "State of the Art of Artificial Neural Networks in Geotechnical Engineering." *Electronic Journal of Geotechnical Engineering* 8:1–26.

Shahnazari, H., M. A. Shahin, and M. A. Tutunchian. 2014. "Evolutionary-Based Approaches for Settlement Prediction of Shallow Foundations on Cohesionless Soils." *International Journal of Civil Engineering* 12(1 B):55–64.

Shams, Mohamed A. 2019. "Analysis and Design of Stiffened Slab Foundations on Reactive Soils Using 3D Numerical Modelling." (March).

Shams, Mohamed A., Mohamed A. Shahin, and Mostafa A. Ismail. 2019. "Computers and Geotechnics Numerical Analysis of Slab Foundations on Reactive Soils Incorporating Sand Cushions." *Computers and Geotechnics* 112(January):218–29. doi: 10.1016/j.compgeo.2019.04.026.

Shariatmadari, N., A. Eslami, and And M. Karimpour-Fard. 2008. “Bearing Capacity of Driven Piles in Sands From Spt–Applied To 60 Case Histories *.” *Iranian Journal of Science & Technology, Transaction B, Engineering* 32(B2):125–40.

Shen, Baohan. 2004. “State-of-the-art of rammed under-expanded piles in china (in Mandarin).” *Industrial Construction* 34(2):45–49.

Shooshpasha, Issa, Ali Hasanzadeh, and Abbasali Taghavi. 2013. “Prediction of the Axial Bearing Capacity of Piles by SPT-Based and Numerical Design Methods.” *International Journal of Geomate* 4(2):560–64.

Singh, Ningombam Thoiba. 2016. “Verification of Pile Load Capacity Using Static Pile Load Test.” Pp. 136–40 in *1st International Conference on Civil Engineering for Sustainable Development – Opportunities and Challenges*.

Srbulov, Milutin. 2010. *Ground Vibration Engineering, Simplified Analyses with Case Studies and Examples*. Vol. 12. Springer Science+Business Media B.V.

Su, Guifeng, and Baoliang Ge. 2005. “Application of the Composite Base Bearaing Piles in Saturated Sand.” *Construction Technology* supp.:2.

Suman, Shakti. 2015. “Prediction of Pile Capacity Parameters Using Functional Networks and Multivariate Adaptive Regression Splines Master of Technology Civil Engineering (Geotechnical Engineering) Prediction of Pile Capacity Parameters Using Functional Networks and Multivar.”

Tan, Xiaochun, and Jizhong Wang. 2010. “RBB Pile Application in Beichuan Middle School in the Rebuild after Earthquake.” *Construction Structure* 40(10):2. doi: 10.1017/CBO9781107415324.004.

Tang, Jiapeng. 2012. “The case analysis of the base bearing piles (in Mandarin).” *Engineeing and Science, Heilongjiang Science Information* 20:245–245.

Tchepak, S. 1986. “Design and Construction Aspects of Enlarged Base Frankipiles.” in *Speciality Geomechanics Symposium Adelaide 18-1 9 August, 1986*.

Tomlinson, Michael, and John Woodward. 2007. *Pile Design and Construction Practice*. 5th ed. Taylor & Francis e-Library.

Wang, Junlin, Caihong Hu, Yanzhi Zhu, and Mingxin Hu. 2006. “Testing Study on the Bearing Capacity of the Ram-Compaction Piles with Composite Bearing Base.” *Rock and Soil Mechanics* 27(Suppl 2):875–78.

Wang, Qingshan. 2014. “The Application Study on Pile with Bearing Base in Dense Sand Stratum of Zhengdong New District (in Mandarin).” Henan Industrial

University.

Wang, Xianfeng. 2007. “Application and Research of the Composite Pile with Bearing Base in Soft and Weak Soil Strata (in Mandarin).” Tongji University.

Wang, Xijiang. 2008. “Application of the Composite Pile with Bearing Base in Engineering (in Mandarin).” Tianjin University.

Wang, Zhan. 2009. “Application of composite rammed bulb pile in Myanmar Tagaung Taung Nickel resource project.” *Non-Ferrous Metal & Metallurgy, China* 25(6):56–60.

William, J. NEELY. 1991. “Bearing Capacity of Expanded-Base Piles with Compacted Concrete Shafts.” *Journal of Geotechnical Engineering* 116(9):1309–24.

Wrana, Bogumił. 2015. “Pile Load Capacity – Calculation Methods.” *Studia Geotechnica et Mechanica* 37(4):4–14. doi: 10.1515/sgem-2015-0048.

Wu, Maozhi, and Jiaxiang Tang. 2000. “Discussion about Variation of Mechanical Property of Bearing Layer Induced by Construction of Dynamic Compaction in Wuhan Area.” *Chinese J Ournal of RockM Echanics and Engineering* 19(3):397–99.

Yang, Jie. 2004. “Research on the Application of the Base Bearing Pile in Luoyang City (in Mandarin).” Tongji Univeristy, China.

Yang, Jingshong. 2011. “Application of the Composite Pile with Bearing Base and Study of the Bearing Characteristics.” Hebei University of Enigneeing.

Yang, Jingsong. 2011. “Research on the Bearing Capacity of the Composite Piles with Bearing Base and Pre-Stressed Casing.” Hebei University of Engineering.

Yang, Q. A., and J. Z. Wang. 2012. “Effect of Ramp-Compacted Bearing Base to Nearby Soils,.” *Foundation Technology Forum (in Mandarin)* 32–33.

Yang, Qi’an, and Jizhong Wang. 2011. “Development of carrier pile technology (in Mandarin).” *Road Subgrade Engineering* 3 (156):68–71.

Yang, Qi An, Jizhong Wang, and Baohan Shen. 2007. “Reasearch on the Construction Effect of Ram-Compacted Piles with Bearing Base.” 473–80.

Yu, Jianmin. 2008. “Carrier Pile Application Study in Hohhot Area.” Xi’an Univerisity of Building and Construction Sciences.

Yu, Minjie. 2007. “Property Comparasion and Application of Cement-Soil Mixed Piles and Rammed Enlarged Composite Bearer Piles (in Mandarin).” Harbin Institute of Technology.

Yue, Yanfeng, and Xiaobin Yang. 2002. “Characteristics and Method of the RBB Pile Test.” *Geotechnical Engineering Regime* 5(10):47–49.

Zein, Abdul Karim M., and Enass M. Ayoub. 2016. “Evaluation of Measured and Interpreted Failure Loads of Bored Piles in Alluvial Soil Deposits.” *Journal of GEOMATE* 10(1):1636–43.

Zergoun, Mustapha, and Derek Harris. 2004. “Vertical Load Carrying Capacity of Concrete Expanded Base Piles.” P. 10 in *Proceedings of the 29th annual conference on deep foundations, 2004, Vancouver, British Columbia, Canada “Emerging Technologies”, (DFI)*, edited by Deep Foundations Institute. Deep Foundations Institute.

Zhang, Houqi. 2014. “The Numerical Analysis and Experimental Study on Mechanical Properties and Settlement Characteristics of Rammed Piles with Composite Bearing Base.” Zhengzhou University.

Zhang, Shuyuan. 2012. “Experimental Research and Comparison on the Bearing Base Piles and the CFG Piles in the Composite Foundations of the High-Speed Railway (in Mandarin).”

Zhang, Yongyang, and Xinchao Chen. 2008. “Research on the Vertical Bearing Capacity per Ram-Compacted Base Bearing Pile.” *Resources Environment & Engineering* 22(addational):3.

Zhu, Hongchang. 2008. “The Test and Application Research of Load-Bearing Mechanics for Bearing Base Pile in Loess Area (in Mandarin).” Xi’an University of Architecture and Technology.

Zhu, Xihu, and Dong Wang. 2005. “Applicaton of ram-compacicton piles with composite bearing base in higher—load lndustrial building (in Mandarin).” *Journal of Anhui Institute of Architecture & Industry* 13(1):44–47.

APPENDIX A: COPYRIGHT HOLDERS PERMISSION STATEMENTS

Every reasonable effort has been made to acknowledge the owners of copyright material. I would be pleased to hear from any copyright owner who has been omitted or incorrectly acknowledged. One permission request has been confirmed, and the correspondences to my other requests have not been received yet, however, the requests are attached as follows.

10/10/2020 Mail - David Du - Outlook

Re: Permission request

Abdul Karim Mohammad Zein <karimzein2000@yahoo.com>

Mon 31/08/2020 9:51 PM

To: David Du <zhaodong.du@postgrad.curtin.edu.au>

Thank you David

I am pleased to know about your interest in my work and I would like to inform you that I have no objection for reprinting through figure you need for your research

Hoping you success

Thank you

Sent from Yahoo Mail on Android

On Sun, Aug 30, 2020 at 3:29 PM, David Du <zhaodong.du@postgrad.curtin.edu.au> wrote:

Dear Dr. Zein,

Greetings to you from Australia!

I am a Master's student at Cur n University in Australia and preparing my thesis for submission. I would like to ask your permission to reprint Figure 1 from your published paper:

"Zein, A. K. M. & Ayoub, E. M. Evaluation of measured and interpreted failure loads of bored piles in alluvial soil deposits. J. GEOMATE 10, 1636–1643 (2016)."

The thesis will be made available online via Curtin's Institutional Repository, espace. The material will be provided strictly for educational purposes and on a non-commercial basis.

If you are not the copyright owner of the material in ques on, I would be grateful for any information you can provide as to who is likely to hold the copyright.

I look forward to hearing from you and thank you in advance for your consideration of my request.

Yours sincerely

David Zhaodong DU

Research Scholar, BE, MSc

School of Civil and Mechanical Engineering
Curtin University
Perth, WA, Australia
Email | zhaodong.du@postgrad.curtin.edu.au
Web | http://scieng.curtin.edu.au/engineering/civil-engineering/

Re: Permission request

David Du <zhaodong.du@postgrad.curtin.edu.au>

Sun 30/08/2020 8:28 PM

To: office@landpac.co.za <office@landpac.co.za>

Dear Berry,

I am a Master's student at Cur n University in Australia and I want your permission to reprint Figure 1 from your published paper:

"Berry, A., Visser, A. T. & Rust, E. State of the Art Review of the Prediction of Ground improvement using impact compaction equipment. in South African Transport Conference, 'Ac on in Transport for the New Millennium' Conference Papers 11 (2000)."

The thesis will be made available online via Cur n's Institutional Repository, espace. The material will be provided strictly for educational purposes and on a non-commercial basis.

If you are not the copyright owner of the material in question, I would be grateful for any information you can provide as to who is likely to hold the copyright.

I look forward to hearing from you and thank you in advance for your consideration of my request. Yours sincerely

David Zhaodong DU

Research Scholar, BE, MSc

School of Civil and Mechanical Engineering

Curtin University

Perth, WA, Australia

Email | zhaodong.du@postgrad.curtin.edu.au

Web | http://scieng.curtin.edu.au/engineering/civil-engineering/

Re: Permission request 许可请求

David Du <zhaodong.du@postgrad.curtin.edu.au>

Sun 30/08/2020 10:11 PM

To: wzjwtr@126.com <wzjwtr@126.com>

Dear Mr. Wang, 亲爱的王先生,

Greetings to you from Australia! 请接受来自澳大利亚的问候!

I am a Master's student at Cur n University in Australia and preparing my thesis for submission. I would like to ask your permission to reprint Figures 1, 2 and 3 from your published paper: 我是科廷大学的硕士生, 正在准备我的硕士论文, 在此请求您的许可, 以使用您发表在下列论文的三幅图片 1, 2 和 3:

"Wang, Z., Zhao, Z., Du, H. & Zhang, Z. Analysis of the economy of the Ram compacted pile with bearing base and the Natural Foundations. Geotech. Inves g. &Surveying 1 Suppl, 118–121 (2009).."

" 王中军等, 载体桩与天然地基的经济分析, 工程勘察, 2009 年增刊第 1 期, 118-121 页.

The thesis will be made available online via Cur n's Institutional Repository. The material will be provided strictly for educational purposes and on a non-commercial basis. 本论文将储藏在科廷大学图书馆. 本资料严格用于教育而非商业用途.

I look forward to hearing from you and thank you in advance for your consideration of my request. 希望得到您的允可和答复.

Yours sincerely, 此致!

David DU

Research Scholar

BE, MSc

School of Civil and Mechanical Engineering

Curtin University

Perth, WA, Australia

Email | zhaodong.du@postgrad.curtin.edu.au

Web | http://scieng.curtin.edu.au/engineering/civil-engineering/

Re: Permission request

David Du <zhaodong.du@postgrad.curtin.edu.au>

Sun 30/08/2020 9:06 PM

To: wrana@limba.wil.pk.edu.pl <wrana@limba.wil.pk.edu.pl>

Dear Bogumil WRANA,

I am a Master's student at Cur n University in Australia and I want your permission to reprint Figure 15 from your published paper:

"Wrana, B. Pile Load Capacity – Calculation Methods. Stud. Geotech. Mech. 37, 4–14 (2015)."

The thesis will be made available online via Cur n's Institutional Repository, espace. The material will be provided strictly for educational purposes and on a non-commercial basis.

If you are not the copyright owner of the material in ques on, I would be grateful for any information you can provide as to who is likely to hold the copyright.

I look forward to hearing from you and thank you in advance for your consideration of my request. Yours sincerely

David Zhaodong DU
Research Scholar, BE, MSc
School of Civil and Mechanical Engineering
Curtin University
Perth, WA, Australia
Email | zhaodong.du@postgrad.curtin.edu.au
Web | http://scieng.curtin.edu.au/engineering/civil-engineering/

Re: Permission request 许可请求

David Du <zhaodong.du@postgrad.curtin.edu.au>

Tue 1/09/2020 10:39 AM

To: zhqzhanghouqi@163.com <zhqzhanghouqi@163.com>

Dear Mr. Zhang Houqi, 亲爱的张厚琦先生,

Greetings to you from Australia! 请接受来自澳大利亚的问候!

I am a Master's student at Cur n University in Australia and preparing my thesis for submission. I would like to ask your permission to reprint Figures 2.6 and 3.11 from your published thesis, 我是科廷大学的硕士生, 正在准备我的硕士论文, 在此请求您的许可, 以使用您发表在下列论文的两幅图片 2.6 和 3.11:

"Zhang, H. The Numerical Analysis and Experimental Study on Mechanical Proper es and Settlement Characteristics of Rammed piles with Composite bearing base. Zhengzhou University, 2014."

The thesis will be made available online via Cur n's Institutional Repository. The material will be provided strictly for educational purposes and on a non-commercial basis. 本论文将储藏在科廷大学图书馆. 本资料严格用于教育而非商业用途. I look forward to hearing from you and thank you in advance for your considera on of my request. 希望得到您的允可和答复.

Yours sincerely, 此致!

David DU

Research Scholar, BE, MSc

School of Civil and Mechanical Engineering

Curtin University

Perth, WA, Australia

Email | 18473768@postgrad.curtin.edu.au

Web | http://scieng.curtin.edu.au/engineering/civil-engineering/

Permissions

As a general rule, permission should be sought from the rights holder to reproduce any substantial part of a copyrighted work. This includes any text, illustrations, charts, tables, photographs, or other material from previously published sources. Obtaining permission to re-use content published by Elsevier is simple. Follow the guide below for a quick and easy route to permission.

Permission guidelines

For further guidelines about obtaining permission, please review our Frequently Asked Questions below:

When is permission required?

When is permission not required?

From whom do I need permission?

How do I obtain permission to use photographs or illustrations?

Do I need to obtain permission to use material posted on a website?

What rights does Elsevier require when requesting permission?

How do I obtain permission from another publisher?

This page is available in the following languages: 

Creative Commons License Deed

Attribution-NonCommercial-NoDerivatives 4.0 International (CC BY-NC-ND 4.0)

This is a human-readable summary of (and not a substitute for) the license.

You are free to:

Share — copy and redistribute the material in any medium or format

The licensor cannot revoke these freedoms as long as you follow the license terms.

Under the following terms:

Attribution — You must give appropriate credit, provide a link to the license, and indicate if changes were made. You may do so in any reasonable manner, but not in any way that suggests the licensor endorses you or your use.

NonCommercial — You may not use the material for commercial purposes.

NoDerivatives — If you remix, transform, or build upon the material, you may not distribute the modified material.

No additional restrictions — You may not apply legal terms or technological measures that legally restrict others from doing anything the license permits.

Notices:

You do not have to comply with the license for elements of the material in the public domain or where your use is permitted by an applicable exception or limitation.

No warranties are given. The license may not give you all of the permissions necessary for your intended use. For example, other rights such as publicity, privacy, or moral rights may limit how you use the material.

https://creativecommons.org/licenses/by-nc-nd/4.0/ 1/1